From Knowledge to Wisdom

Geological Resource and Engineering

Volume 1, Number 1, December 2013

David Publishing Company
www.davidpublishing.com

ISSN 2328-2193

Journal of Geological Resource and Engineering

Volume 1, Number 12, December 2013 (Serial Number 1)

David Publishing Company
www.davidpublishing.com

Publication Information:
Journal of Geological Resource and Engineering is published monthly in hard copy (ISSN 2328-2193) by David Publishing Company located at 240 Nagle Avenue #15C, New York, NY 10034, USA.

Aims and Scope:
Journal of Geological Resource and Engineering, a monthly professional academic journal, particularly emphasizes practical application of up-to-date technology in realm of geological resource and engineering and other relevant fields. And articles interpreting successful policies, programs or cases are also welcome.

Manuscripts and correspondence are invited for publication. You can submit your papers via web submission, or E-mail to geology@davidpublishing.com. Submission guidelines and web submission system are available at http://www.davidpublishing.com.

Editorial Office:
240 Nagle Avenue #15C, New York, NY 10034, USA
Tel: 1-323-984-7526, 323-410-1082; Fax: 1-323-984-7374, 323-908-0457
E-mail: geology@davidpublishing.com

Abstracted / Indexed in:
Chinese Database of CEPS, CNKI, China
Chinese Scientific Journals Database, VIP Corporation, Chongqing, China
ProQuest
CiteFactor (USA), Ulrich's International Periodicals Directory, USA
Google Scholar
Summon Serials Solutions
Pubicon Science Index
SJournal Index
Scientific Indexing Services

Subscription Information:
Price (per year):
Print $520; Online $360; Print and Online $680

David Publishing Company
240 Nagle Avenue #15C, New York, NY 10034, USA
Tel: 1-323-984-7526, 323-410-1082; Fax: 1-323-984-7374, 323-908-0457
E-mail: order@davidpublishing.com

Journal of
Geological Resource and
Engineering

Volume 1, Number 1, December 2013 (Serial Number 1)

Contents

Journal of Geological Resource and Engineering 1 (2013) 1-10

Impact Analysis of the 2011 Fukushima Nuclear Power Plant Accidents by Running Spectrum Analysis on Newspaper

Muneyoshi Numada and Kimiro Meguro

International Center for Urban Safety Engineering (ICUS), Institute of Industrial Science (IIS), University of Tokyo, Tokyo153-8505, Japan

Abstract: Huge amount of digital data of the Great East Japan Earthquake is provided by the highly-developed digital data technology. But the method and technique for analysis of these huge digital data are not developed sufficiently. This paper proposes a running spectrum technique for text data and analyzing changes of disaster phase during the disaster management cycle. Impact analysis of the nuclear power plant accidents have been performed by using Fukushima Minpo newspaper for its verification. The result shows the dynamic characteristics of the nuclear power plant accidents. As the time interval B becomes longer, the analysis data is used from wide range period along with the smoothing effect. When observing different time intervals B, fewer keywords have been ranked in the longer time intervals of B. The proposed technique is a powerful tool to analyze effectively the huge amount of digital data for the effective and efficient disaster response and management.

Key words: Impact analysis, Fukushima nuclear power plant accident, running spectrum analysis, newspaper.

1. Introduction

Huge amount of digital information related to the Great East Japan Earthquake has been published by newspapers, wire agencies and TV stations. The volume of information has exceeded that of past disasters because the tools by using to send out information have dramatically changed; Internet-based platforms are now widely used as popular sources for news updates. The contents covered include many different kinds of events and problems that were caused simultaneously by the earthquake. Reports on regional damage induced by the earthquake, tsunami and economic problems in the[1] Tokyo metropolitan area, Fukushima nuclear power plant accident and much other information spread out at the same time.

Cloud computing technology can evaluate more and more digital contents that produced and stored in the digital world. This new innovative environment and incorporating powerful delivery data system enable us to use information more easily for different purposes. However, the quality of data analysis technique in the disaster management field is far from enough. We need efficient means to distinguish important events out of the vast amount of information. Furthermore, we can get the movements within a certain time frame and know the changes occurring in the disaster management phase and so on.

Some algorithms in literature evaluation method suggest using association rules such as TF-IDF (term frequency-inverse document frequency) [1, 2], Z-score [3] and MIM (mutual information measure) [4]. The association rules and TF-IDF are based on term co-occurrence frequencies, while Z-score and MIM are based on term co-occurrence probabilities [5]. The characteristics of disaster-related-information change or shift in accordance with each disaster management

Corresponding author: Muneyoshi Numada, Ph. D, research field: disaster management. E-mail: numa@iis.u-tokyo.ac.jp.

cycle phase, which are namely damage mitigation, preparedness, prediction and early warning, damage assessment, emergency disaster response, recovery, and reconstruction/restoration.

When handling this kind of information with characteristics that depend on time-changing, it is necessary to make analysis within a certain time span. Therefore, we propose a dynamic analysis technique of literature with considerations on time series to offer proper and appropriate responses. This paper shows the overview of proposed techniques. News from the newspaper of Fukushima Minpo has been used for its verification. The proposed technique is a powerful tool to effectively analyze the huge amount of digital data, thereby responding to the upcoming society with growing volume of information.

2. Running Spectrum Analysis of Text Data

2.1 Running Spectrum Analysis

Running spectrum analysis is a method widely used in the seismic ground motion analysis for understanding the wave characteristics in time and frequency domain. It is an approach that shifts a time interval of analysis points to conduct analysis within a certain time frame. In our research, the target is further expanded to the literature field. It can be seen in Fig. 1 that moving-average method which is widely used to smooth short-term data fluctuations in time series is applied for dynamic analysis. The time interval B is defined as the calculating range for smoothing the data fluctuations.

2.2 Flow of Text Data Running Spectrum Analysis

Fig. 2 shows the flowchart diagram of running spectrum analysis on text data proposed in this research.

Firstly, Japanese Kanji letters, Katakana letters, numbers and alphabets are extracted from the documents separately as keywords. For this purpose, we have developed an EKP (extract-keyword-program). The EKP can extract each keyword individually and accurately. For example, “hinan” (“evacuation” in English) and “hinansya” (“evacuee” in English) are identified as different keywords within the same document. The EKP can also count the frequency of appearance within one certain day or all the days during the specified period. Users can freely reset the period depending on purposes.

Secondly, keywords are reviewed and analyzed. The weights of all extracted keywords are calculated respectively. Suggested algorithms for keyword analysis are: clustering, TF-IDF, LSI (latent semantic indexing), and co-occurrence. Our proposed system can choose the most suitable weighing approach according to the purposes and requirements of each user. In this paper, we have used TF-IDF in the time span B. TF-IDF is a statistical measurement method to evaluate the importance degree of a specified keyword in a document among a collection of numerous documents. The importance level is determined by the frequency and distribution within the collection of all documents [5].

To apply TF-IDF for the running spectrum analysis, TF-IDF value is calculated as:

$$TF \cdot IDF\,(t, j) = TF\,(t, j) \times IDF\,(t, j) \tag{1}$$

Where,

$$TF\,(t, j) = \frac{Kj(t)}{K(t)} \tag{2}$$

$$IDF\,(t, j) = \log \frac{T(t)}{Tj(t)} \tag{3}$$

where $Kj(t)$ is number of occurrence of keyword (j), $K(t)$ is total number of occurrence keywords in the time interval B, $Tj(t)$ is number of literatures which includes keyword (j) and $T(t)$ is total number of literatures in the time interval B.

Thirdly, after the evaluation of the importance of each keyword in certain time interval B, all keywords are ranked according to its weights.

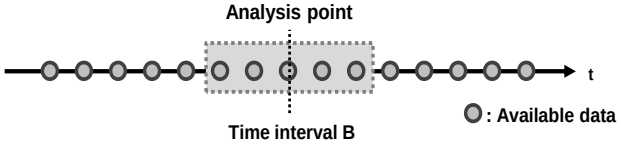

Fig. 1 Time interval B of moving average method.

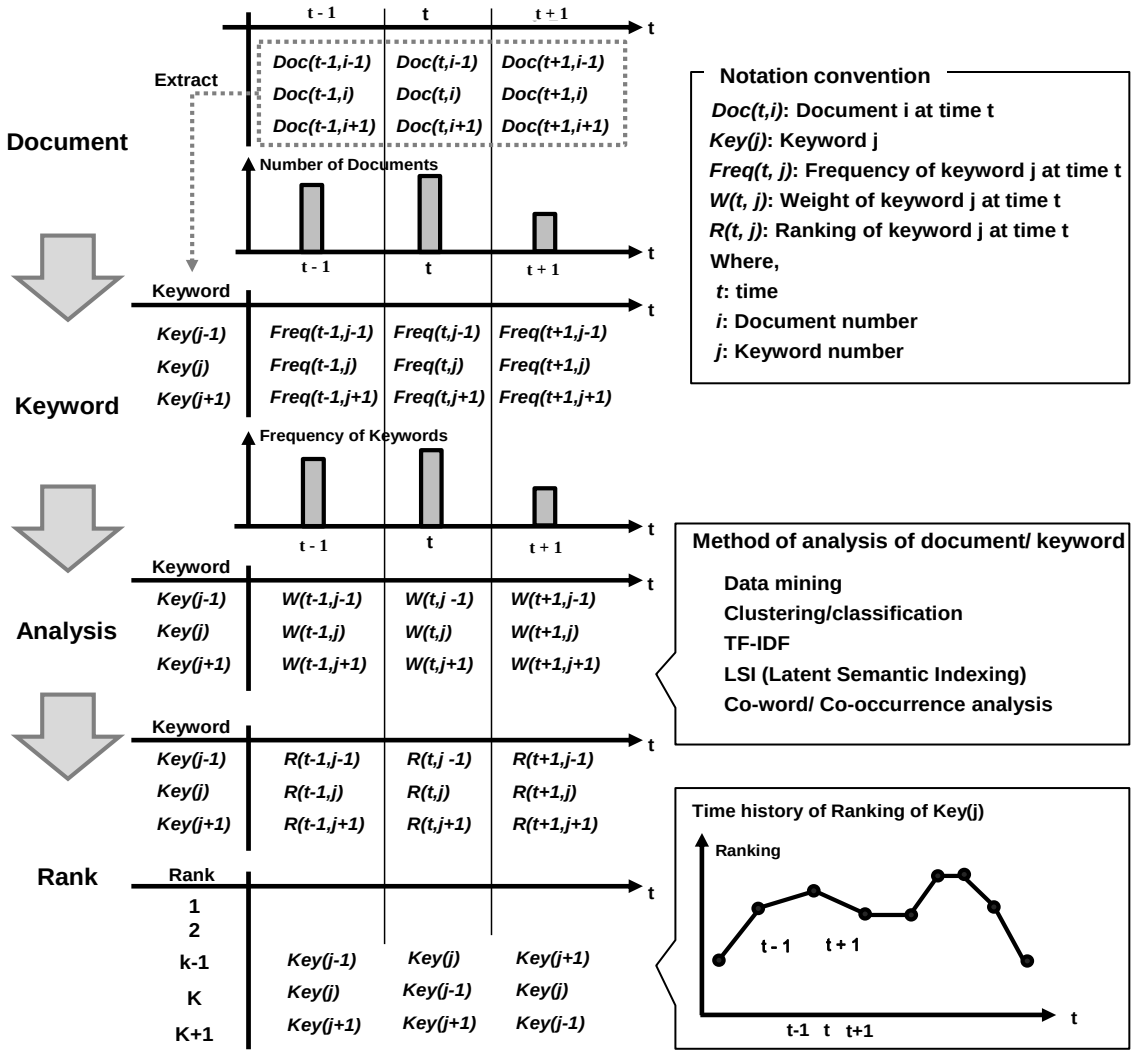

Fig. 2 Flowchart diagram for running spectrum technique.

3. Case Study of Fukushima Minpo Newspaper

3.1 Newspaper data

Fukushima Minpo is a local newspaper with circulation of 250 thousand copies per day and the largest in Fukushima Prefecture [6]. Newspaper repeatedly reports on nuclear power plant accidents as the company office is located near the site.

Some impact analysis of Fukushima nuclear disaster are carried out [7, 8], but a few researches analyze a newspaper to understand the time changing of the disaster.

Fig. 3 shows news report archives from March 2011 to May 2012, analyzing articles by the running spectrum approach described above.

Fig. 3 includes the reports about not only nuclear plant accidents but also earthquake, tsunami, and damages to analyze all impacts of this disaster.

3.2 Extracting Keywords

Fig. 4 shows the number of keyword items and its frequency. Total of 67,881 different keywords have been extracted. For example, frequency is shown as “1” in 44,022 items (64.85% of the total), indicating that the keyword appears only one time. Most newspaper articles report the name, gender and age of those dead or injured, therefore the number of keywords with only one-time appearance equals the number of items.

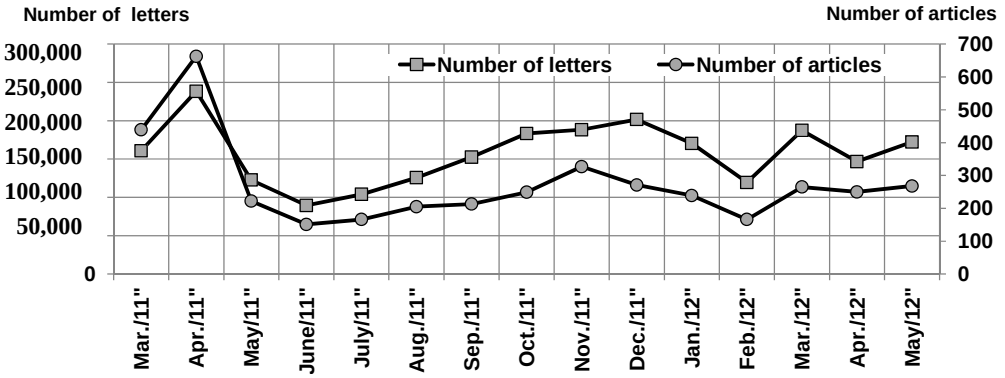

Fig. 3 Archives of Fukushima Minpo newspaper.

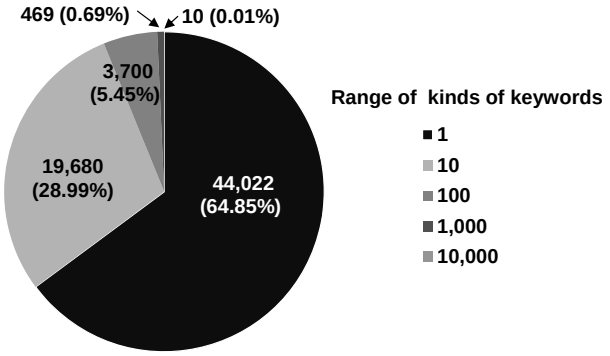

Fig. 4 The number of keyword items and its appearance within a certain range.

Fig. 5 represents keywords with high frequency. “Refuge” is listed as the most frequently used keyword with 1,696 appearances, followed by “residents” with 1,614 times over the period from March 2011 to May 2012. Because both tsunami and nuclear plant accidents induced the emergency evacuation and long-term evacuation to the people, refuge and residents are frequently used.

Keywords related to nuclear power accidents such as “decontamination”, “nuclear power plant accident”, “influence”, “radioactive material”, “children”, “dose of radiation” etc., are ranked high. In this study, one-letter words have been omitted because the keyword often has no meaning in itself and therefore should be interpreted within idioms, phrases and contexts.

3.3 Results of Running Spectrum Analysis

All keywords are given the rank respectively according to the weighting algorithm on daily or monthly level by proposed method. We get to understanding which keywords received attention at the time and tracing down the hottest keywords changing with the circumstances of the moment.

(1) Time-chart of the top ranked keywords: Table 1 shows the time chart of the top three ranked keywords having top ranking in a day in March 2011 as a sample period for B = 3, 7 and 31 days respectively due to space limit of paper.

Taking a look at the B = 3 cases, frequently used keywords in this emergency period immediately after the quake include “tsunami”, “evacuation”, “disaster victim” and “debris”; “Blanket” was another important word since the earthquake occurred during the winter season and blankets were strongly required by the evacuees.

On March 19th, due to worries about the spread of radiation from the nuclear power plant accident, the word “pregnant” was seen for the first time. On March 30th, “temporary home return” was ranked top. This was when the evacuees who had to leave their hometown for fear of radiation and were allowed to pay a brief visit home just to bring their valuables. The B = 7 case, which is similar to the B = 3 case, covers the time when the earthquake hit. Keywords described as emergency terms such as “tsunami”, “evacuation” and “debris” are seen. On March 16th and 17th, “pregnant” was ranked top indicating the serious concerns of radiation by pregnant women as in the B = 7 case. As for B = 31, “evacuation” and “refuge” were the most

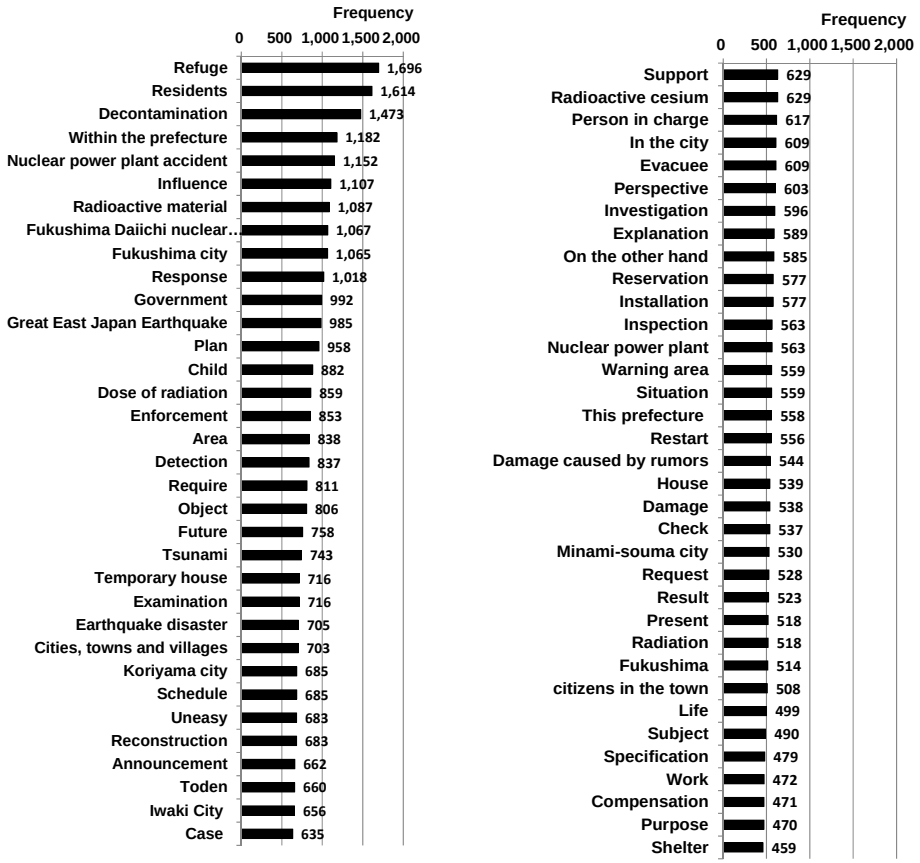

Fig. 5 List of Keywords and their appearance frequency (high frequency part).

used keywords for some days during emergency period. From March 22nd, “election” was ranked high because the nationwide local elections in April were also another issue of attention.

(2) Effect of different time interval B: Comparing the short and long time intervals in terms of “B” , top ranked keywords change day by day in B = 3 (in which the target time interval days are shorter). On the other hand, some specific keywords, such as “evacuation”, “refugee”, “acceptance” and “election”, tend to be ranked higher in the longer time intervals. Therefore, because the time interval B becomes longer, the analysis data is used from wide range period along with the smoothing effect.

The characteristics of the duration effect of time interval B can be explained by how many kinds of keywords were ranked No. 1 at least once as shown in Fig. 6. When observing different time intervals B = 3, 7 and 31 days, fewer keywords have been ranked in the longer time intervals of B. For example, the B = 31 case shows only 42 kinds of keywords ranked No. 1 while the B = 3 case shows as many as 248.

(3) Keywords ranked No. 1: Fig. 7 shows the keywords which were ranked No. 1, and how many times the keyword has reached the No. 1 position. The most frequently ranked as No. 1 include: “decontamination” with 15 times for B = 3 days, “sludge” with 22 times for B = 7 days and “planting” with 36 times for B = 31 days. From this result, we see that specific keywords were constantly listed high for the longer B due to the effect of soothing.

Table 2 shows the time-history of keywords that remained No. 1 for a month. By reviewing this table, the timeline of events are observed. Unfortunately, only the top three are shown in this table due to the limitation of paper space even though many keywords remained in the No. 1 position for a month. Focusing on the B = 31 case, keywords of the months in

Table 1 Time chart of ranking of keywords.

		B = 3			B = 7			B = 31		
		1	2	3	1	2	3	1	2	3
2011/3/11	Keyword	Fukushima city	Tsunami	Center	Tsunami	Evacuation	Disaster victim	Evacuation	Refuge	Response
	TF-IDF	0.015884	0.015884	0.015884	0.018549	0.017122	0.014268	0.011379	0.008302	0.007007
2011/3/12	Keyword	Tsunami	Center	Evacuation	Koriyama city	Disaster victim	Evacuation	Evacuation	Refuge	Response
	TF-IDF	0.015694	0.015694	0.013079	0.012868	0.012433	0.010568	0.010424	0.007525	0.006362
2011/3/13	Keyword	Center	Generating	Offer	Disaster victim	Koriyama city	Evacuation	Evacuation	Refuge	Acceptance
	TF-IDF	0.007838	0.006532	0.006532	0.010186	0.007478	0.007099	0.009608	0.006706	0.005774
2011/3/14	Keyword	Koriyama city	Disaster victim	Suffering a calamity	Disaster victim	Evacuation	Koriyama city	Evacuation	Refuge	Acceptance
	TF-IDF	0.013906	0.008126	0.005794	0.004954	0.004817	0.004578	0.008486	0.005925	0.005415
2011/3/15	Keyword	Koriyama city	Debris	Business	Debris	Acceptance	Activity	Evacuation	Refuge	Acceptance
	TF-IDF	0.004075	0.003943	0.003943	0.003477	0.003367	0.003134	0.007612	0.005316	0.005158
2011/3/16	Keyword	Business	Work	Part	Pregnant	Debris	Niigata prefecture	Evacuation	Acceptance	Refuge
	TF-IDF	0.003505	0.002804	0.002804	0.004234	0.003024	0.003024	0.006876	0.004736	0.004668
2011/3/17	Keyword	Directions	Woman	Blanket	Pregnant	Numerical value	Detection	Evacuation	NPPA	Acceptance
	TF-IDF	0.002985	0.002985	0.002985	0.003366	0.002512	0.002476	0.005918	0.004135	0.004135
2011/3/18	Keyword	Pregnant	Citizen	Niigata prefecture	Last spring	Detection	Citizen	Evacuation	Acceptance	NPPA
	TF-IDF	0.004228	0.003020	0.003020	0.002930	0.002916	0.002287	0.005239	0.003820	0.003747
2011/3/19	Keyword	Detection	Pregnant	Postponement	Last spring	Citizen	Detection	Evacuation	Acceptance	NPPA
	TF-IDF	0.003803	0.003803	0.003260	0.002767	0.002754	0.002046	0.005153	0.003757	0.003433
2011/3/20	Keyword	Last spring	Goods	Water supply	Citizen	Restart	Holding	Evacuation	Acceptance	NPPA
	TF-IDF	0.002857	0.002711	0.002449	0.002561	0.002292	0.002167	0.004497	0.003283	0.003125
2011/3/21	Keyword	Student	Successful applicant	Citizen	Citizen	Postponement	Holding	Evacuation	NPPA	Acceptance
	TF-IDF	0.004139	0.003726	0.003312	0.002103	0.002103	0.001896	0.003873	0.002961	0.002885
2011/3/22	Keyword	Difficulty	Aizuwakamatsu	Holding	Holding	Last spring	Postponement	Evacuation	Election	NPPA
	TF-IDF	0.002421	0.002421	0.002118	0.001622	0.001622	0.001523	0.003244	0.002655	0.002600
2011/3/23	Keyword	Postponement	Holding	Life in refuge	Student	Holding	Last spring	Evacuation	Election	Acceptance
	TF-IDF	0.001976	0.001874	0.001606	0.001690	0.001598	0.001598	0.003221	0.002636	0.002519

(Table 1 continued)

		B = 3			B = 7			B = 31		
		1	2	3	1	2	3	1	2	3
2011/3/24	Keyword	Holding	Large scale disaster	Life in refuge	Student	Holding	Last spring	Evacuation	Election	Acceptance
	TF-IDF	0.001555	0.001333	0.001333	0.001740	0.001646	0.001646	0.003200	0.002619	0.002503
2011/3/25	Keyword	Restoration	Tokyo metropolitan	Large scale disaster	Student	Holding	Election	Evacuation	Election	Acceptance
	TF-IDF	0.001899	0.001625	0.001625	0.001907	0.001804	0.001704	0.002723	0.002609	0.002493
2011/3/26	Keyword	Attendance	Tomioka	Tokyo metropolitan	Election	Reservation	Holding	Election	Acceptance	Detection
	TF-IDF	0.003176	0.002117	0.002117	0.002433	0.001899	0.001778	0.002573	0.002458	0.002356
2011/3/27	Keyword	Radioactive material	Tomioka	Sea water	Election	Reservation	Acceptance	Election	Acceptance	Detection
	TF-IDF	0.004758	0.003569	0.003569	0.002681	0.002053	0.001967	0.002539	0.002426	0.002325
2011/3/28	Keyword	Acceptance	Investigation	Residents	Attendance	Acceptance	Radioactive material	Election	Acceptance	Detection
	TF-IDF	0.006747	0.003680	0.003169	0.002556	0.002283	0.001886	0.002553	0.002440	0.002338
2011/3/29	Keyword	Reservation	Fukushima	Accident	Hotel	Victim	Japanese style hotel	Election	Acceptance	Postponement
	TF-IDF	0.002896	0.002896	0.002779	0.004085	0.003682	0.003156	0.002503	0.002392	0.002222
2011/3/30	Keyword	Temporary back-home	Inside Shelter	Accident	Victim	Hotel	Japanese style hotel	Election	Postponement	Acceptance
	TF-IDF	0.002826	0.002826	0.002711	0.004175	0.003578	0.003227	0.002442	0.002418	0.002334
2011/3/31	Keyword	Victim	Hotel	Restart	Victim	Hotel	Japanese style hotel	Postponement	Election	Acceptance
	TF-IDF	0.005895	0.005359	0.003751	0.004514	0.003870	0.003490	0.002508	0.002360	0.002214

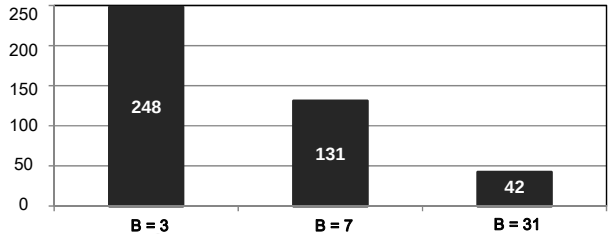

Fig. 6 Comparison of items of keywords ranked No. 1.

chronological order at the top are observed. "Evacuation" was the most important keyword in March 2011, followed by "disaster victim" (April), "temporary payment" (May), "sludge" (June), "specification" (July), "compensation" (August), "two points" (September), "forest for disaster mitigation" (October), "compost" (November), "rice" (December). Moving onto 2012, "rice" (January), "planting" (February), "center" (March) and "detection" (April and May). By following the top keywords, the outline and the stream of this complex disaster despite them intertwined problems and difficulties.

(4) Trend of each keyword: this system also analyzes the trend of specific keywords that a system user might take interest. For example, focusing on the top ranked keyword "planting" in Fig. 7c, the trend of its ranking is presented as seen in Fig. 8. The nuclear power plant accidents have given the impact to the planting of rice in the rice fields. The case B = 3 shows high discontinuity, while continuity is clearly shown in B = 31 due to the soothing effects. From around October 2011, the problems related to "planting" constantly emerge as shown in the B = 31 case.

4. Conclusions

We have proposed the running spectrum system for analyzing text data in the advanced society having digital data. The news reported by Fukushima Minpo newspaper is used for the verification of the technique and analyze of the impact of nuclear power plant accidents in Japan. The result shows the dynamic characteristics of the nuclear power plant accidents.

As time goes on, more digital information on natural disasters will become available. Then, the proposed technique serves efficiently and effectively to analyze huge amount of digital information, thus providing appropriate understanding of the impact of the nuclear power plant accidents.

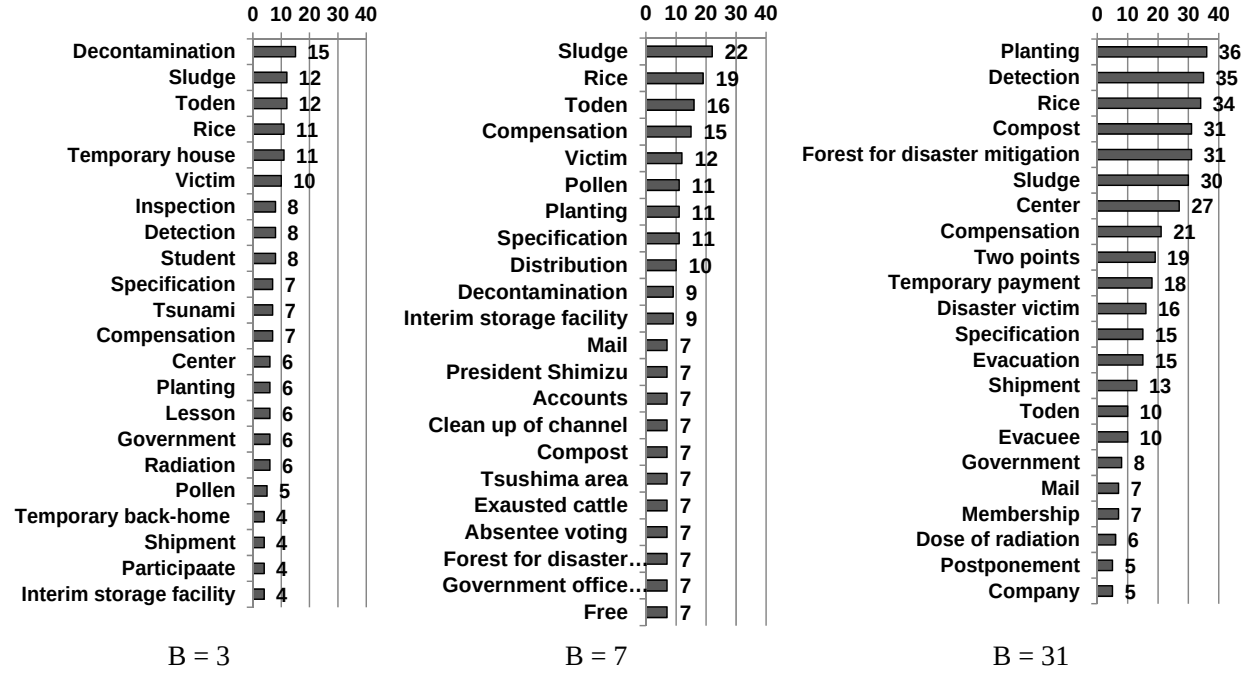

Fig. 7 Keywords ranked as No. 1 and their frequency.

Table 2 Time-history of keywords that ranked as No. 1 with their frequency.

		B = 3		B = 7		B = 31	
Year	Month	Keyword	Number of No. 1	Keyword	Number of No. 1	Keyword	Number of No. 1
2011	3	Center	3	Last spring	3	Evacuation	15
		Pregnant	2	Student	3	Election	5
		Tsunami	2	Pregnant	2	Postponement	1
	4	Student	3	President Shimizu	7	Disaster victim	12
		Move in	3	Danger	4	Evacuee	5
		Vegetables	2	Move in	4	Request	5
	5	Japan Agriculture	3	Temporary payment	5	Temporary payment	18
		Temporary back-home	3	Toden	5	Government	8
		Temporary payment	3	Japan agriculture	4	Toden	5
	6	Sludge	3	Sludge	7	Sludge	19
		Temporary house	3	Clean up of channel	7	Company	5
		Clean up of channel	3	Measurement	5	Temporary back-home	2
	7	Specification	4	Specification	9	Specification	15
		Participate	3	Shipment	4	Shipment	13
		Ratio of adjustment	3	Beef cattle	4	Farmhouse	3
	8	Student	3	Sludge	3	Compensation	11
		Specification	3	Compensation	3	Evacuee	5
		Pension for survivor	2	Announcement	3	Refuge	5
	9	Reconciliation	3	Two points	6	Two points	16
		Prime minister Noda	3	Compensation	5	Compensation	6
		Mediation	3	Guardian	4	Temporary place	4
	10	Rice	3	Rice	7	Forest for disaster mitigation	23
		Landslide	3	Forest for disaster mitigation	7	Two points	3
		Forest for disaster mitigation	3	Interim storage facility	4	Compensation	3
	11	Wild boar	3	Compost	7	Compost	22
		Compost	3	Absentee voting	7	Forest for disaster mitigation	8
		Absentee voting	3	Government office building	7	-	-
	12	Golf course	3	Tsushima area	7	Rice	13
		Sludge	3	Bark	6	Compost	9
		Recycle	3	Membership	6	Membership	7
2012	1	Decontamination	6	Toden	7	Rice	21
		Hanami Yama mountain	3	Rice	4	Planting	5
		Government	3	Decontamination	4	Donation	2
	2	Rice	4	Victim	7	Planting	29
		Subsidy for reconstruction	3	Pollen	6	-	-
		Planting	3	Subsidy for reconstruction	5	-	-
	3	Free	3	Accounts	7	Center	27
		Area where is difficult to return	3	Distribution	7	Planting	2
		Distribution	3	Free	7	Iodine	1
	4	Exhausted cattle	3	Mail	7	Detection	12
		Mail	3	Exhausted cattle	7	Mail	7
		Personnel	3	Pollen	4	Exhausted cattle	5
	5	Cherry blossom	3	Sludge	7	Detection	23
		Sludge	3	Yanagisawa	7	Sludge	8
		Subsidy	3	Buying credit	4	-	-

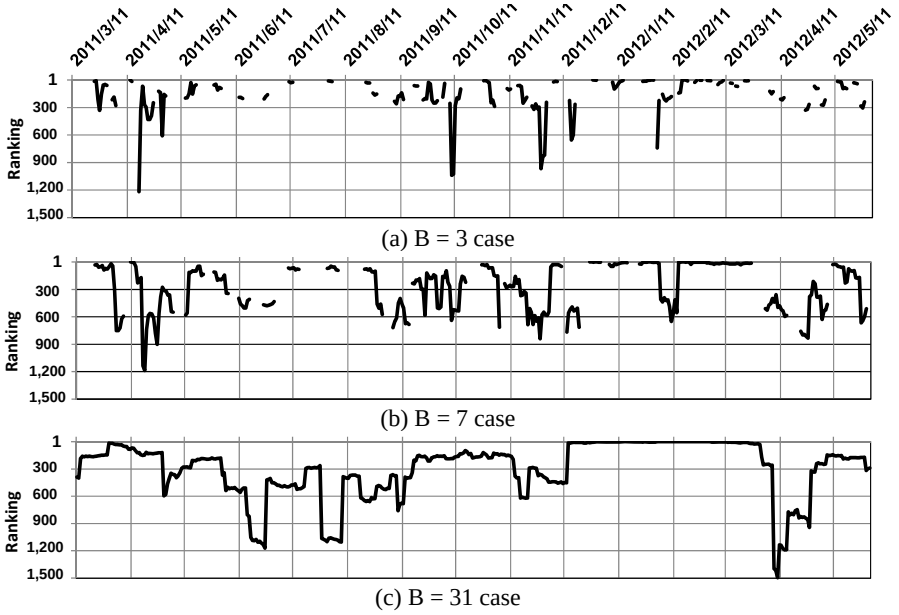

(a) B = 3 case

(b) B = 7 case

(c) B = 31 case

Fig. 8 Time history of ranking of "Planting".

References

[1] R.K. Lindsay, M.D. Gordon, Literature based discovery by lexical statistics, Journal of the American Society for Information Science and Technology 49 (1999) 674-685.

[2] P. Srinivasan, Generating hypotheses from MEDLINE, Journal of the American Society for Information Science and Technology 55 (2004) 396-413.

[3] M. Yetisgen-Yildiz, W. Pratt, Using statistical and knowledge-based approaches for literature based discovery, Journal of Biomedical Informatics 39 (2006) 600-611.

[4] J.D. Wren, Extending the mutual information measure to rank inferred literature relationship, BMC Bioinformatics 5 (2004) 145.

[5] Y.Y. Meliha, P. Wanda, A new evaluation methodology for literature-based discovery systems, Journal of Biomedical Informatics 42 (4) (2009) 633-643.

[6] Tohoku earthquake reports, Fukushima-Minpo Co., http://www.fukushimaminponews.com/ about.html (accessed Jun 28, 2012).

[7] S.K. Yeo, M.A. Cacciatore, D. Brossard, D.A. Scheufele, K. Runge, L.Y. Su, J. Kim, M. Xenos, E.A. Corley, Partisan amplification of risk: American perceptions of nuclear energy risk in the wake of the Fukushima Daiichi disaster, Energy Policy, 67 (2014) 727-736.

[8] H.A. Hassard, J.K.Y. Swee, M. Ghanem, H. Unesaki, Assessing the impact of the fukushima nuclear disaster on policy dynamics and the public sphere, Procedia Environmental Sciences, 17 (2013) 566-575.

Journal of Geological Resource and Engineering 1 (2013) 11-24

Stability Analysis of Piles Subjected to Lateral Load in Static and Seismic Conditions

José Medina, Nicolás Sau, Qutberto Acuña and Jesús Quintana

Department of Civil Engineer and Mining, University of Sonora, Hermosillo, Sonora 83000, México

Abstract: It is disclosed a method for the stability analysis of foundation piles and piers subjected to lateral loading, both static and seismic conditions. The stability analysis for stratified soil is based upon the models of foundation soil-structure interaction and the Rankine´s theory of earth passive pressure. In addition, its application is simpler and it can be solved using a spreadsheet. The procedure described in this work can be used in homogeneous soils as in stratified soils, considers the horizontal drag forces exerted by the soil mass against the foundation during an earthquake, can be used easily in the four pile and piers boundary cases, and considers the pore pressure generated in a fine saturated soil during an earthquake or during a rapid application of the horizontal load. The solution of two examples are shown, one in static condition and one in seismic condition, detailing the procedure step by step.

Key words: Ultimate lateral resistance of piles and piers, lateral bearing capacity of piles and piers, piles, piers, soil-structure interaction in piles and piers.

1. Introduction

In a deep foundation subjected to lateral loading, it should be checked that the supporting soil is able to withstand the contact pressure induced by the foundation to the soil mass. This article presents a method for the analysis of stability of foundation piles and piers subjected to lateral loading, both in static and seismic conditions. The stability analysis for stratified soil is based upon the models of foundation soil-structure interaction proposed by Medina [1-4] as well as in the Rankine's theory of earth passive pressure [5]. This methodology has the advantage that it considers the excessive hydrostatic pressure that is generated in a fine saturated soil during a seismic event. In addition, its application is simpler and it can be solved using a spreadsheet.

2. Ultimate Lateral Resistance

According to Rankine theory shown in Terzaghi [5], the passive horizontal stress is determined by Eqs. (1) and (2):

$$\sigma'_h = N\varphi\ \sigma'_z + 2\,C\sqrt{N\varphi} \quad (1)$$

$$N\varphi = \tan^2(45° + \varphi/2) \quad (2)$$

where, σ'_h is the horizontal effective stress, σ'_z is the vertical effective stress, C is the material cohesion, and φ is the soil internal friction angle.

For a pile subjected to a lateral force P and a moment M (Fig. 1), the ultimate lateral resistance of a layered soil is determined by Eq. (3):

$$Q_{LU} = \sum_{0}^{ZP} \left[N\varphi_i\ \sigma'_{ZMi} + 2\,C_i\sqrt{N\varphi_i} \right] H_i\ D \quad (3)$$

where, Q_{LU} is the ultimate lateral resistance of the pile, $N\varphi_i$ is the i-th layer passive coefficient, σ'_{ZMi} is the vertical effective average stress at the center of the i-th layer. C_i is the cohesion and H_i is the thickness of the i-th layer, D is the diameter of the pile or pier. ZP is the depth of the passive region (Fig. 1).

The factor of safety against the foundation passive failure is determined by Eq. (4):

$$Fs = \frac{Q_{LU}}{\sum_{0}^{ZP} R_i} \geq 2.5 \quad (4)$$

where, $\sum_{0}^{ZP} R_i$ is the sum of the soil-foundation contact reactions to the depth ZP.

Corresponding author: José Medina, M. Eng./professor, research fields: foundation and geotechnical engineering. E-mail: jose.medina@prolas.com.mx.

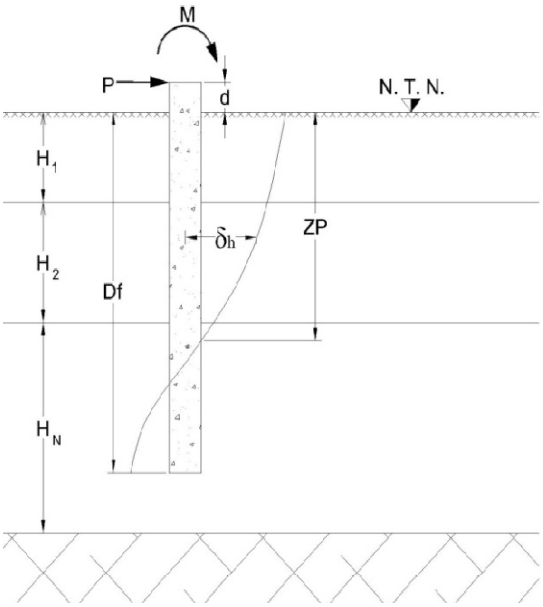

Fig. 1 Pile placed upon a layered soil.

To ensure that the foundation is stable to lateral load, it should be checked that the lateral displacement of the foundation complies with the stipulated maximum value in the project. In addition, it should be verified that it complies with the maximum allowable slope of the superstructure.

In pile groups, it should also be considered the stability of the group against lateral load, which it may be carried out with the same procedure described herein, but considering the rotation of the pile group as a rigid body, so that the soil-structure interaction analysis is considerably simplified.

3. Soil-Foundation Structure Interaction

The passive zone depth *ZP* and the lateral contact soil-foundation reactions can be determined by the methods of soil-structure interaction for piles and piers, distinguishing the following boundary cases (Fig. 2):

Case I: It occurs when a pile or an isolated foundation pier exists and the foundation tip does not penetrate the resistant stratum. In this condition, it is considered that the foundation is free to rotate on both ends. The solution of this case is available at Medina [1].

Case II: When the pile or pier is embedded in the head and it can rotate freely on the base. The pile is cast integrally with the foundation structure. The head of the pile may or may not have a restricted rotation due to the deformation of the material that surrounds the top of the pile. The solution of this case can be found in Medina [4].

Case III: When the pile or pier can freely rotate at its upper end and is fixed at its base. The foundation tip penetrates the resistant layer. The base of the foundation can or cannot have a restricted rotation, due to deformation of the material surrounding the tip of the foundation. The solution of this case can be found

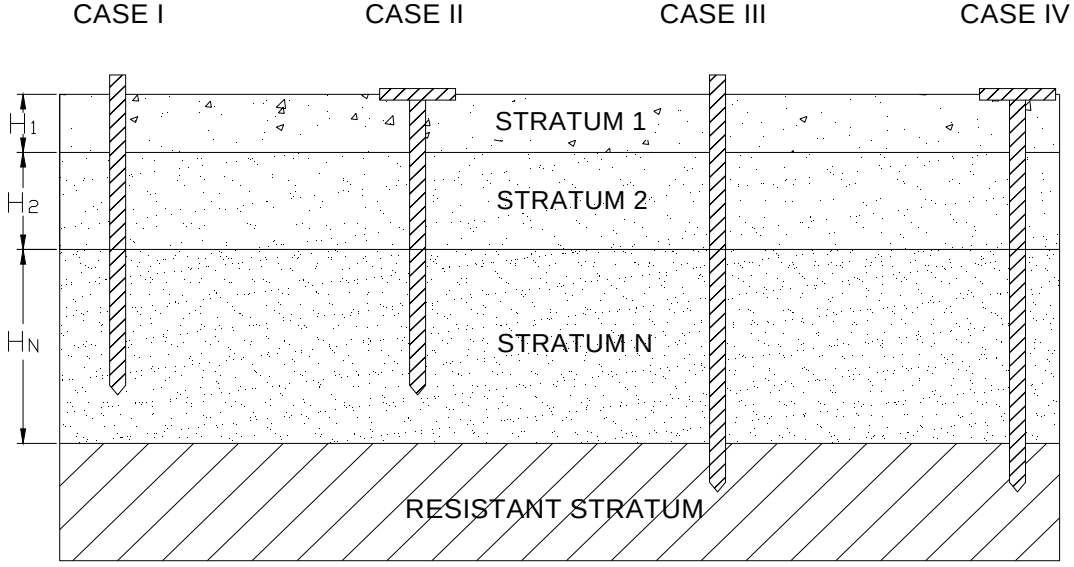

Fig. 2 Different boundary conditions cases in piles and piers.

in Medina [2].

Case IV: In this case, the foundation is fixed at both ends. The pile or pier is cast integrally with the foundation structure and the tip penetrates the resistant stratum. Both the head and the tip of the foundation may or may not have a restricted rotation due to deformation of the material surrounding the ends of the foundation. The solution can be found in Medina [3].

4. Example of a Pile in Static Condition

4.1 Statement of the Problem

The stability analysis for a pier with the following features was developed:

Pier foundation using Case I, EI = 4.8168E+06 kN/m^2 (E is the Young's modulus of reinforced concrete and I is the moment of inertia of the cross section of the pier). P = 230 kN; M = 180 kN-m; d = 0.50 m; D = 1.40 m; and Df = 6.00 m.

Considering the subsoil characteristics shown in Table 1, with a Poisson's ratio of subsoil, ν = 0.3 and assuming that it is a soil deposit in arid zones, where there is no groundwater level in the subsoil foundation. It is considered that there is a permitted maximum lateral displacement of 20 mm and an inclination with respect to the vertical of no more than 1°.

4.2 Solution

4.2.1 Soil-Foundation Structure Interaction

The soil-foundation structure interaction was conducted according to Medina [1]. The methodology consists on dividing the foundation pile in dowels *a*, 1, 2,.., n and *b* and the soil mass in the sections A, B, C, …, and F (Fig. 3). Zeevaert [6], with the application of the flexibility method to the soil mass, obtains the horizontal displacements matrix equation (5).

$$\begin{bmatrix} \delta_{aa} & \delta_{a1} & \delta_{a2} \ \dots \ \delta_{an} & \delta_{ab} \\ \delta_{1a} & \delta_{11} & \delta_{12} \ \dots \ \delta_{1n} & \delta_{1b} \\ \delta_{2a} & \delta_{21} & \delta_{22} \ \dots \ \delta_{2n} & \delta_{2b} \\ & & \vdots & \\ \delta_{na} & \delta_{n1} & \delta_{n2} \ \dots \ \delta_{nn} & \delta_{nb} \\ \delta_{ba} & \delta_{b1} & \delta_{b2} \ \dots \ \delta_{bn} & \delta_{bb} \end{bmatrix} \begin{vmatrix} R_a \\ R_1 \\ R_2 \\ \vdots \\ R_n \\ R_b \end{vmatrix} = \begin{vmatrix} \delta_a \\ \delta_1 \\ \delta_2 \\ \vdots \\ \delta_n \\ \delta_b \end{vmatrix} \quad (5)$$

R_i is the horizontal reaction in the dowel i.

δ_i is the lateral displacement in the dowel i.

δ_{ji} is the lateral displacement in the center of slice j, produced by a unitary load acting upon slice i, R_i is the reaction in the dowel i and δi is the lateral displacement of the dowel i.

δ_{ji} is obtained with equation (6):

$$\delta_{ji} = \left[\ I_{ji}^{A}\alpha_i^{A} + I_{ji}^{B}\alpha_i^{B} + \ldots + I_{ji}^{F}\alpha_i^{F} \ \right] / a_i \quad (6)$$

$$\alpha_i^{N} = M_{hi}^{N}\Delta x \quad (7)$$

M_{hi}^{N} is the soil deformation modulus; Δx is the width of the section of soil; a_i is the area of slice i.

I_{ji}^{N} is the influence upon the center of slice j, produced by a unit load acting upon slice i and upon the center of section N. The influence values are obtained with the proposed equation by Zeevaert [6] and improved by Medina [7].

Table 1 Foundation subsoil characteristics corresponding to Example 4.

	Depth (m)	Description	*Mh*	γ_m	*C*	φ
Ground Level	0.00		(m^2/kN):	(kN/m^3)	(kN/m^2)	(^{O})
	1.50	Clayey coarse sand	1.9750E-04	18.142	15.298	34
	3.50	Clayey coarse sand	1.7375E-04	18.338	18.437	34
	7.00	Clayey coarse sand	1.5125E-04	19.123	19.613	35
	10.00	Rock layer		22.555		

Mh is the soil deformation modulus, γ_m is the unit weight, *C* is the cohesion and φ is the internal friction angle.

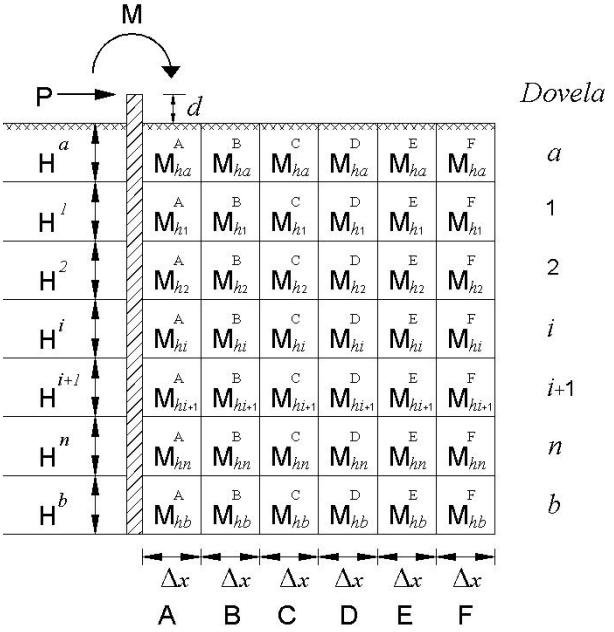

Fig. 3 Foundation and soil mass discretization.

With the application of the flexibility method to the foundation structure, (Fig. 4), Medina [1], the flexibility matrix equation (8) is obtained.

$$\begin{bmatrix} d_{11} & d_{12} \dots d_{1n} \\ d_{21} & d_{22} \dots d_{2n} \\ & \vdots \\ d_{n1} & d_{n2} \dots d_{nn} \end{bmatrix} \begin{vmatrix} R_1 \\ R_2 \\ \vdots \\ R_n \end{vmatrix} = \begin{vmatrix} \Delta_1 \\ \Delta_2 \\ \vdots \\ \Delta_n \end{vmatrix} + \begin{vmatrix} \delta_1^A \\ \delta_2^A \\ \vdots \\ \delta_n^A \end{vmatrix} - \begin{vmatrix} \delta_1 \\ \delta_2 \\ \vdots \\ \delta_n \end{vmatrix} \qquad (8)$$

d_{ji} is the deflection in j due to a unitary load applied at i (condition $R_i = 1$); Δ_i is the deflection at point i for condition $R_i = 0$ and δ_i^A is the displacement at point i, by deformation of the supports *a* y *b*, considered the pier as a rigid body.

Note that with matrix Equations (5) and (8) there are 2n+2 equations with 2n+4 unknowns, therefore the two remaining equations are obtained from the sum of moments at supports *a* and *b* with which the system of equations can be resolved, obtaining the equations (9) to (11).

By the sum of moments at the supports *a* and *b*:

$$R_a = R_{a0} - (\psi_1 R_1 + \psi_2 R_2 + \dots + \psi_n R_n) \qquad (12)$$

$$R_b = R_{b0} - (\xi_1 R_1 + \xi_2 R_2 + \dots + \xi_n R_n) \qquad (13)$$

$$\psi_i = y'_i / L'; \qquad \xi_i = z'_i / L' \qquad (14)$$

where, y'_i, z'_i are the position coordinates of point i and L′ is the distance -center to center- between slices *a* and *b* (Fig. 4).

R_{a0} and R_{b0} are the reactions at the supports *a* and *b*, respectively, for condition $R_i = 0$ (Fig. 4).

From equations (5) are obtained: δ_a, δ_1, δ_2, …, δ_n and δ_b.

The problem was solved by a computer program developed in a spreadsheet.

Foundation pier was divided into eight segments: *a*,

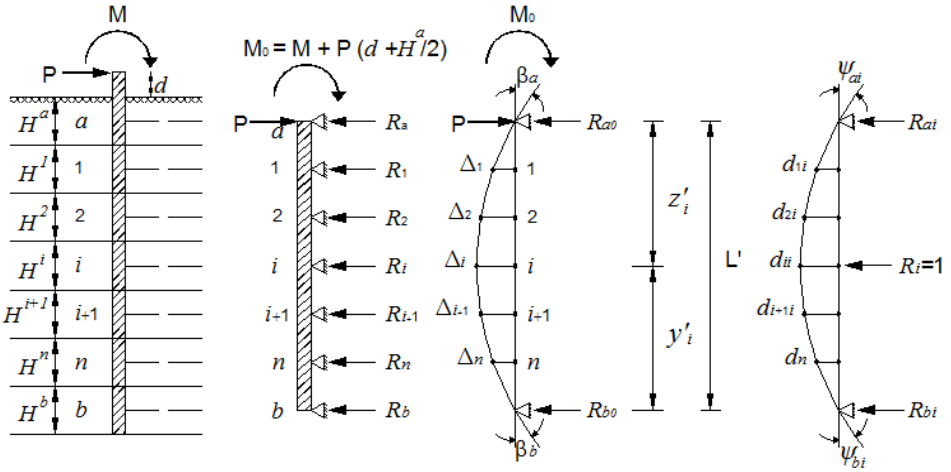

Fig. 4 Application of the flexibilities method: a) real foundation; b) discreteness of foundation; c) condition $R_i = 0$; d) condition $R_i = 1$.

1, 2, 3, 4, 5, 6 and *b*. It was chosen a value of Δx = 2.10 m and six sections in the soil mass: A, B, C, D, E and F. Discretization of the foundation and soil mass are shown in Table 2.

Table 3 shows the unitary lateral displacements matrix $[\delta_{ji}]$.Table 4 shows the matrix $[d_{ji}]$; Table 5 shows the matrix $[m_{ji}]$; Table 6 shows the vectors N_i and Δ_i.

Table 2 Soil mass and pier discretization.

Dowel	Thickness (m)	*Zi* (m)	*Mhi* (m^2/kN)
a	0.75	0.375	1.9750E-04
1	0.75	1.125	1.9750E-04
2	0.67	1.833	1.7375E-04
3	0.67	2.500	1.7375E-04
4	0.67	3.167	1.7375E-04
5	0.83	3.917	1.5125E-04
6	0.83	4.750	1.5125E-04
b	0.83	5.583	1.5125E-04

Zi is the depth measured from the ground surface to the center of the dowel *i*, *Mhi* is the soil deformation modulus in the dowel *i*.

Table 3 Unitary lateral displacements matrix, $[\delta_{ji}]$(m/kN).

a	1	2	3	4	5	6	*b*
9.0916E-05	4.5826E-05	2.1267E-05	1.3411E-05	9.4665E-06	6.7703E-06	4.8351E-06	3.5456E-06
4.5826E-05	7.0746E-05	4.1064E-05	1.9291E-05	1.1825E-05	7.9969E-06	5.5424E-06	3.9916E-06
1.8793E-05	3.6291E-05	6.0191E-05	3.6254E-05	1.6414E-05	9.3361E-06	6.0428E-06	4.2088E-06
1.1820E-05	1.7062E-05	3.6254E-05	5.9060E-05	3.5436E-05	1.4749E-05	8.0547E-06	5.2945E-06
8.3368E-06	1.0425E-05	1.6414E-05	3.5436E-05	5.8453E-05	3.1735E-05	1.2379E-05	7.1066E-06
5.1805E-06	6.1172E-06	8.0914E-06	1.2690E-05	2.7309E-05	4.9236E-05	2.4556E-05	9.8723E-06
3.7004E-06	4.2411E-06	5.2494E-06	6.9855E-06	1.0674E-05	2.4556E-05	4.9023E-05	2.4396E-05
2.7138E-06	3.0549E-06	3.6585E-06	4.6000E-06	6.1666E-06	9.8723E-06	2.4396E-05	4.8901E-05

Table 4 Matrix, $[d_{ji}]$(m/kN).

1	2	3	4	5	6
1.4855E-07	2.3359E-07	2.6205E-07	2.4954E-07	1.9753E-07	1.0741E-07
2.3359E-07	3.9737E-07	4.6281E-07	4.4859E-07	3.5882E-07	1.9623E-07
2.6205E-07	4.6281E-07	5.7040E-07	5.7216E-07	4.6665E-07	2.5783E-07
2.4954E-07	4.4859E-07	5.7216E-07	6.0476E-07	5.1174E-07	2.8807E-07
1.9753E-07	3.5882E-07	4.6665E-07	5.1174E-07	4.6295E-07	2.7232E-07
1.0741E-07	1.9623E-07	2.5783E-07	2.8807E-07	2.7232E-07	1.7661E-07

Table 5 Matrix, $[m_{ji}]$(m/kN).

1	2	3	4	5	6
-1.1065E-05	6.2932E-06	9.5147E-06	9.2990E-06	7.2856E-06	2.6421E-06
8.4802E-06	2.1181E-05	2.2043E-05	1.9915E-05	1.5722E-05	7.3866E-06
1.0939E-05	2.1648E-05	2.2541E-05	2.0864E-05	1.7153E-05	8.1568E-06
1.0307E-05	1.9399E-05	2.0677E-05	1.9804E-05	1.6974E-05	7.7585E-06
8.8375E-06	1.6117E-05	1.7831E-05	1.7869E-05	1.6033E-05	6.5776E-06
3.8212E-06	7.8044E-06	8.7980E-06	8.6410E-06	6.5533E-06	-4.6770E-06

$$\left[\begin{bmatrix}\delta_{11} & \delta_{12} & \dots & \delta_{1n}\\ \delta_{21} & \delta_{22} & \dots & \delta_{2n}\\ & \vdots & & \\ \delta_{n1} & \delta_{n2} & \dots & \delta_{nn}\end{bmatrix}+\begin{bmatrix}d_{11} & d_{12} & \dots & d_{1n}\\ d_{21} & d_{22} & \dots & d_{2n}\\ & \vdots & & \\ d_{n1} & d_{n2} & \dots & d_{nn}\end{bmatrix}+\begin{bmatrix}m_{11} & m_{12} & \dots & m_{1n}\\ m_{21} & m_{22} & \dots & m_{2n}\\ & \vdots & & \\ m_{n1} & m_{n2} & \dots & m_{nn}\end{bmatrix}\right]\begin{vmatrix}R_1\\ R_2\\ \vdots\\ R_n\end{vmatrix}=\begin{vmatrix}n_1\\ n_2\\ \vdots\\ n_n\end{vmatrix}+\begin{vmatrix}\Delta_1\\ \Delta_2\\ \vdots\\ \Delta_n\end{vmatrix} \quad (9)$$

where:

$$\begin{bmatrix} m_{11} & m_{12}\ldots & m_{1n} \\ m_{21} & m_{22}\ldots & m_{2n} \\ & \vdots & \\ m_{n1} & m_{n2}\ldots & m_{nn} \end{bmatrix} = \begin{bmatrix} \psi_1 & \xi_1 \\ \psi_2 & \xi_2 \\ & \vdots & \\ \psi_n & \xi_n \end{bmatrix} \begin{bmatrix} \delta_{aa} & \delta_{ab} \\ & \\ \delta_{ba} & \delta_{bb} \end{bmatrix} \begin{bmatrix} \psi_1 & \psi_2\ldots & \psi_n \\ \xi_1 & \xi_2\ \ldots & \xi_n \end{bmatrix} - \begin{bmatrix} \psi_1 & \xi_1 \\ \psi_2 & \xi_2 \\ & \vdots & \\ \psi_n & \xi_n \end{bmatrix} \begin{bmatrix} \delta_{a1} & \delta_{a2}\ldots & \delta_{an} \\ \delta_{b1} & \delta_{b2}\ldots & \delta_{bn} \end{bmatrix} -$$

$$- \begin{bmatrix} \delta_{1a} & \delta_{1b} \\ \delta_{2a} & \delta_{2b} \\ & \vdots & \\ \delta_{na} & \delta_{nb} \end{bmatrix} \begin{bmatrix} \psi_1 & \psi_2\ldots\psi_n \\ \xi_1 & \xi_2\ldots\xi_n \end{bmatrix} - \begin{bmatrix} d_{1b} \\ d_{2b} \\ \vdots \\ d_{nb} \end{bmatrix} \begin{bmatrix} B_1\ B_2\ldots B_n \end{bmatrix} - \begin{bmatrix} (\delta_{1a} - \delta_{1b)} \\ (\delta_{2a} - \delta_{2b}) \\ \vdots \\ (\delta_{na} - \delta_{nb}) \end{bmatrix} \begin{bmatrix} D_1\ D_2\ldots D_n \end{bmatrix} +$$

$$+ \begin{bmatrix} \psi_1 & \xi_1 \\ \psi_2 & \xi_2 \\ & \vdots & \\ \psi_n & \xi_n \end{bmatrix} \begin{bmatrix} (\delta_{aa} - \delta_{ab}) \\ (\delta_{ba} - \delta_{bb}) \end{bmatrix} \begin{bmatrix} D_1\ D_2\ldots D_n \end{bmatrix} \tag{10}$$

$$\begin{vmatrix} n_1 \\ n_2 \\ \vdots \\ n_n \end{vmatrix} = \left[\begin{bmatrix} \psi_1 & \xi_1 \\ \psi_2 & \xi_2 \\ & \vdots & \\ \psi_n & \xi_n \end{bmatrix} \begin{bmatrix} \delta_{aa} & \delta_{ab} \\ & \\ \delta_{ba} & \delta_{bb} \end{bmatrix} - \begin{bmatrix} \delta_{1a} & \delta_{1b} \\ \delta_{2a} & \delta_{2b} \\ & \vdots & \\ \delta_{na} & \delta_{nb} \end{bmatrix} \right] \begin{vmatrix} R_{a0} \\ R_{b0} \end{vmatrix} - \begin{bmatrix} (\delta_{1a} - \delta_{1b}) \\ (\delta_{2a} - \delta_{2b}) \\ \vdots \\ (\delta_{na} - \delta_{nb}) \end{bmatrix} \begin{vmatrix} D_0 \end{vmatrix} -$$

$$- \begin{bmatrix} d_{1b} \\ d_{2b} \\ \vdots \\ d_{nb} \end{bmatrix} \begin{vmatrix} B_0 \end{vmatrix} + \begin{bmatrix} \psi_1 & \xi_1 \\ \psi_2 & \xi_2 \\ & \vdots & \\ \psi_n & \xi_n \end{bmatrix} \begin{bmatrix} (\delta_{aa} - \delta_{ab}) \\ (\delta_{ba} - \delta_{bb}) \end{bmatrix} \begin{vmatrix} D_0 \end{vmatrix} \tag{11}$$

Solving the matrix above are obtained R_1, R_2, R_3, … and R_6. With the equations (12) and (13) are obtained R*a* and R*b*. The lateral displacements are obtaining whit equation (5). The reactions and lateral displacements are shown in Table 7.

Fig. 5 shows the lateral displacement-depth diagram, while Fig. 6 shows the lateral contact pressure-depth diagram.

4.2.2 Ultimate lateral resistance in static condition

In Fig. 5, the depth of the passive zone, ZP is 4.40 m, so the calculation of the ultimate lateral resistance of the pier is considered up to the bottom of the dowel 5, at a depth of 4.33 m.

Table 6 Vectors N_i and Δ_i Reactions R*a*o and R*b*o.

Vector Ni	Vector Δi	
(m)	(m)	
9.3750E-03	8.1867E-05	R*a*o = 303.20 kN
1.3499E-02	1.2408E-04	
1.1844E-02	1.3760E-04	R*b*o = - 73.20 kN
9.1850E-03	1.3029E-04	
6.0153E-03	1.0278E-04	
2.7172E-03	5.5790E-05	

Soil structure interaction matrix equation (EMISE):

(m/kN)						(kN)		(m)
5.9830E-05	4.7591E-05	2.9068E-05	2.1374E-05	1.5480E-05	8.2919E-06	R_1		9.4569E-03
4.5005E-05	8.1769E-05	5.8759E-05	3.6777E-05	2.5417E-05	1.3626E-05	R_2		1.3623E-02
2.8263E-05	5.8364E-05	8.2172E-05	5.6872E-05	3.2369E-05	1.6469E-05	R_3		1.1982E-02
2.0981E-05	3.6262E-05	5.6685E-05	7.8862E-05	4.9220E-05	2.0425E-05	R_4	=	9.3153E-03
1.5152E-05	2.4567E-05	3.0988E-05	4.5690E-05	6.5732E-05	3.1406E-05	R_5		6.1181E-03
8.1698E-06	1.3250E-05	1.6041E-05	1.9603E-05	3.1381E-05	4.4522E-05	R_6		2.7729E-03

Table 7 Reactions and lateral displacements.

Dowel	zi (m)	Ri (kN)	δi (m)
a	0.375	152.321	1.8558E-02
1	1.125	50.946	1.5112E-02
2	1.833	97.132	1.1835E-02
3	2.500	37.006	8.7400E-03
4	3.167	27.646	5.6412E-03
5	3.917	13.682	2.1533E-03
6	4.750	-11.123	-1.7232E-03
b	5.583	-137.611	-5.6005E-03

Ri is the reaction of soil-foundation contact in the dowel i and δi is the lateral displacement of the pier at the center of dowel i.

With equation (3), it is obtained the ultimate lateral resistance of the pier shown in Table 8.

4.2.3 Factor of Safety against the Foundation Passive Failure

$$Fs = \frac{1\,264.51}{378.73} = 3.34$$

4.2.4 Discussion of Results

The safety factor obtained against the foundation passive failure is satisfactory.

It was obtained a maximum lateral displacement of 18.6 mm for this foundation, so that for a depth *ZP* of 4.4 m there is a pier rotation of 0.24° with respect to the vertical, so that the foundation meets the maximum lateral displacement and tilt.

The definition of the factor of safety against passive failure according to Eq. (4) is correct since the $\sum_{0}^{ZP} R_i$ = 378.73 kN is higher by 65% than the horizontal load P of 230 kN, applied to the head of the pile. We conclude that the foundation is stable and is not suitable to reduce the diameter of the pier.

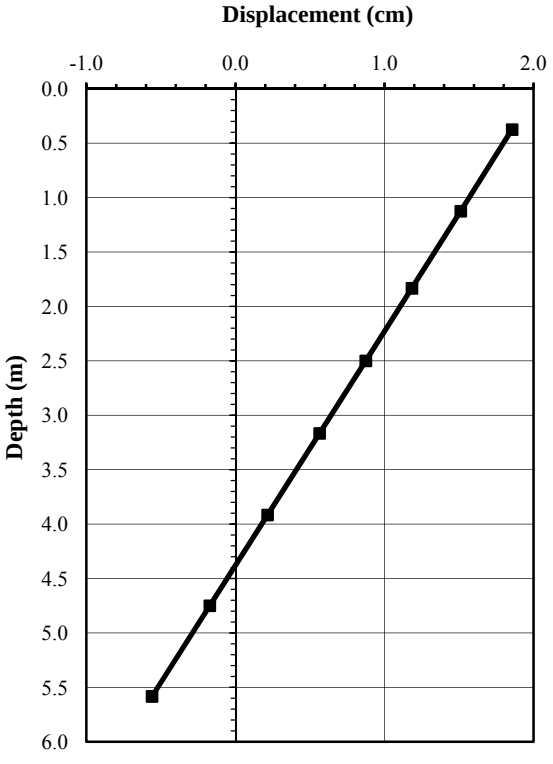

Fig. 5 Lateral displacement diagram.

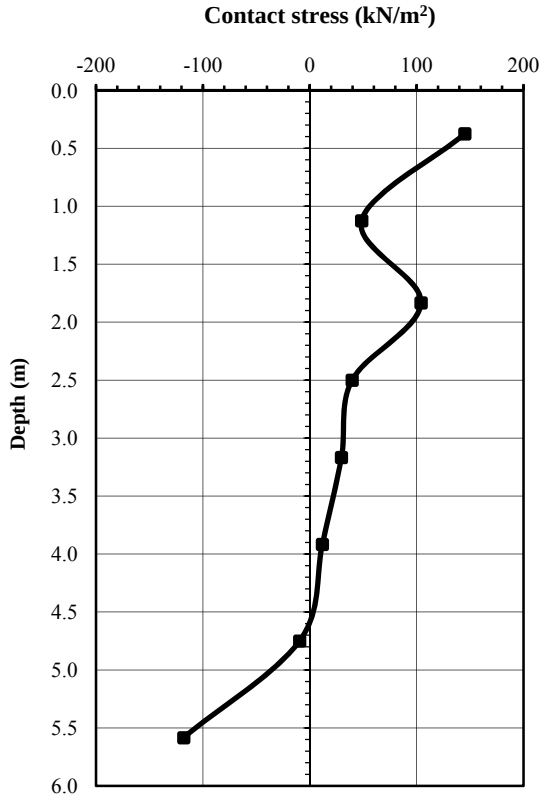

Fig. 6 Lateral contact pressure diagram.

5. Example of a Pier in Seismic Condition

5.1 Statement of the Problem

The stability analysis for the pier was developed with the following features:

Foundation pier using Case II, EI = 4.8168E+06 kN/m^2 (E is the Young's modulus of reinforced concrete and I is the moment of inertia of the cross section of the pier).

P = 400 kN; M = 0.0 kN-m; d = 0.00 m; D = 1.40 m; Df = 15.00 m. Considering subsoil foundation characteristics shown in Table 9, with the water level on the ground surface and hydrostatic water condition, and Poisson's ratio of subsoil, ν = 0.5.

When estimating the drag forces exerted by the soil mass against the pier during the earthquake, the seismic horizontal displacements of the soil mass shown in Table 10 were considered. It is considered a permitted maximum lateral displacement of 10 mm and an inclination with respect to the vertical of no more than 1°.

Table 8 Calculation of the ultimate lateral resistance in static condition.

Dowel	Hi (m)	Ri (kN)	γ_m (kN/m^3)	C (kN/m^2)	φ (^{O})	$N\varphi$	σ'_{zM} (kN/m^2)	ΔQ_{LU} (kN)	$\Sigma\Delta Q_{LU}$ (kN)	$\Sigma\Delta Ri$ (kN)
a	0.75	152.32	18.142	15.298	34	3.54	6.80	85.689	85.689	152.321
1	0.75	50.95	18.142	15.298	34	3.54	20.41	136.224	221.913	203.267
2	0.67	97.13	18.338	18.437	34	3.54	33.33	174.746	396.659	300.399
3	0.67	37.01	18.338	18.437	34	3.54	45.55	215.106	611.765	337.405
4	0.67	27.65	18.338	18.437	34	3.54	57.78	255.467	867.232	365.051
5	0.83	13.68	19.123	19.613	35	3.69	71.86	397.277	1,264.509	378.734
ΣRi (kN) =		378.73				Q_{Lu} (kN) =		1,264.509		

Table 9 Foundation subsoil characteristics corresponding to Example 5.

	Depth (m)	Description	γ_m	C	φ
Ground and water label	0.00		(kN/m^3)	(kN/m^2)	(^{O})
	3.50	Saturated fine soil	16.181	39.227	30
	6.00	Saturated fine soil	12.945	34.323	28
	8.00	Saturated fine soil	11.768	31.381	26
	10.50	Saturated fine soil	13.729	41.678	28
	12.00	Saturated fine soil	11.768	32.362	26
	14.00	Saturated fine soil	13.729	35.304	28
	16.00	Saturated fine soil	14.220	40.207	30
	18.00	Resistant stratum	15.691	-	-

Table 10 Seismic displacement and characteristics of the soil mass, δ_{Si}.

Dowel	Thickness (m)	Unit weight (kN/m^3)	μ_i (kN/m^2)	*Mhi* (m^2/kN)	*Zi* (m)	δ_{Si} (m)
a	1.50	16.181	14,700	2.2676E-05	0.75	2.3870E-02
1	2.00	16.181	14,700	2.2676E-05	2.50	2.3529E-02
2	2.50	12.945	3,730	8.9366E-05	4.75	2.0854E-02
3	2.00	11.768	2,750	1.2121E-04	7.00	1.5060E-02
4	2.50	13.729	6,370	5.2329E-05	9.25	9.5442E-03
5	1.50	11.768	24,520	1.3594E-05	11.25	7.0659E-03
6	2.00	13.729	8,340	3.9968E-05	13.00	5.2276E-03
b	1.00	14.220	8,830	3.7750E-05	14.50	3.7648E-03

μ_i is the shear modulus of dowel *i*, *Mhi* is the horizontal deformation modulus of dowel *i*, *Zi* is the depth at the center of dowel *i* and δ_{Si} is the horizontal seismic displacement of the soil mass at the center of dowel *i*.

5.2 Solution

5.2.1 Soil-Foundation Structure Interaction

The soil-foundation structure interaction was conducted according to Medina [4]. The foundation pier was divided into eight segments: *a*, 1, 2, 3, 4, 5, 6 and *b*. We worked with Δx = 2.10 m and six sections in the soil mass: A, B, C, D, E and F. Discretization of the foundation and soil mass are shown in Table 11.

By applying the flexibility method (Fig. 7) Medina [4], it is obtained the flexibility matrix equation that corresponds to case II, equation (15).

Observe that with matrix Equations (5) and (15) there are 2n+3 equations with 2n+5 unknowns, therefore the two remaining equations are obtained from the sum of moments at supports *a* and *b* with which the system of equations can be resolved, obtaining equations (16) to (25).

Table 11 Soil mass and pier discretization.

Dowel	Thickness (m)	*Zi* (m)	*Mhi* (m^2/kN)	$\Delta\delta_{Si}$ (m)
a	1.50	0.75	2.2676E-05	0.0000E+00
1	2.00	2.50	2.2676E-05	2.2176E-03
2	2.50	4.75	8.9366E-05	2.8330E-03
3	2.00	7.00	1.2121E-04	3.2908E-04
4	2.50	9.25	5.2329E-05	-1.8972E-03
5	1.50	11.25	1.3594E-05	-1.4511E-03
6	2.00	13.00	3.9968E-05	-7.3052E-04
b	1.00	14.50	3.7750E-05	0.0000E+00

$\Delta\delta_{si}$ is the soil mass relative seismic displacement with respect to dowels a and b.

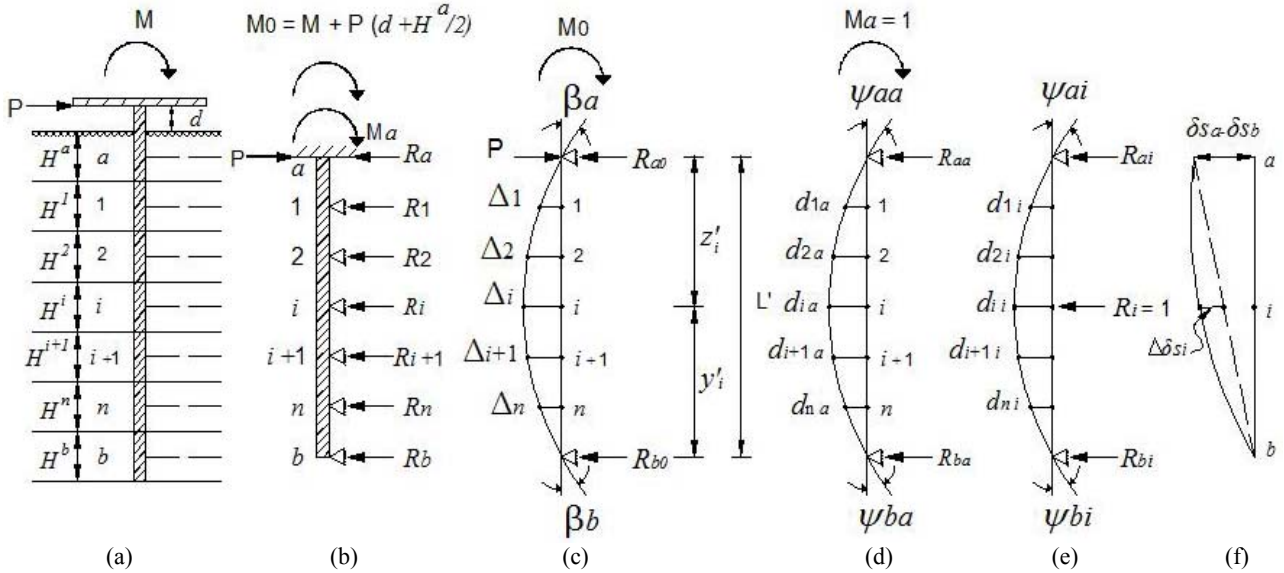

Fig. 7 Application of the flexibilities method: a) real foundation; b) discreteness of foundation; c) condition R_i = 0; d) condition Ma = 1; e) condition R_i = 1; f) relative seismic displacement of soil mass.

$$\begin{bmatrix} \psi_{aa} & \psi_{a1} & \psi_{a2} \ldots \psi_{an} \\ d_{1a} & d_{11} & d_{12} \ldots d_{1n} \\ d_{2a} & d_{21} & d_{22} \ldots d_{2n} \\ & & \vdots \\ d_{na} & d_{n1} & d_{n2} \ldots d_{nn} \end{bmatrix} \begin{vmatrix} M_a \\ R_1 \\ R_2 \\ \vdots \\ R_n \end{vmatrix} = \begin{vmatrix} \beta_a \\ \Delta_1 \\ \Delta_2 \\ \vdots \\ \Delta_n \end{vmatrix} + \begin{vmatrix} 0 \\ \delta_1^A \\ \delta_2^A \\ \vdots \\ \delta_n^A \end{vmatrix} - \begin{vmatrix} \theta_a \\ \delta_1 \\ \delta_2 \\ \vdots \\ \delta_n \end{vmatrix} \tag{15}$$

Where Ma is the moment at the head of the pier; β_a is the rotation of support a for condition $R_i = 0$, θ_a is the rotation of head of pier for deformation of material where the pier is fitted; ψ_{ai} is the rotation of the support a due to a unit load applied at i (condition $R_i = 1$); ψ_{aa} is the rotation of the support a due to a unit moment applied at a (condition $M_a = 1$).

$$\left[\begin{bmatrix} \delta_{11} & \delta_{12} \ldots & \delta_{1n} \\ \delta_{21} & \delta_{22} \ldots & \delta_{2n} \\ & \vdots & \\ \delta_{n1} & \delta_{n2} \ldots & \delta_{nn} \end{bmatrix} + \begin{bmatrix} d_{11} & d_{12} \ldots & d_{1n} \\ d_{21} & d_{22} \ldots & d_{2n} \\ & \vdots & \\ d_{n1} & d_{n2} \ldots & d_{nn} \end{bmatrix} + \begin{bmatrix} m_{11} & m_{12} \ldots & m_{1n} \\ m_{21} & m_{22} \ldots & m_{2n} \\ & \vdots & \\ m_{n1} & m_{n2} \ldots & m_{nn} \end{bmatrix} \right] \begin{vmatrix} R_1 \\ R_2 \\ \vdots \\ R_n \end{vmatrix} = \begin{vmatrix} n_1 \\ n_2 \\ \vdots \\ n_n \end{vmatrix} + \begin{vmatrix} \Delta_1 \\ \Delta_2 \\ \vdots \\ \Delta_n \end{vmatrix} + \begin{vmatrix} \Delta\delta_{S1} \\ \Delta\delta_{S2} \\ \vdots \\ \Delta\delta_{Sn} \end{vmatrix} \tag{16}$$

$$\begin{bmatrix} m_{11} & m_{12} \ldots & m_{1n} \\ m_{21} & m_{22} \ldots & m_{2n} \\ & \vdots & \\ m_{n1} & m_{n2} \ldots & m_{nn} \end{bmatrix} = \begin{bmatrix} \psi_1 & \xi_1 \\ \psi_2 & \xi_2 \\ & \vdots & \\ \psi_n & \xi_n \end{bmatrix} \begin{bmatrix} \delta_{aa} & \delta_{ab} \\ \delta_{ba} & \delta_{bb} \end{bmatrix} \begin{bmatrix} \psi_1 & \psi_2 \ldots & \psi_n \\ \xi_1 & \xi_2 \ldots & \xi_n \end{bmatrix} - \begin{bmatrix} \psi_1 & \xi_1 \\ \psi_2 & \xi_2 \\ & \vdots & \\ \psi_n & \xi_n \end{bmatrix} \begin{bmatrix} \delta_{a1} & \delta_{a2} \ldots & \delta_{an} \\ \delta_{b1} & \delta_{b2} \ldots & \delta_{bn} \end{bmatrix} -$$

$$- \begin{bmatrix} \delta_{1a} & \delta_{1b} \\ \delta_{2a} & \delta_{2b} \\ & \vdots & \\ \delta_{na} & \delta_{nb} \end{bmatrix} \begin{bmatrix} \psi_1 & \psi_2 \ldots \psi_n \\ \xi_1 & \xi_2 \ldots \xi_n \end{bmatrix} - \begin{vmatrix} d_{1a} \\ d_{2a} \\ \vdots \\ d_{na} \end{vmatrix} \left| A_1 \; A_2 \ldots A_n \right| - \begin{vmatrix} (\delta_{1a} - \delta_{1b}) \\ (\delta_{2a} - \delta_{2b}) \\ \vdots \\ (\delta_{na} - \delta_{nb}) \end{vmatrix} \left| C_1 \; C_2 \ldots C_n \right| +$$

$$+ \begin{bmatrix} \psi_1 & \xi_1 \\ \psi_2 & \xi_2 \\ & \vdots & \\ \psi_n & \xi_n \end{bmatrix} \begin{vmatrix} (\delta_{aa} - \delta_{ab}) \\ (\delta_{ba} - \delta_{bb}) \end{vmatrix} \left| C_1 \; C_2 \ldots C_n \right| \tag{17}$$

$$\begin{vmatrix} n_1 \\ n_2 \\ \vdots \\ n_n \end{vmatrix} = \left[\begin{bmatrix} \psi_1 & \xi_1 \\ \psi_2 & \xi_2 \\ & \vdots & \\ \psi_n & \xi_n \end{bmatrix} \begin{bmatrix} \delta_{aa} & \delta_{ab} \\ \delta_{ba} & \delta_{bb} \end{bmatrix} - \begin{bmatrix} \delta_{1a} & \delta_{1b} \\ \delta_{2a} & \delta_{2b} \\ & \vdots & \\ \delta_{na} & \delta_{nb} \end{bmatrix} \right] \begin{vmatrix} R_{a0} \\ R_{b0} \end{vmatrix} - \begin{vmatrix} (\delta_{1a} - \delta_{1b}) \\ (\delta_{2a} - \delta_{2b}) \\ \vdots \\ (\delta_{na} - \delta_{nb}) \end{vmatrix} \left| C_0 \right| -$$

$$-\begin{vmatrix} d_{1a} \\ d_{2a} \\ \vdots \\ d_{na} \end{vmatrix} \begin{vmatrix} A_0 \end{vmatrix} + \begin{bmatrix} \psi_1 & \xi_1 \\ \psi_2 & \xi_2 \\ \vdots & \\ \psi_n & \xi_n \end{bmatrix} \begin{vmatrix} (\delta_{aa} - \delta_{ab}) \\ (\delta_{ba} - \delta_{bb}) \end{vmatrix} \begin{vmatrix} C_0 \end{vmatrix} \quad (18)$$

$$A_0 = \frac{\beta_a + \gamma_{sa} - C_{\theta a} M_0}{\psi_{aa} + C_{\theta a}} \quad (19)$$

$$A_i = \frac{\psi_{ai}}{\psi_{aa} + C_{\theta a}} \quad (20)$$

$$C_0 = A_0 / L' \quad (21)$$

$$C_i = A_i / L' \quad (22)$$

$$M_a = A_o - (A_1 R_1 + A_2 R_2 + ... + A_n R_n) \quad (23)$$

$$R_a = R_{a0} - (\psi_1 R_1 + \psi_2 R_2 + ... + \psi_n R_n) + M_a / L' \quad (24)$$

$$R_b = R_{b0} - (\xi_1 R_1 + \xi_2 R_2 + ... + \xi_n R_n) - M_a / L' \quad (25)$$

The problem was solved by a computer program developed in a spreadsheet.

Table 12 shows the unit lateral displacements matrix $\left[\delta_{ji}\right]$. Table 13 shows the matrix $\left[d_{ji}\right]$; Table 14 show the matrix $\left[m_{ji}\right]$; Table 15 shows the vectors N_i, Δi and $\Delta\delta_{Si}$.

Solving the matrix (EMISE) are obtained R1, R2, R3, … and R6. With the equations (23), (24) and (25) are obtaining Ma, Ra and Rb. The lateral displacements are obtaining whit equation (5). The reactions and lateral displacements are shown in Table 17.

Fig. 8 shows the lateral displacement-depth diagram, while Fig. 9 shows the lateral contact pressure-depth diagram.

M*a* = -1 034.071 kN/m; θ_a = -8.8544E-04 rad. Table 18 shows the horizontal stress increment matrix indicated by the pier in seismic condition.

5.2.2 Lateral Bearing Capacity in Seismic Condition

In Fig. 8, the depth of the passive zone *ZP* is 8.50 m, so the calculation of the lateral bearing capacity is considered down to the bottom of the dowel 3 at a depth of 8.00 m.

The lateral bearing capacity of the pier is obtaining from equation (3). Table 19 shows the calculation of the lateral bearing capacity of the pier. Hydraulic pressure is calculated on the center of the section, and at the center of each of the dowels with equation (26),

$$u = uh + \Delta u \quad (26)$$

where u is the hydraulic pressure, uh is the hydrostatic pressure and Δu is the increase in hydrostatic pressure generated in seismic condition. Δu is obtained from Table 18 and it is considered on section A.

5.2.3 Factor of Safety against the Foundation Passive Failure

$$Fs = \frac{1\,718.32}{558.70} = 3.08$$

5.2.4 Discussion of results

The 558.70 kN is higher by 40% than the horizontal load P of 400 kN applied to the head of the foundation pier.

Table 12 Unitary lateral displacements matrix, $\left[\delta_{ji}\right]$ (m/kN).

a	1	2	3	4	5	6	*b*
8.4242E-06	2.0443E-06	6.0611E-07	2.6068E-07	1.2780E-07	7.0637E-08	4.4137E-08	2.9907E-08
1.9302E-06	7.0450E-06	1.3420E-06	4.4180E-07	2.0016E-07	1.0567E-07	6.4058E-08	4.2368E-08
2.3349E-06	5.0529E-06	2.4603E-05	4.9158E-06	1.6949E-06	8.0956E-07	4.6488E-07	2.9527E-07
1.3847E-06	2.3616E-06	6.9861E-06	3.7143E-05	6.9406E-06	2.4607E-06	1.2938E-06	7.7848E-07
2.9162E-07	4.5841E-07	9.9247E-07	2.8589E-06	1.4357E-05	3.2651E-06	1.3177E-06	7.1775E-07
4.2348E-08	6.3658E-08	1.2490E-07	2.7863E-07	9.4655E-07	4.6605E-06	1.0976E-06	4.1848E-07
7.7505E-08	1.1291E-07	2.0928E-07	4.2661E-07	1.0214E-06	3.0313E-06	1.2236E-05	3.6144E-06
4.9908E-08	7.0991E-08	1.2641E-07	2.4474E-07	5.2974E-07	1.1734E-06	3.9160E-06	1.4380E-05

Table 13 Matrix, $[d_{ji}]$(rad/kN; m/kN).

a	1	2	3	4	5	6
9.5153E-07	1.3608E-06	2.3063E-06	2.5066E-06	2.1336E-06	1.4598E-06	7.0515E-07
1.3608E-06	2.2195E-06	3.9046E-06	4.2854E-06	3.6630E-06	2.5109E-06	1.2138E-06
2.3063E-06	3.9046E-06	7.6550E-06	8.8185E-06	7.6890E-06	5.3160E-06	2.5790E-06
2.5066E-06	4.2854E-06	8.8185E-06	1.1059E-05	1.0110E-05	7.1274E-06	3.4857E-06
2.1336E-06	3.6630E-06	7.6890E-06	1.0110E-05	1.0022E-05	7.3861E-06	3.6757E-06
1.4598E-06	2.5109E-06	5.3160E-06	7.1274E-06	7.3861E-06	5.8609E-06	3.0345E-06
7.0515E-07	1.2138E-06	2.5790E-06	3.4857E-06	3.6757E-06	3.0345E-06	1.6993E-06

Table 14 Matrix, $[m_{ji}]$(m/kN).

1	2	3	4	5	6
2.4826E-06	2.6582E-06	2.2512E-06	1.9293E-06	1.7144E-06	1.3125E-06
7.4930E-07	7.7608E-07	8.1268E-07	1.2678E-06	1.8843E-06	1.9510E-06
7.1174E-07	7.0744E-07	1.0081E-06	1.8321E-06	2.7807E-06	2.8134E-06
1.2113E-06	1.4800E-06	2.1608E-06	3.3253E-06	4.4945E-06	4.3537E-06
1.2276E-06	2.0164E-06	3.2187E-06	4.7972E-06	6.2183E-06	5.9515E-06
8.3184E-07	1.7259E-06	2.8971E-06	4.2446E-06	5.2957E-06	4.3715E-06

Table 15 Vectors N_i, Δi and $\Delta\delta_{Si}$. βa and Reactions R*a*o and R*b*o Constants A_0 y C_0.

Vector Ni	Vector Δi	Vector $\Delta\delta_{Si}$		
(m)	(m)	(m)		
3.0330E-03	4.0823E-04	2.2176E-03	βa = 2.8546E-4 rad	A_0 = -7.1306E+02
3.1135E-03	6.9189E-04	2.8330E-03		
3.1569E-03	7.5198E-04	3.2908E-04	R*a*o = 421.818 kN	C_0 = -5.1859E+01
2.8608E-03	6.4009E-04	-1.8972E-03		
2.0936E-03	4.3795E-04	-1.4511E-03	R*b*o = - 21.818 kN	
1.1070E-03	2.1155E-04	-7.3052E-04		

Table 16 Vectors Ai and Ci.

	1	2	3	4	5	6
Ai	6.3065E-01	1.0689E+00	1.1617E+00	9.8883E-01	6.7657E-01	3.2680E-01
Ci	4.5865E-02	7.7735E-02	8.4486E-02	7.1915E-02	4.9205E-02	2.3768E-02

Soil structure interaction matrix equation (EMISE):

(m/kN)					(kN)		(m)
1.1747E-05	7.9047E-06	6.9785E-06	5.7925E-06	4.3310E-06	2.5903E-06	R_1	5.6588E-03
9.7067E-06	3.3034E-05	1.4547E-05	1.0652E-05	8.0098E-06	4.9949E-06	R_2	6.6384E-03
7.3588E-06	1.6512E-05	4.9210E-05	1.8882E-05	1.2369E-05	7.5928E-06	R_3	4.2380E-03
5.3327E-06	1.0161E-05	1.5129E-05	2.7705E-05	1.5146E-05	9.3472E-06	R_4	1.6037E-03
3.8021E-06	7.4573E-06	1.0625E-05	1.3130E-05	1.6740E-05	1.0084E-05	R_5	1.0805E-03
2.1585E-06	4.5142E-06	6.8094E-06	8.9417E-06	1.1361E-05	1.8307E-05	R_6	5.8801E-04

= (between the kN and m columns)

Table 17 Reactions and lateral displacements.

Dowel	*Zi* (m)	*Ri* (kN)	δh (m)
a	0.75	-91.384	2.0577E-04
1	2.50	453.341	3.1285E-03
2	4.75	86.102	4.1835E-03
3	7.00	19.258	1.8603E-03
4	9.25	-40.071	-4.2816E-04
5	11.25	-62.937	-2.6916E-04
6	13.00	8.903	4.4393E-05
b	14.50	26.788	3.6821E-04

Table 18 shows that under Section A, it is presented the largest increase in the hydraulic pressure. Neglecting the frictional forces of the water flow in the soil mass and the pier contact with the soil foundation, with the excess hydrostatic pressure generated during the earthquake in dowel 1 and under section A, the water would rise 4.9 m above the ground surface, which is consistent with the removal of water observed in the contact of the pile or pier and

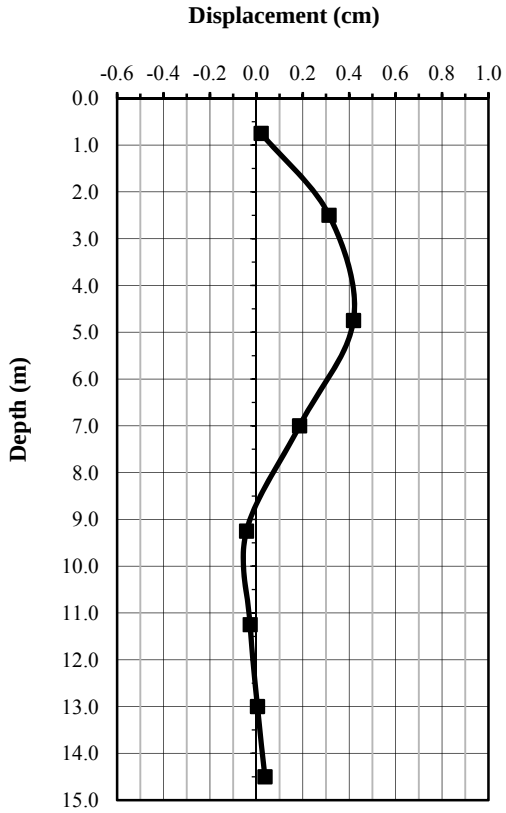

Fig. 8 Lateral displacement diagram.

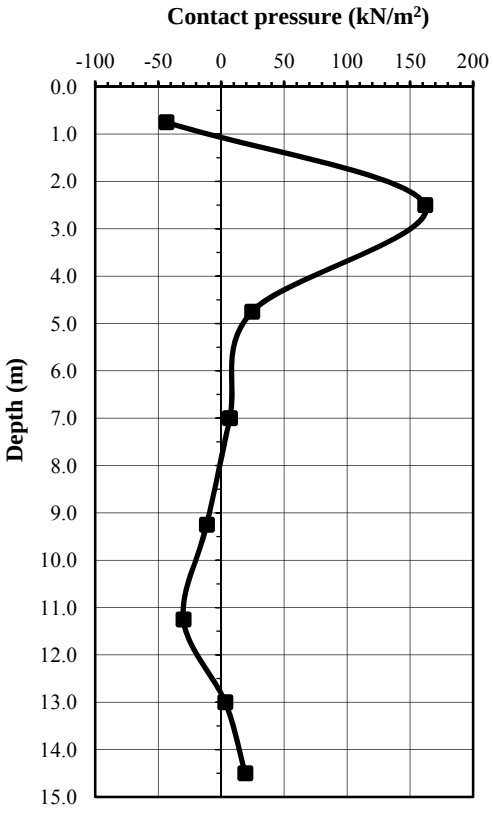

Fig. 9 Lateral contact pressure diagram.

the soil mass during an earthquake. This phenomenon of ejection of water does not necessarily mean failure of the soil during the earthquake.

Table 18 shows that the excess of hydrostatic pressure generated during the earthquake, decreases rapidly with increasing distance from the shaft of the foundation pier, which justifies the use of Eq. (26), with the estimate of excess hydrostatic pressure under Section A.

From Table 18, it was found that the increase in the hydraulic pressure in the dowel "*a*" and under the section A is negative, and this was considered positive for the calculation of effective stress because it can change sign during an earthquake.

The hydraulic pressure in dowels "*a*" and "1" generated during the earthquake is greater than the total stress in the soil, so that the vertical effective stress is considered zero in the calculation of the ultimate lateral resistance of the subsoil foundation in contact with dowels "*a*" and "1".

Table 18 Soil mass increased horizontal stress matrix (kN/m^2).

A	B	C	D	E	F
-6.2331	3.8568	2.7880	1.8169	1.2263	0.8663
48.0806	9.5550	3.8071	2.0672	1.2991	0.8893
9.9355	5.6483	3.0207	1.7578	1.1357	0.7940
2.3594	1.3986	1.2234	0.9775	0.7580	0.5916
-3.9642	-0.9824	-0.0163	0.3086	0.3850	0.3731
-8.0163	-1.4907	-0.3537	0.0298	0.1769	0.2257
0.7065	-0.2620	-0.1531	-0.0023	0.0949	0.1450
3.9238	0.4653	0.0521	0.0304	0.0693	0.1038

The reaction obtained in the slice "*a*" is negative, which means that in this section the pile charges to the left side, which agrees with the lateral displacement diagram shown in Fig. 8 For this reason in the calculation of $\sum_{0}^{ZP} R_i$ the reaction was not considered in dowel "*a*".

The factor of safety against passive failure of the foundation is satisfactory.

Maximum lateral displacement of the foundation is 4.2 mm, so that the foundation meets maximum lateral displacement and tilt.

Table 19 Calculation of lateral bearing capacity in seismic condition.

Dowel	Hi	Ri	γ_m	C	φ	$N\varphi$	σ_{zM}	u	σ'_{zM}	ΔQ_{LU}	$\Sigma\Delta Q_{LU}$	$\Sigma\Delta Ri$
	(m)	(kN)	(kN/m^3)	(kN/m^2)	(^{O})		(kN/m^2)	(kN/m^2)	(kN/m^2)	(kN)	(kN)	(kN)
a	1.50	-91.384	16.181	39.227	30	3.00	12.136	13.588	0.000	285.36	285.36	-91.384
1	2.00	453.341	16.181	39.227	30	3.00	40.452	72.597	0.000	380.48	665.84	453.341
2	2.50	86.102	12.945	34.323	28	2.77	72.814	56.517	16.297	557.86	1 223.69	539.443
3	2.00	19.258	11.768	31.381	26	2.56	100.763	71.006	29.757	494.63	1 718.32	558.702
ΣRi (kN) =		558.702						Q_{LU} (kN) =		1,718.32		

Therefore, the foundation is stable in seismic condition for lateral passive failure, maximum lateral displacement and permissible tilt.

5. Conclusions

It has been explained a procedure for estimating the lateral bearing capacity of foundation piles and piers subjected to lateral loading, both in static and seismic conditions. The method is based upon the Rankine theory of passive earth pressure, and as discussed herein, the frictional force developed in the contact of the shaft of the foundation with the soil is not considered. So the bearing capacity obtained with the method presented here is on the side of safety, i.e., the real capacity will be higher than the calculated. The procedure described has the following advantages:

(1) It can be used in homogeneous soils as in stratified soils;

(2) It is applicable in both static and earthquake condition;

(3) It is easy to program in a spreadsheet and solved with simplicity;

(4) It considers the horizontal drag forces exerted by the soil mass against the foundation during an earthquake;

(5) It can be used easily in the four pile and piers boundary cases;

(6) It considers the pore pressure generated in a fine saturated soil during an earthquake or during a rapid application of the horizontal load.

References

[1] J. Medina, Interacción sísmica suelo-estructura en pilotes y pilas: Caso I, in: 14th Pan-American Conference on Soil Mechanic and Geotechnical Engineering, Toronto, Ontario, Canada, 2011.

[2] J. Medina, Seismic soil-structure interaction in piles and piers: Case III, in: 14th Pan-American Conference on Soil Mechanic and Geotechnical Engineering, Toronto, Ontario, Canada, 2011.

[3] J. Medina, Seismic soil-structure interaction in piles and piers: Case IV, in: 5th International Conference on Earthquake Geotechnical Engineering, Santiago de Chile, Chile, 2011.

[4] J. Medina, Interacción sísmica suelo-estructura en pilas y pilotes: Caso II, in: Proceedings of the XX Congreso Argentino de Mecánica de Suelos e Ingeniería Geotécnica, Mendoza, Argentina, 2010, pp. 281-288.

[5] K. Terzaghi, Theoretical Soil Mechanics, John Wiley and Sons, New York, 1943.

[6] L. Zeevaert, Foundation Engineering for Difficult Subsoil Conditions, Van Nostrand Reinhold Company, New York, 1983.

[7] J. Medina, Esfuerzo horizontal producido por una carga rectangular horizontal uniforme aplicada en el interior de un sólido, in: Proceedings of XXV Reunión Nacional de la Sociedad Mexicana de Ingeniería Geotécnica, Acapulco, Guerrero, México, 2010, Vol. 3, pp. 871-876.

Journal of Geological Resource and Engineering 1 (2013) 25-30

A Stability Analysis of the Cantilevered Blocks in the Underground Gold Mine of Akka (Anti-Atlas of Morocco)

Taha Ezzarrouk[1], Toufik Remmal[1]and Rachid El Hamdouni[2]

1. Department of Geology, Faculty of sciences of Ain Choc, University of Hassan II-Casablanca, Casablanca 5366, Morocco

2. Department of Civil Engineering, University of Granada, Granada 18071, Spain

Abstract: A cantilevered block is instable rock which results from a combination of several discontinuities, in interaction with an underground mining excavation giving a mass rocky under-gangway without natural support. Since the starting of the gold mine of Akka in 1998, 4 deaths and 26 grave accidents happened that are associated to the falling of the cantilevered blocks. However, this study analyzes the causes of apparition of this instability in the underground gold mine of Akka which is in the buttonhole of Tagragra (Anti-Atlas, Morocco) taking into account the geological and geotechnical aspects. The more utilized geotechnical approaches were used to evaluate the quality of rocky mass including RQD, RMR and Q System method besides laboratory tests and geomechanical stations. After development of some classical formulas and using of simulation software and analytical methods, a way of support by bolting is proposed to stabilize the risk of blocks collapse inherent to the mining operations. Also we discuss here other technical solutions and theirs application limits in these cases. Finally, we confirmed the reliability of our conclusions and the type of the support proposed during 2012 and 2013 because we did not register any accident associated to cantilevered block falling.

Key words: Stability, block cantilevered, support.

1. Introduction

A cantilevered block is a structural element embedded in one end and free at the other. This is the result of a combination of several discontinuities, interacting with the excavation, without giving a natural support block. In the mining jargon, it is a mass rock suspended without abutment. Since the starting of the gold mine of Akka in the Anti-Atlas of Morocco (Fig. 1) in 1998, 4 deaths and 26 grave accidents happened that are associated to the falling of blocks. To overcome this problem, a method of retaining bolting is proposed, taking into account the geometry of the fracture, and the geomechanical properties of the blocks. An analog simulation is discussed to evaluate the safety factor inherent to this approach.

Corresponding author: Taha Ezzarrouk, Ph.D. Student, research field: geotechnical mining. E-mail: taha_zarouk@yahoo.fr.

2. Materials

2.1 Geological Background of Mine Site

The Precambrian buttonhole of Tagragra Akka is located in the western Anti-Atlas at about 280 km south-east of Agadir. The central portion of the buttonhole that houses the mining district contains several mineralized structures of EW direction and spaced by 30 m to 50 m with a dip to the north. These structures move dolerite dykes and gabbro to the right side oriented NE with a decametric extension to hectometric. The mineralized thickness varies between 0.5 m and 5 m, with tight areas in places (Fig. 1). Some satellites of low thickness and limited extension structures are associated to the main EW structures.

2.2 Cantilevered Blocks

The gold mine of Akka show abundantly cantilevered blocks which is consecutively behind the major risk to

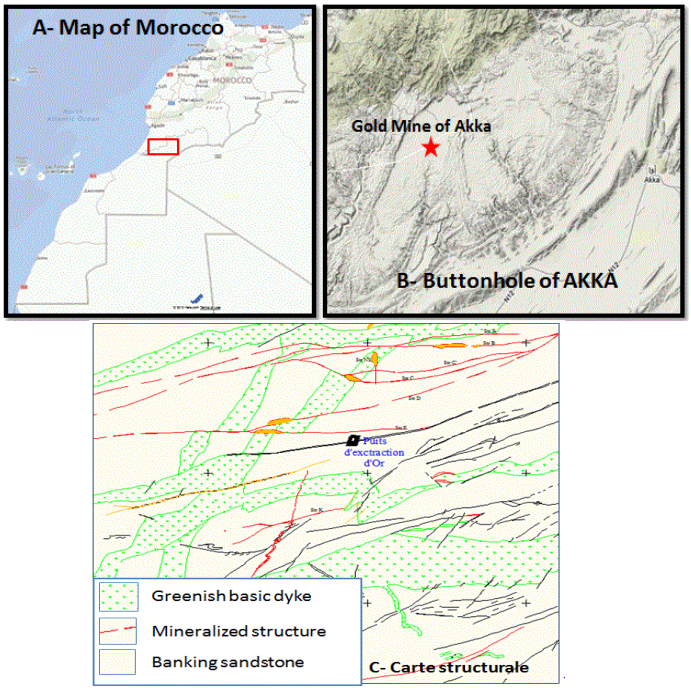

Fig. 1 A—Map of Morocco; B—Buttonhole of Akka; and C—Structural map of the area studied.

minors falling blocks. The detailed structural study of the gold deposit showed three main families of discontinuities that have shaped geometry of cantilevered blocks (Fig. 2).

It is the F1-F3 or F2-F3 combination with the excavation during the cull of ore [1], which form the hanging and unstable blocks (Fig. 3). In the case where the thickness of the vein coincides with the width of the underground gallery, which is of the order of 1.6 m required for movement of extraction machines (scoop), the risk of cantilevered blocks is no longer possible.

Despite the good rheological competence of sandstone rocky matrix, there are the density and the orientation of fractures that weaken the rock mass and induce the creation of cantilevered blocks.

2.2.1 Simulation by Unwedge Logiciel

For a spatial scene of the structure, we performed a 3D (three-dimensional) view by Unwedge Software (Fig. 4) simulation, which also allows to calculate the safety factor of cantilevered blocks and in this case it is in the order of $F = 0.778$ and when the weight is $W = 0.093$ *MN*. The views following various angles are taken to geometrically model such instability in the non-shot sterile area.

The analysis of the effect of the orientation of the excavation realized by a 3D graph by the same software Unwedge (Fig. 5), shows that certain directions promote stable operation including directions of 0° and 200°, regardless of the dip of the excavation.

2.2.2 Geomechanical Proprietes of Blocs

Geomechanical properties of sandstone which constitute the bulk of the material cantilevered blocks of the mine are reflected in the tables (Tables 2-5) below [2].

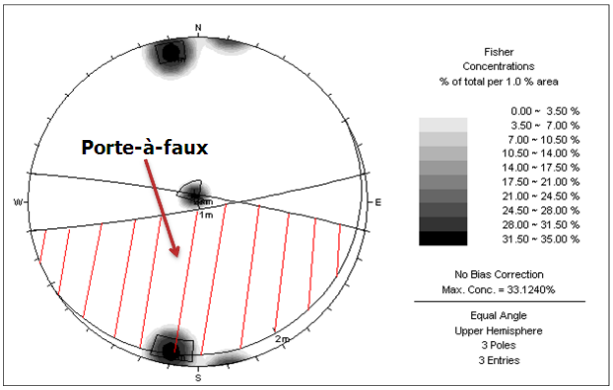

Fig. 2 Stereographic projection by DIPS software of the three main families of fractures which cause the apparition of cantilevered blocks.

Table 1 The three main families of fractures which cause the apparition of cantilevered blocks.

Sandstone letite facies	Direction	DIP
Famille 1 (F1)	N80	85SE
Famille 2 (F2)	N100	88NNE
Famille 3 (F3)	N60	10SSE

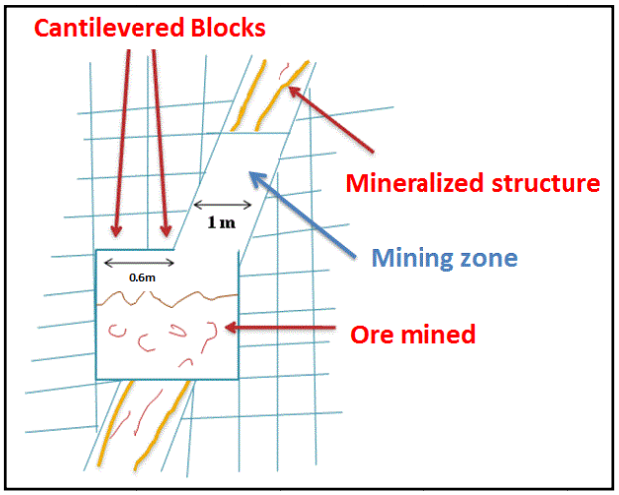

Fig. 3 Mining of the mineralised structure.

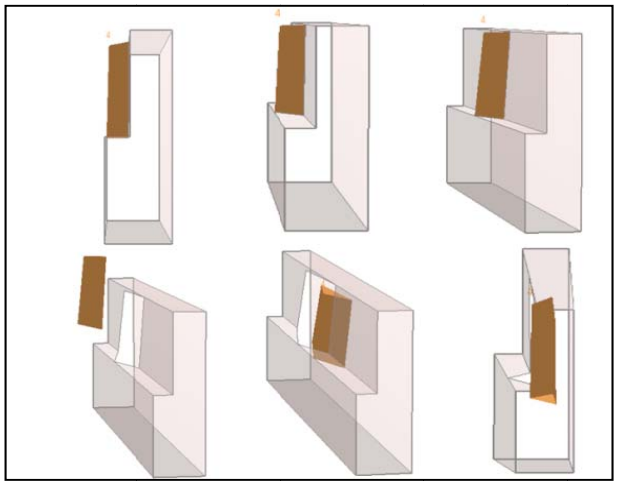

Fig. 4 3D views of a cantilevered block.

In conclusion, the results are allowed to characterize the quality of the mass rock from good to moderate.

2.3 Simulation by the Method of Finite Element

To understand the reaction amongst all geological compositions taking into account the geotechnical aspects [3], we used the finite element method which originally was a numerical technique for finding approximate solutions to boundary value problems for differential equations.

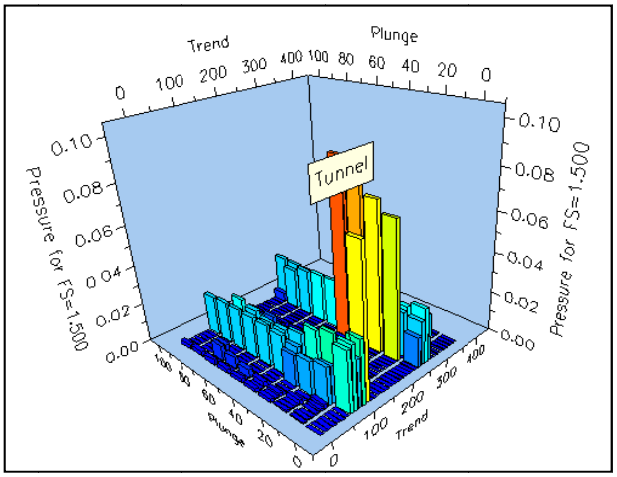

Fig. 5 Effect of orientation on the stability of the excavation for a safety factor of 1.5.

We used a numerical simulation by finite element method proposed by Phase 2 software, which could identify the major tensile stresses around the excavation and therefore deduce the magnitude of the instability associated with cantilevered blocks (Fig. 6). The latter in this case exceed 2 m for a safety factor of 1.57.

2.4 Mode of Support

Among the tested methods of support to deal with the risk of falling blocks, we tested the anchor bolts. To estimate the number as well as the length of anchor bolts required to support the cantilevered block, we developed the analytical calculations proposed by Stillborg [4] and Hadjigeorgiou [5] and the results were as following.

$$N = Wf/T \quad (1)$$

where: N: number of anchor bolts;

W: weight of cantilevered bloc;

2.4.1 Suspended Cantilevered Bloc

T: sum of the bolts in tension;

f: safety factor.

$$s \leq 3e \quad (2)$$

$$p \geq L + 1 \quad (3)$$

$$2 \leq f \leq 5 \quad (4)$$

where: s: spacing between bolts;

Table 2 Mechanical tests of laboratory.

Rc MPa	*E* GPa	*v*	*Is* MPa	*Rt* MPa	*Rtri* MPa
101	54	0.28	5.3	4	141

Table 3 In situ characterization via RocLab software.

Hoek-brown classification	Hoek-brown criterion	Mohr-Coulomb fit	Rock mass parameters
GSI: 63 Mi: 25 Distrubance factor: 0	mb: 6.669 s: 0.0164 a: 0.502	Cohesion: 12.905 Friction angle: 43.34°	Tensile strength: 0.406 MPa Uniaxial compressive strength: 20.926 MPa Global strength: 58.433 MPa Modulus of deformation: 21234.89 MPa

Table 4 Empirical classification "RMR" (rock mass rating) [6].

Rc = 101 MPa	RQD = 75	Spacing of the joints 0.5 m
12	13	20
Joint conditions (smooth, planar)	Filtrations (no water influx)	Adjustment factor (low orientation)
12	10	-5
RMR corrected = 62 (Roch with moderate quality)		

Tabel 5 "Q system" method. [7] & [8]

RQD = 75	Jn = 9 Three families	Jr = 1 Joints plans lisses
Ja = 1 Joints slightly altered	Jw = 1 Low water inflows	SRF = 2.5 Shear zones
Q = 3.33 Moderate mass rock quality		

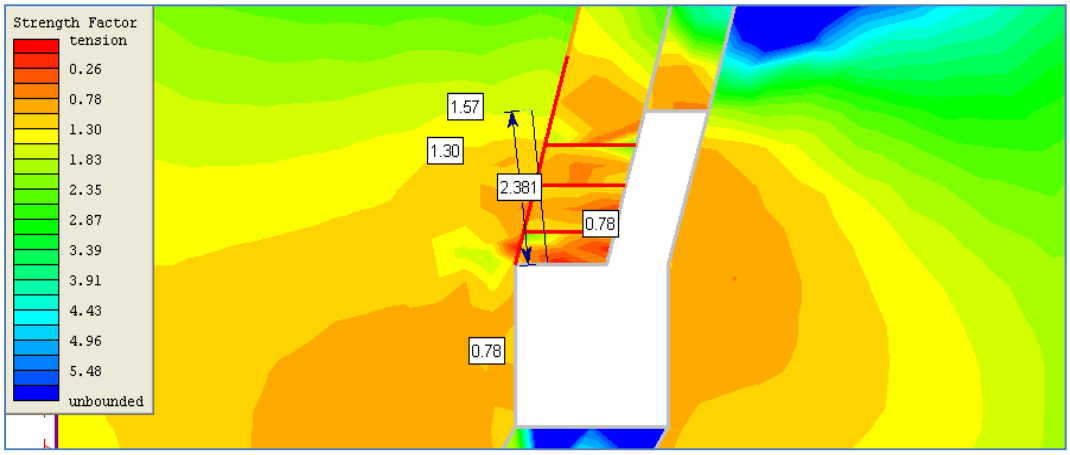

Fig. 6 Simulation of unstable areas by Phase 2 software.

e: spacing between joints;

L: length of bolts;

p: reach of excavation.

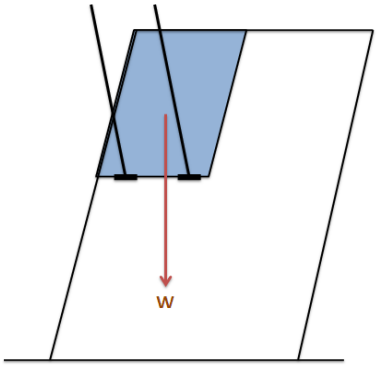

2.4.2 Slippery Cantilevered Bloc

$$N = \frac{W\cdot(f\cdot sin\beta - \cos\beta\cdot tg\varphi) - CA}{B\cdot(cos\alpha\cdot tg\alpha + f\cdot sin\alpha)} \quad (5)$$

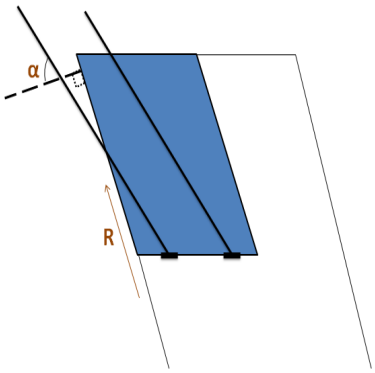

where: B: bearing capacity of the bolt (t);

A: area of the sliding surface;

α: angle between the bolts and the normal to the sliding surface;

β: inclination of the sliding surface;

C: cohesion along the sliding surface;

φ: angle of friction of the sliding surface;

R: slip resistance.

$$\text{With: } R = CA + W\cos\beta\ \text{tg}\varphi \quad (6)$$

$$f = 2 \quad (7)$$

2.4.3 Calculation of Length Bolt Anchors

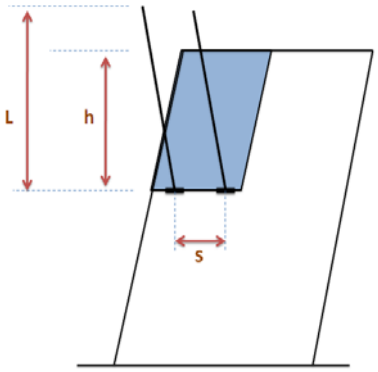

$$L - h \geq \frac{W}{A} \text{ then } L \geq \frac{W}{A} + h \quad (8)$$

$$W = f(s.c.h.\gamma) \quad (9)$$

$$B = 1.5W \quad (10)$$

h: Cantilevered block height;

γ: specific weight of the rock (t / m³);

s: spacing bolts perpendicular to the axis of the excavation (m);

c: spacing between bolts along the axis of the excavation (m);

A: anchoring capability (ton / m);

B: bolt capacity (metric tons);

W: weight of cantilevered block supported by a single bolt (metric tons).

2.4.4 Digital Application

(1) Case of a cantilevred block suspended

Block dimensions: 1×1.5×1 m^3, with a density of 2.7;

N = 2 boulons split set ach 1 m laterally;

N = 1 boulon swellex each 1 m laterally;

Also: e = 0.5, then bolts spacing = 1.5 m.

Fig. 7 Cantilevered block supported by bolts of the Swellex type.

(2) Case of a cantivelered sliping bloc:

N = 3 split set bolts each 1 m laterally;

N = 2 swellex bolts each 1 m laterally.

(3) Length of bolts:

$L \geq 2$ m;

Reach of the excavation: P = 3 m.

3. Conclusions

Bolt of the Swellex type seems the most effective since it does not unshod because of the vibrations induced by the firing explosives, against the bolt shell, in addition to its high capacity of anchoring compared to the first two (Fig. 7). This bolt will also affect the containment seal as it will append the blocks to each other.

Bolting is done before the initiation of slaughter, that is, before the land destabilization by explosives. Note that the holes can be only inclined if the drilling is done using a conventional hammer, given the difficulty of parking this heavy tool vertically. Other solutions can be recommended to address these instabilities in similar conditions, including connectable Swellex, and lashings.

References

[1] L. Jun, L.Zhongkui, Z. Zhuoyuan, Stability analysis of block in the surrounding mass rock of a wide underground

excavation, Ed Tunneling and Underground Space Technology (1) (2003) 10.

[2] J.L. Giafferi, Useful characterization of the rock to the study and implementation of underground structures, in: Ed French Association of Tunnels and Underground Space (AFTES), Paris, France, 2003, p. 54.

[3] J. Guillaume, The choice of parameters and geotechnical testing useful for the design, dimensioning, and execution of the excavated underground works, in: Ed French Association of Tunnels and Underground Space (AFTES), Paris, France, 1994, p. 22.

[4] B. Stillborg, Professional Users Handbook for Rock Bolting, Trans Tech Publications, Vol. 18, Series on Rock and Soil Mechanics, Quebec, 1994, p. 56.

[5] F. Charrette, J. Hadjigeorgiou, Practical guide to mining support, in: Ed Mining Association of Quebec, Canada. 2009, p.120.

[6] L. Jun, L.Zhongkui, Cantilevered structures and probability approaches of failures, Ed Tunneling and Underground Space Technology (1) (2002) 45.

[7] Z. Zhuoyuan, Important geotechnical considerations to evaluate a mass rock in underground excavations, Ed Tunneling and Underground Space Technology (1) (2003) 13.

[8] J. Guillaume. Modelling of geological and geotechnical parameters in underground mines, in: Ed French Association of Tunnels and Underground Space (AFTES), Paris, France, 1996, p. 31.

Journal of Geological Resource and Engineering 1 (2013) 31-38

Evaluation of Mine Productivity and Economics by Effective Blast Instrumentation—A Techno Economic Proposition

Ajay Kumar Jha

Blasting Cell, PAD Division, Central Mine Planning and Design Institute (Coal India Limited), Ranchi 834008, India

Abstract: Coal is the mainstay of power generation in India. The manifold increase in demand for coal puts a huge pressure on augmenting production, primarily from opencast mines. The increase in production necessitates heavy blasting in overburden and coal benches of opencast mines which poses numerous challenges in carrying out blasting operation techno-economically. Presently, the consumption of industrial explosives and accessories in Coal India has touched a whopping figure of 350 million USD per annum. The present paper discusses some of key challenges faced in various mines of coal in India during blasting where blast instrumentation may contribute to the mine productivity and economics significantly. Blast Instrumentation at mine level will prove to a harbinger for practicing blasting engineers. The blast instrumentation at Sonepur Bazari project resulted in direct savings in explosives cost by 29.5%. The use of well characterized explosives obtained by using MASW (multi channel analysis of surface waves) technique at Umrer project of Coal India Limited resulted in improvement in fragment size by 12.76%. It may be concluded with high degree of confidence that blast instrumentation at mine level will influence the mine productivity and economics.

Key words: Blast instrumentation, blast simulation, mine productivity, fragmentation.

1. Introduction

Coal shall remain India's most important energy sources till 2031-2032 and possibly beyond. Coal dominates the energy mix in India, contributing to major share of the total primary energy production. Coal is a crucial and enduring element in a modern, balanced energy portfolio, providing a bridge to the future as an important low cost and secure energy solution to sustainability challenges. The manifold increase in demand for coal puts a huge pressure on augmenting production primarily from opencast mines as well as from underground mines [1-3]. The need of carrying out heavy blasting in overburden and coal benches of opencast mines requires blast instrumentation at mine level. The blast performance is significantly influenced by use of proper instrumentation. The present paper discusses the case study carried at Umrer project and Sonepur Bazari project of Coal India Limited using advanced blast instrumentation and their influence on the mine productivity and economics.

2. Materials and Methods

Sonepur Bazari project of Eastern Coalfields Limited is located in the eastern part of Raniganj Coalfields in India. It is well connected by rails and roads. The Raniganj railway station on Howrah-Delhi line is about 20 km from the project. The Grand Trunk Road passes at 14 km west of the project. Four coal seams, viz., R-IV, R-V, R-VI and R-VII are mainly exposed in the mine. Presently, seams R-V and R-VI are being extracted by opencast method of mining. The mine was producing about 4 Mt of coal and removal of overburden was about 15 million cubic meters during 2010-2011. The average stripping ratio of the mine is 4.63 m^3/t coal produced. The total reserve of the project

Corresponding author: Ajay Kumar Jha, Ph.D., research field: rock blasting in mines and construction. E-mail: ajayk_jha_in@yahoo.com.

is 188.26 million t. The overview of the Sonepur Bazari project is shown in Fig. 1.

2.1 Influence of Scattering/Delay Timings on Vibration and Fragmentation

Precise surface and down-the-hole delay timing affects explosives energy utilisation in terms of blast results, i.e., optimum fragmentation, looseness of muck pile, and favourable muck pile angle. The detonator timing do not only have influence upon the fragmentation but also upon other factors, viz., displacement of rock and swellings of rock, over break and intensity of vibration and overpressure. It is technically desirable to use precise detonators with accurate delay timings to achieve desired blast results in terms of improved fragmentation, lower level of vibration and air overpressure. Presently, scattering in initiation systems is a matter of serious concern to the mine operators as the blast performance is getting affected adversely. Delay timing is primarily provided using delay element made up of pyrotechnic composition placed between the ignition system and the primer charge. Initiation system made with pyrotechnic delay compositions has inherent scattering in their delay timings. In order to understand the effect of detonator timing and delay sequences on blast vibration, the field experimentation was carried out at Sonepur Bazari project, CIL and actual blast results were compared with the simulated blast results obtained by using simulation techniques. The simulation software named 2D Bench of JKSimblast, Australia, has been used for obtaining the simulated blast results.

3. Results and Discussion

3.1 Actual and Simulated Ground Vibration due to Scattering at Sonepur Bazari, CIL

The drilling and blasting parameters practiced at dragline bench of Sonepur Bazari project is shown in Table 1. The plan showing blast design layout along with the initiation sequence and output of simulated blast design obtained by using the software 2D, Bench (JKSimblast) is shown in Fig. 2. The simulated detonation timing contours along with the number of decks detonated vs. detonation time is shown in Fig. 3.

Fig. 1 Overview of Sonepur Bazari project.

Table 1 Drilling and blasting parameters practiced at dragline bench of Sonepur Bazari project.

Sl. No.	Particulars	Existing pattern	Modified pattern
1	Drill diameter (mm)	270	270
2	Average bench height (m)	28	28
3	Burden (m)	7.5	8.5
4	Spacing (m)	8.5	9.5
5	No. of rows	5	5
6	Holes per row	15	15
7	Pattern of holes	Staggered	Staggered
8	Bottom charge (kg)	600	600
9	Top charge (kg)	325	300
10	Linear density (kg/m)	52	50
11	Volume per blast (m^3)	133,875	169,575
12	Total explosive quantity (kg)	69,375	67,500
13	Powder factor (m^3/kg)	1.93	2.50

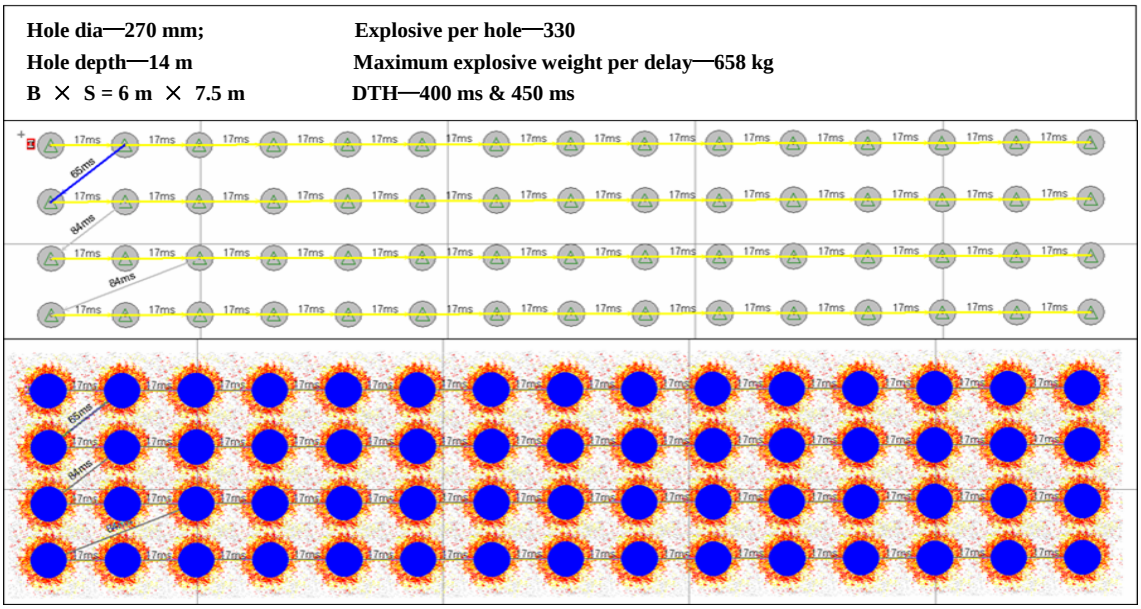

Fig. 2 Plan showing blast design layout along with the initiation sequence and simulated blast result.

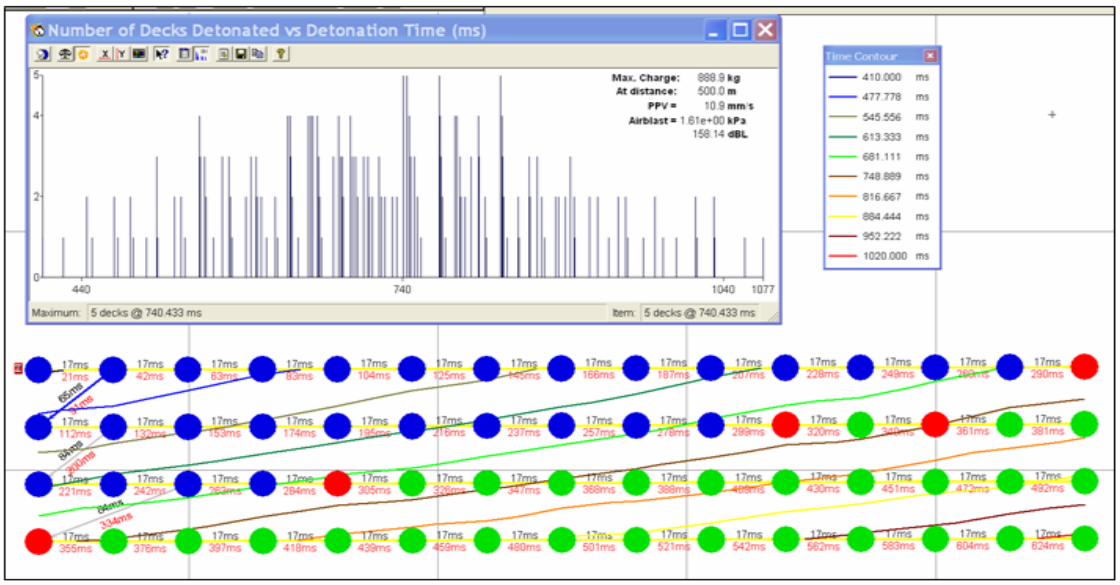

Fig. 3 Detonation timing contours along with the number of decks detonated vs. detonation time.

Ground vibration data were recorded at Sonepur Bazari project by using multi channel seismograph, i.e., Minimate Plus manufactured by Instantel, Canada. The changes in explosives charge weight per delay (Q_{max}) between the designed Q_{max} and actual Q_{max} due to scattering in delay detonators used during blasting for the blast design shown in Fig. 2, at a distance of 500 m was simulated by 2D Bench software (JKSimblast) using Monte Carlo simulation and is tabulated in Table 2. Fifteen experiments were simulated with scattering percentage varying from 1 to 15 using Monte Carlo simulation algorithm in 2D Bench software. It is evident from the results that scattering in the delay detonator has affected the actual explosive charge per delay which will result into increase in blast induced ground vibration.

3.2 Fragmentation Assessment by WipFrag

The dragline bench of Umrer project, CIL, as facing the problem of low productivity as a result of handling

Table 2 Changes in explosives charge weight per delay due to scattering in detonator timing at Sonepur Bazari project.

Designed experiment number	% of scattering	Q_{max} (with designed delay)	Q_{max} (with actual delay)
1	1	658	889
2	2	658	1,021
3	3	658	1,021
4	4	658	889
5	5	658	1,350
6	6	658	1,152
7	7	658	1,021
8	8	658	988
9	9	658	1,021
10	10	658	1,218
11	11	658	1,251
12	12	658	1,119
13	13	658	1,218
14	14	658	922
15	14	658	1,218

more oversized boulders by the dragline bucket, tight muck pile and adverse muck pile profile. The bucket size of the dragline was 10 m^3. Originally, there was no blast instrumentation at Dragline bench and the drilling and blasting parameters were optimised by trial and error method by conducting blasting experiments, using experience of blasting engineers. The drilling and blasting parameters practiced at Umrer project, before using any blast instrumentation methodology is mentioned in Table 1.

The burden relief rate of 3 ms/m was used at the mine on the basis of past experiences without using any scientific study using high speed camera. The fragmentation assessment was carried out by adopting digital image analysis technique and using the granularity software, i.e., WipFrag. The graph showing the fragment size distribution and percentage of oversized boulders was 12.76% and is shown in Fig. 4. It is evident that poor productivity of Dragline was due to significant percentage of oversized boulders.

3.3 Fragmentation Improvement by Blast Instrumentation

In order to improve the blast fragmentation at the mine, 1,000 frames per second high speed camera manufactured by MREL, Canada was used and coloured markers were suspended freely on the blast face to calculate the optimum burden relief rate. The captured photographs were analysed by using the ProAnalyst software. It was inferred that a minimum of 10 ms/m is needed at the dragline bench of Umrer project for proper onset of movement for getting the optimum fragmentation. After knowing the optimum burden relief rate, intra deck, inter hole and inter row delay interval was calculated. The modified drilling and blasting parameters after suitable blast instrumentation at Umrer project is mentioned in Table 1.

By adopting the modified drilling and blasting parameters, the percentage of oversized boulders was brought to 0%, which led to improvement in mine productivity. In order to select the suitable explosives techno-economically, geophysical technique such as seismic survey method was to characterize the rock mass using MASW (multi channel analysis of surface waves) system (Coal S&T Report MT/146). The MASW system with its various components is shown in Fig. 5. The layer wise VOD (confined velocity of detonation) at various depths of the rock mass for achieving optimal explosives energy utilisation is shown in Fig. 6. Based on the results of MASW, emulsion explosives having VOD of 5,500 m/s was used at the dragline bench as against the normal practice of using emulsion explosives having VOD of 4,500 m/s. The inter hole delay and inter row delay was computed from the burden relief rate obtained by using high

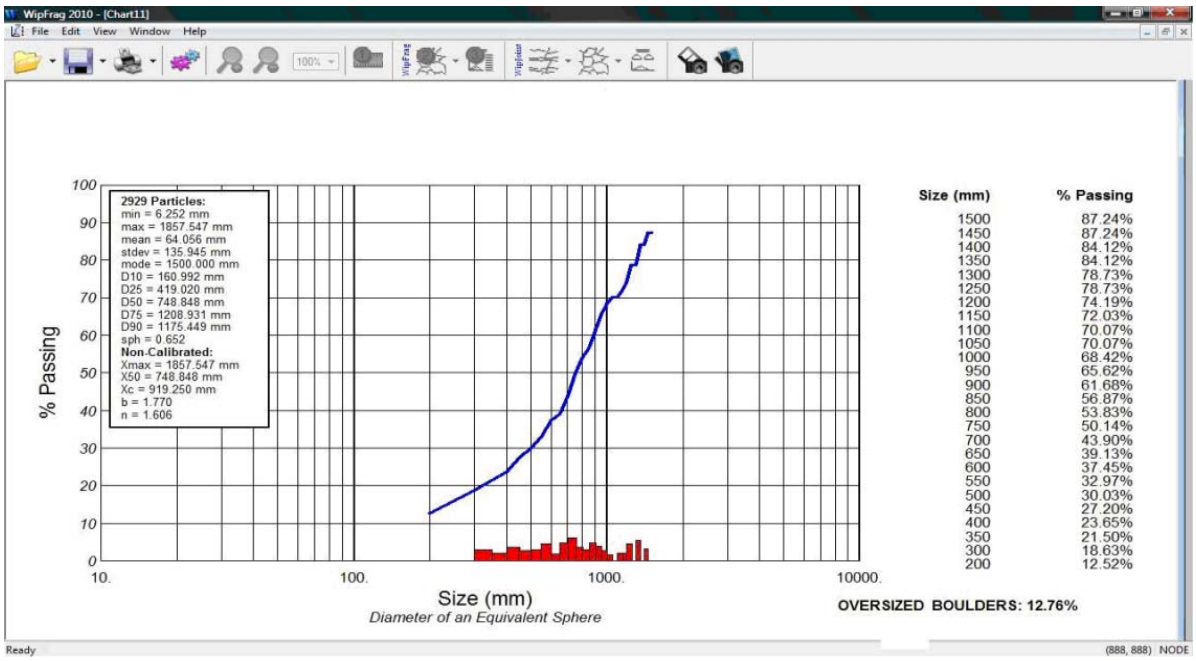

Fig. 4 Fragmentation results by using Wipfrag software at Umrer project.

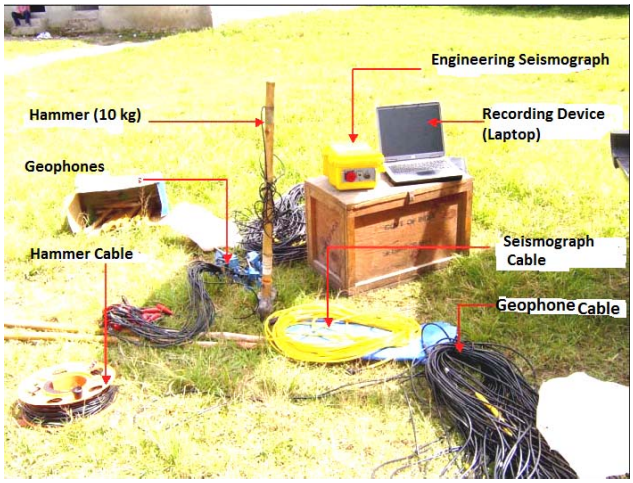

Fig. 5 Various components of the MASW system.

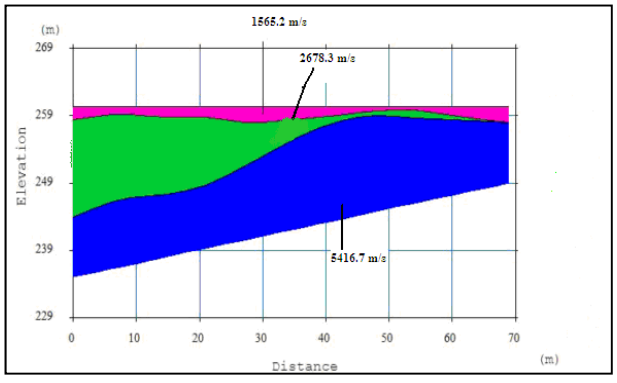

Fig. 6 VOD of explosives profile of major cluster of layers of overburden bench at Umrer project.

speed camera and ProAnalyst software. The average toe burden was obtained by using the instrument Burden finder manufactured by MDL, UK.

The fragmentation assessment, after using necessary blast instrumentation was carried out by adopting Digital Image Analysis technique and using the granularity software, i.e., WipFrag, is shown in Fig. 7. It was observed that the percentage of oversized boulders got reduced to zero and there was an increase in powder factor resulting into saving of explosives cost by 28%.

3.4 Minimum Deck Thickness between Deck Charges

Decking is a technique that enables the blaster to divide the explosives in a blast hole into two or more locations. This is accomplished by loading an inert material, such as crushed stone or drill cuttings between the explosives charges. Decking is used primarily for the following purposes:

(1) To give confinement of explosion gases where a soft seam or void is encountered;

(2) To give a better energy utilization;

(3) To cope up with vibration constraints and reduce the explosives weight per delay.

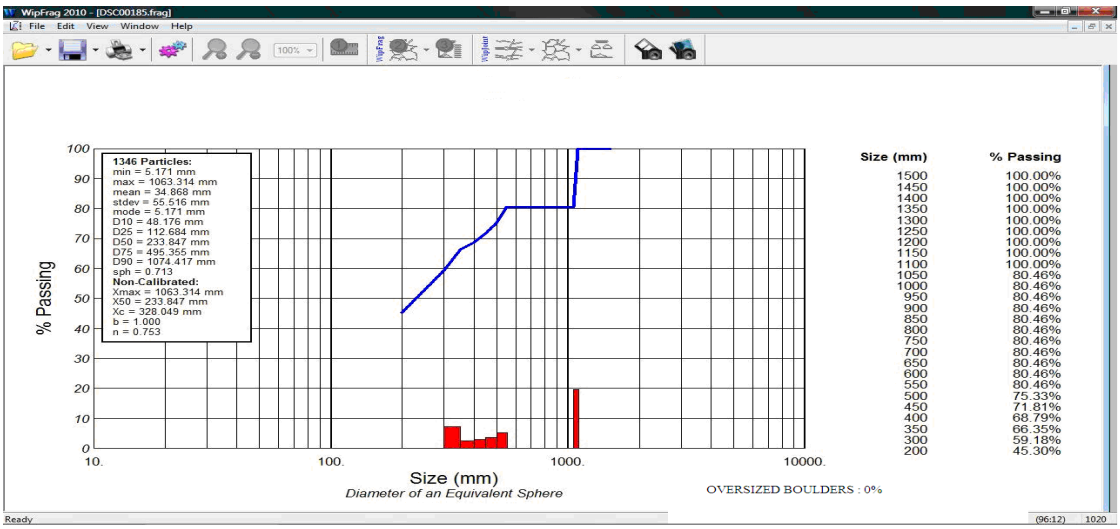

Fig. 7 Fragmentation results by using WipFrag software at Umrer project.

The reason for minimal deck thickness is to ensure that sympathetic detonation and/or cross propagation between charges does not occur. The minimal deck thickness will also ensure that there is no pressure desensitisation of explosives in upper decks due to detonation of explosives column of lower decks or adjacent boreholes arising out of pressurisation of nearby detonated boreholes. The pressure desensitisation in receptor explosive column may be classified as follows:

(1) sympathetically initiate the detonator (i.e., instantaneous detonation);

(2) sympathetic desensitisation of upper decks;

(3) sympathetic detonation of upper deck.

Pressurise the detonator in the booster and thereby increase its firing time.

The pressurisation may result into density increase or fall of sensitivity of explosives column in adjacent boreholes

In opencast blasting, the minimum bench height necessary for effective decked charges should be such as to give the ratio of $H/D > 70$, where H is the bench height (m) and D is the drill diameter (mm) [2-7]. In order to understand the role of decking on pressure desensitisation in a borehole deck, thickness was varied from 4D to 12D between the upper and bottom explosives charge columns, where D shows the borehole diameter (mm). The in-the-hole VOD of the explosives column in top deck and bottom deck explosives column was measured by Datatrap-II manufactured by MREL with the help of VOD probe cable of high resistivity, i.e., 10.8 Ω/m.

When the deck thickness was not optimum, detonation of bottom explosives column affected the top explosives column as recorded by DataTrap-II, i.e., top deck got detonated prior to the designed time delay between top and bottom explosives columns due to pressurisation. When the deck thickness was optimum, the top and bottom decks were monitored as independent events. The in-the-hole VOD of explosives plot vividly shows the actual time delay between the decks along with the in-the-hole VOD of explosives values of top and bottom explosives columns. Fig. 8 shows the typical in-the-hole VOD of explosives plots recorded in both the explosives columns in the blast hole (bottom charge and top charge) at Umrer project.

Similarly, the recorded in-the-hole VOD of explosives at Umrer project for bottom and top decks are presented in Table 3. In some cases, the top column of the explosives in the blast hole got affected due to bottom explosives pressurisation. The designed time interval between the detonators in bottom and top explosives column and the length of the deck between

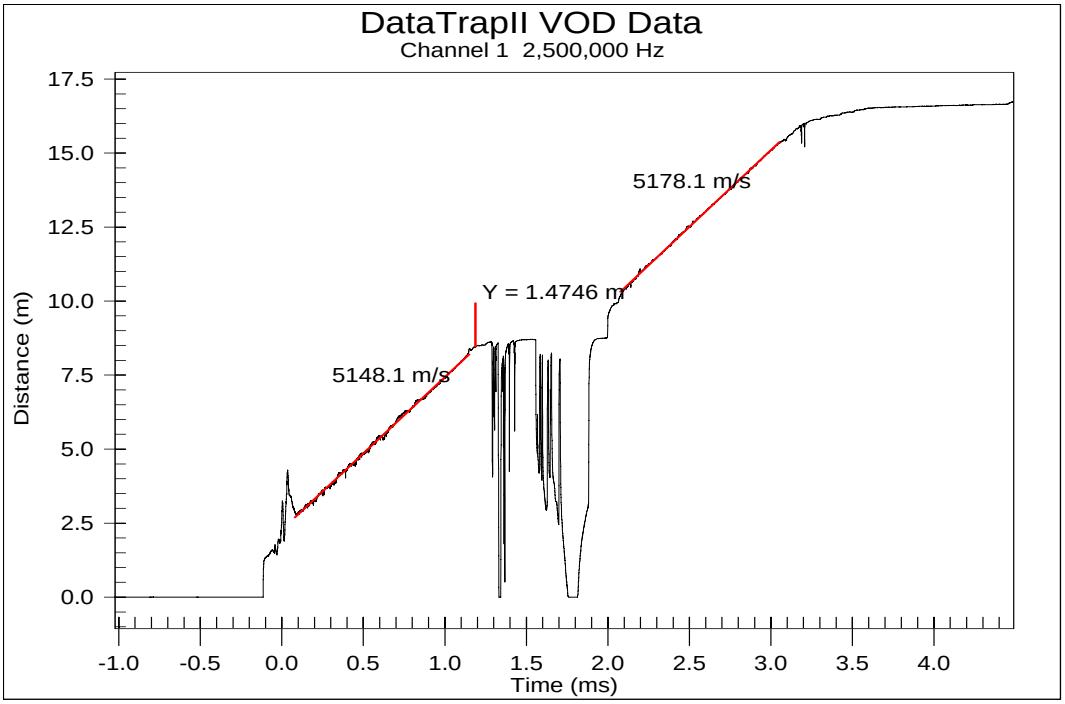

Fig. 8 In-the-hole VOD of explosives plot recorded at Umrer project.

Table 3 Designed and actual time gap between top and bottom explosives column along with measured in-the-hole VOD of explosives at Umrer project.

Sl. No.	Deck thickness in terms of drill diameter	Hole-dia-meter (mm)	In-the-hole VOD of bottom explosives column (m/s)	In-the-hole VOD of top explosives column (m/s)	Actual time gap between top and bottom explosives column (ms)	Designed Time Gap between top and bottom explosives column (ms)	Remark
UMR-1	4D	270	5,148.1	5,178.1	2.2	50	Top column got affected
UMR-2	4D	270	4,820.5	4,825.1	2.1	50	Top charge got affected
UMR-3	6D	160	4,882	4,840	3.1	25	Top charge got affected
UMR-4	6D	160	5,648	5,438	3.6	50	Top charge got affected
UMR-5	6D	250	4,778.8	4,619	3.8	50	Top charge got affected
UMR-6	8D	160	5,152	4,787	3.94	50	Top charge got affected
UMR-7	8D	270	5,019	4,567	4.8	50	Top charge got affected
UMR-8	8D	270	5,049	4,835	4.14	50	Top charge got affected
UMR-9	8D	270	5,155	4,637	3.9	50	Top charge got affected
UMR-10	10D	160	5,610.1	5,100	56	50	Top charge not affected
UMR-11	10D	270	5,270.7	5,068	58	50	Top charge not affected
UMR-12	10D	270	4,638	4,416	53	50	Top charge not affected
UMR-13	12D	160	5,213	5,014	55	50	Top charge not affected

two charges is also presented in the Table 3.

Based on the field experimentation, the optimal deck length between two explosive charges in the blast holes to obviate any chance of occurrences of pressure desensitization inside a borehole may be approximated to 10*D* as shown in Fig. 9. Thus, deck length of 10*D* may be considered as optimal deck length for Umrer project to have no likelihood of pressure desensitisation of upper deck due to detonation of bottom deck explosives charge [8]. The cast booster was positioned at a distance of 4*D* from the floor of the blasthole.

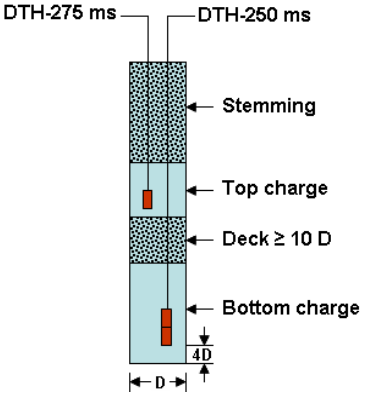

Fig. 9 Optimal deck length between explosives column in a borehole.

4. Conclusions

The scattering in delay detonators affects the techno economics of the blasting which has adverse impact on the mine productivity and economics. The scattering affects the blast performance significantly by worsening the overall blast performance by increased blast induced vibration and reduced fragmentation. There is significant impact of detonators timing and delay sequences on blast vibration characteristics and scattering in detonator timing influences the energy utilisation in rock fragmentation. The minimum deck thickness for mines of Coal India Limited using drill cuttings as decking materials should be 10*D*, where *D* shows the drill diameter to have no likelihood of pressure desensitisation of upper deck due to detonation of bottom deck explosives charge. The blast instrumentation provides improved blast performance with high degree of confidence at mine level by influencing the mine productivity. It may be concluded that blast instrumentation is a key to mine productivity and economics.

References

[1] A.K. Jha, H.K. Mishra, Chopra R.K, Safety, Security & Recent Trends in Explosives, Explo Safe Press, Nagpur, India, 2013.

[2] A.K. Debnath, A.K. Jha, Blast instrumentation-a key to mine productivity, in: Proceedings of the 23rd World Mining Congress, Montreal, Quebec, Canada, 2013, pp. 301-313.

[3] A.K. Jha, A. Biswas, IT enablement in drilling and blasting, in: Proceeding of the XXVI International Mneral Processing Congress IMPC 2012, New Delhi, India, 2012, pp. 2318-2334.

[4] C.L. Jimeno, E.L. Jimeno, F.J.A. Carcedo, Drilling and Blasting of Rocks, CRC Press, Brookfield, Rotterdam, 1995, pp. 156-157.

[5] K.W Xia, S. Huang, A.K.Jha, Dynamic tensile strength of coal, shale and sandstone using split Hopkinson pressure bar: A tool for blast and impact assessment, International Journal of Geotechnical Earthquake Engineering 7 (12) (2010) 24-37.

[6] A.K. Jha, D. Deb, N.C. Jha, Impact assessment of surface mine blasting on adjacent underground mine structures using field measurements and numerical techniques, in: J.A Sanchidrian(Ed), Rock Fragmentation by Blasting, CRC Press, Granada, Spain, 2009, pp. 571-577.

[7] A.K. Singh,A.K. Jha, A critical analysis of application of ANFO and ANFO blends in opencast coal mine blasting in India, Visfotak 6 (2011).

[8] A.K. Jha, Characterisation of Rock and Explosive Parameters for Optimal Explosives Energy Utilization in Opencast Blasting, technical report for Ministry of Coal, Government of India, India, Mar. 2010.

Journal of Geological Resource and Engineering 1 (2013) 39-45

Simulation of the Continental Plates Movement for the Earthquake Investigation

Mihail Borisovich Ignatyev[1], Tat'jana Sergeevna Katermina[2] and Vadim Aleksandrovich Nenashev[1]

1. Computer Science Department, Saint-Petersburg State University of Aerospace Instrumentation, St-Petersburg 190000, Russia

2. Computer Science Department, Niznevartovsk State University, Niznevartovsk 628605, Russia

Abstract: Predicting earthquake is old, but a very real issue. On our planet the earthquake killed thousands of people. Predicting earthquake can reduce the number of victims. There are many hypotheses about the nature of earthquakes, and one of the popular hypothesis is that the source of earthquakes links from the point of collision of continental plates, which seemed to float on the surface of the magma. Plate tectonics are confirmed by direct measurements of the speed of plates by interferometric methods and means of satellite navigation systems. The report addresses the problem of modeling the movement of continental plates. Earthquake prediction system should consist of a block of modeling movements of continental plates, the unit of measurement of the real position of slabs and blocks consideration of additional factors affecting the occurrence of earthquakes. Creating a real system of earthquake prediction requires extensive international cooperation.

Key words: Earthquake, combinatorial simulation, uncertainty, appearance, essence, cybernetical geology.

1. Introduction

As the geological studies show, the location of the continents in the past (Fig. 1) was not like in our time (Fig. 2).

Continental plates continue to move, causing earthquakes. Around the Pacific Ring of Fire, a zone of high seismic activity formed.

The prediction of the earthquakes is a very old and complicate problem [1, 2]. We try to simulate the movement of the continental plates and to measure the real movements of continental plates by means of satellite systems.

2. Linguo-combinatorial Modeling the Movement of Continental Plates

Only a small number of real systems have the mathematical models. First of all, the system described using natural language. Method to transition from description on neutral language to mathematical equations is proposed. For example, suppose there is a phrase:

$$\text{WORD1} + \text{WORD2} + \text{WORD3} \quad (1)$$

This phrase denotes the words and only implies the meaning of words. The sense in the current structure of natural language is not indicated. It is proposed to introduce the concept of meaning in the following form:

$$(\text{WORD1}) \times (\text{SENSE1}) + (\text{WORD2}) \times (\text{SENSE2}) + (\text{WORD3}) \times (\text{SENSE3}) = 0 \quad (2)$$

A_i denote Appearances, Ei denote Essences. Then Eq. (2) can be represented as:

$$A_1E_1 + A_2E_2 + A_3E_3 = 0 \quad (3)$$

Eqs. (2) and (3) patterns are phrases (1). If we have a mathematical equation $F(x_1, x_2, x_3) = 0$, we can obtain a form (3) by differentiating this equation, then A_i will be partial derivative and E_i—time derivatives of variables.

This model is an algebraic ring and we can resolve the Eq. (3) or of the A_i or of the E_i by the introduction of the third group of variables — the arbitrary coefficients of Us [3, 4].

Corresponding author: Mihail Borisovich Ignatyev, professor, research fields: computer science, cybernetical geology. E-mail: ignatmb@mail.ru.

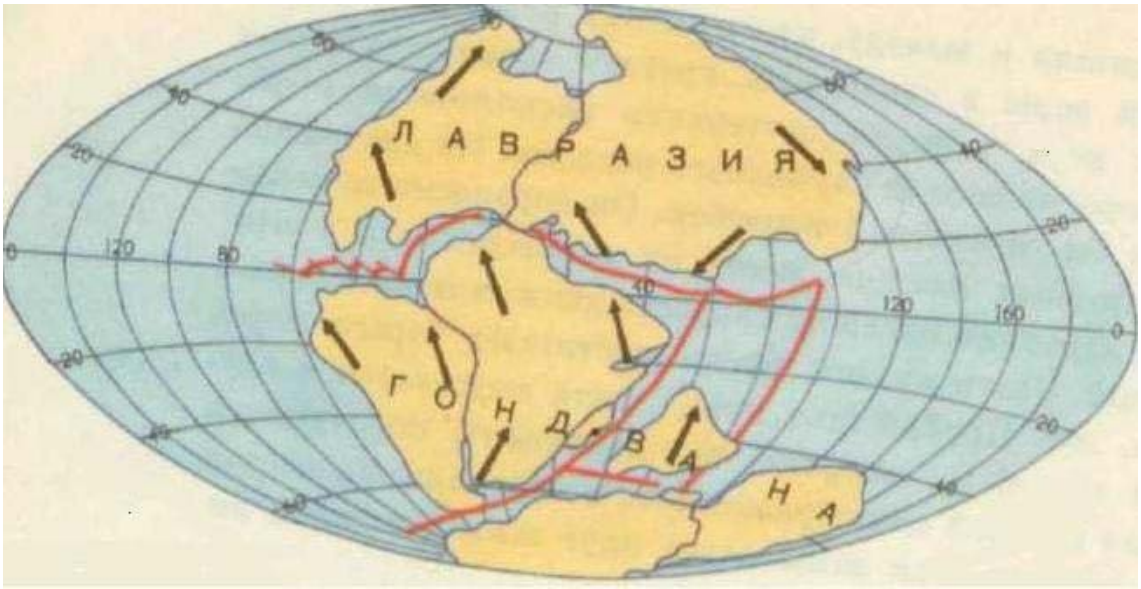

Fig. 1 Location of the continents in the past.

Fig. 2 The location of the continents nowadays.

$$A_1 = U_1 E_2 + U_2 E_3, A_2 = -U_1 E_1 + U_3 E_3,$$
$$A_3 = -U_2 E_1 - U_3 E_2 \quad (4)$$

$$\text{or } E_1 = U_1 A_2 + U_2 A_3, E_2 = -U_1 A_1 + U_3 A_3,$$
$$E_3 = -U_2 A_1 - U_3 A_2 \quad (5)$$

where U_1, U_2, U_3—the arbitrary coefficients, which can be used for the most extensive range of tasks on the manifold (3). For example, if we want to reach the maximum of the variable x_3, we can assign arbitrary coefficients $U_2 = -b A_1$, $U_3 = -b A_2$, and then obtain

$$dx_1/dt = U_1A_2 - bA_1A_3, dx_2/dt =$$
$$-U_1A_1 - bA_2A_3, \quad (6)$$
$$dx_3/dt = b(A_1A_1 + A_2A_2)$$

And if $b > 0$, then the variable x_3 consistently committed to the maximum, and to manipulate the trajectory remains the coefficient U_1.

If we have two phrases:

$$A_{11}E_1 + A_{12}E_2 + A_{13}E_3 + A_{14}E_4 = 0 \quad (7)$$
$$A_{21}E_1 + A_{22}E_2 + A_{23}E_3 + A_{24}E_4 = 0 \quad (8)$$

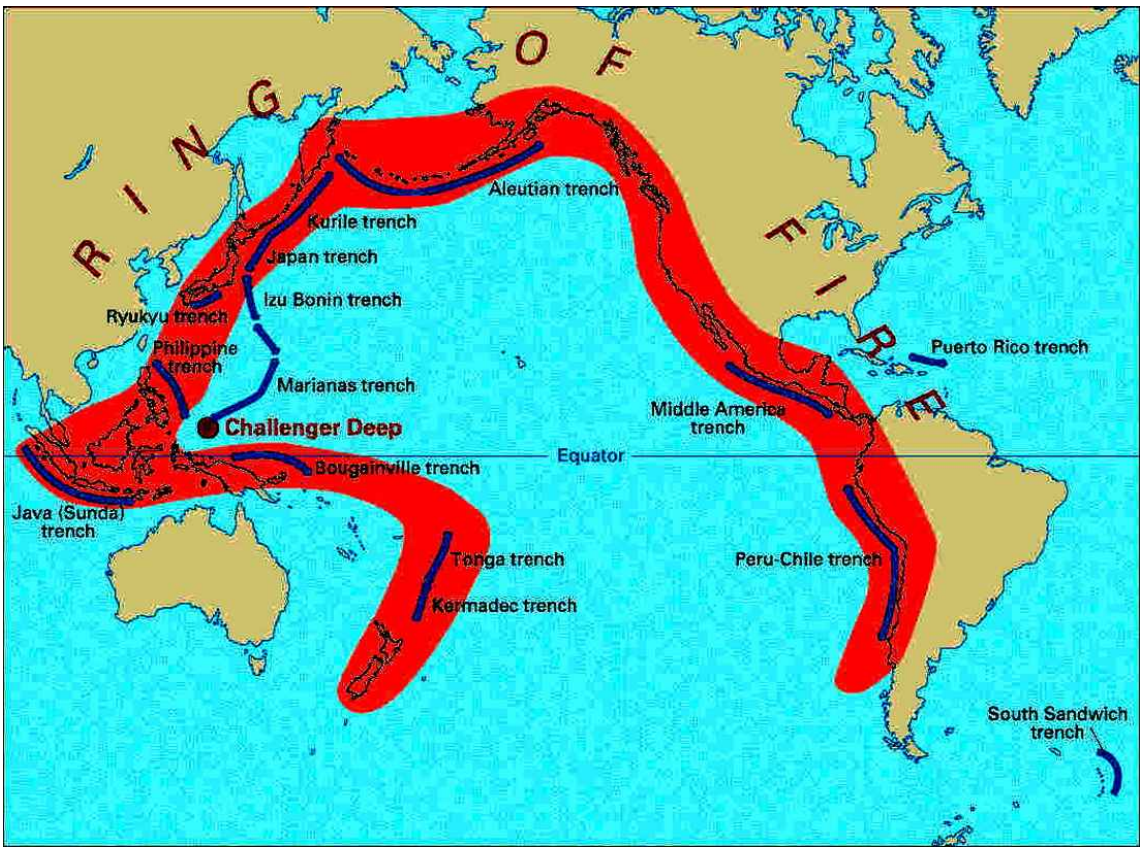

Fig. 3 Zone of high seismic activity.

then the structure of the equivalent equations will contain four arbitrary coefficients and these equations:

$E_1 = U_1D_{23} + U_2D_{24} + U_3D_{34}$, $E_2 = -U_1D_{13} - U_2D_{14} + U_4D_{34}$, $E_3 = U_1D_{12} - U_3D_{14} - U_4D_{24}$, $E_4 = U_2D_{12} + U_3D_{13} + U_4D_{23}$ (9)

Where U_1, U_2, U_3, U_4—arbitrary coefficients, $D_{12} = (A_{11}A_{22} - A_{21}A_{12})$, etc..

In general, if we have n variables and m manifolds limits, the number S is an arbitrary coefficient equal to the number of combinations of n to $m + 1$ [3-14] refer to (Table 1).

$$S = C_n^{m+1}, \qquad n > m \tag{10}$$

The number of arbitrary coefficients is a measure of uncertainty and adaptability. Linguo combinatorial modeling is that in a particular subject area highlights key words, which are combined into phrases like Phrase. (1), which are constructed on the basis of equivalent systems of equations with arbitrary coefficients. In the particular case, they may be differential equations and their study can be used by a well-developed mathematical tools. Linguo-combinatorial modeling includes all combinations of embodiments and all solutions and is useful in the study of heuristics badly formalized systems [3-5].

Geologists distinguish the 8 major plates, which cover 90% of the Earth's surface, including plates—Australian, Antarctic, African, Eurasian, Hindustan, the North American, Pacific and South American. There are more medium sized tectonic plates.

Each of the plates can be considered as a single word, and the method of linguistic and combinatorial modeling determine the structure of the equations with arbitrary coefficients. These equations define the entire structure of the interactions between the plates, all the combinatorial interactions. It is obvious that a large number of plates structure equivalent equations will contain a large number of arbitrary coefficients,

Table 1 The number of arbitrary coefficients depending on *n* and *m*.

m/*n*	1	2	3	4	5	6	7	8
2	1							
3	3	1						
4	6	4	1					
5	10	10	5	1				
6	15	20	15	6	1			
7	21	35	35	21	7	1		
8	28	56	70	56	28	8	1	
9	36	84	126	126	84	36	9	1

which determines the difficulty of predicting earthquakes. Simulation of the motion of plates is an important area of research and we need to define the ultimate capabilities of this method.

If we denote the characteristic Australian plate A_1^1 through A_2^1 characteristic Antarctic plate, A_3^1—the African plate, A_4^1 — the Eurasian plate, A_5^1 — Hindustan plate, A_6^1 — North American, A_7^1 — Pacific, A_8^1 — South America, in accordance with Refs. [3, 4], the equation will be the Earth's surface:

$$A_1^1 \times E_1 + A_2^1 \times E_2 + \ldots + A_8^1 \times E_8 = 0 \quad (11)$$

where E_1 — to change the characteristics of the Australian plate, E_8—changing characteristics of the South American plate, and when you consider that the plates are placed on the surface of the geoid, which is the second restriction on the variables of the system.

$$A_1^2 \times E_2 + A_2^2 \times E_3 + \ldots + A_8^2 \times E_8 = 0 \quad (12)$$

Then the structure will contain the equivalent equations with arbitrary coefficients

$$S = C_8^3 = 56$$

The structure will look like

$$\begin{aligned} E_1 &= U_1 \times D_{23}^1 + U_1 \times D_{24}^1 + \ldots + U_{21} \times D_{78}^1; \\ E_2 &= -U_1 \times D_{13}^2 - U_2 \times D_{14}^2 + \ldots + U_{36} \times D_{78}^2; \\ &\ldots\ldots\ldots\ldots\ldots\ldots\ldots\ldots\ldots\ldots\ldots\ldots \\ E_8 &= U_6 \times D_{12}^8 + U_{11} \times D_{13}^8 + \ldots + U_{56} \times D_{67}^8 \end{aligned} \quad (13)$$

where U_1, U_2, ..., U_{56}—arbitrary coefficients, which can be used to set the various movements of the continental plates at the geoid, and

$$D_{12} = A_1^1 \times A_2^2 - A_2^1 \times A_1^2 \text{ etc.}$$

Each board has its own shape. To simulate the movement of plates and visualize these movements in an accelerated time scale, each of the plates is the intersection of a cone, which is the source of the direct image of the center of the earth and pass through the plate boundary on the surface of the geoid. So we can put these plates on the model of the globe, and set plate movement by assigning appropriate values of arbitrary factors, not thinking yet about the forces that affect the movement of plates. For simplicity, we can model each of the plates placed on a separate bowl, and then consider these balls together, analyzing the possibility of a collision of plates, based on their shape [5]. In solving these complex computational problems it is advisable to use cloud recursive structures.

3. The Measurement of the Movement of Continental Plates

Each of the tectonic plates is several thousand square kilometers of the Earth's surface located on its forests, rivers, lakes, deserts, steppes, and in many places they go far into the ocean. They move through the interaction of different forces within the Earth, and outside of it (Fig. 3). The problem is that moving these crustal blocks that make up the Earth's upper shell—the lithosphere—in different directions. Some of them are moving away from the old neighborhood, and some the contrary—come closer to them too close. As a result, there is tension on the borders that appear at one point, the rapid release of energy. In continental or oceanic part of bark there are various, a pore of

enormous force shifts, breaks, resets, bursts. They turn in earthquakes, tsunamis, volcanic eruptions and other natural disasters.

People have long tried to predict the time of occurrence of such disasters, resulting in casualties. Significant results achieved so far failed, and why scientists are still working on new methods of forecasting.

To get a picture of the plate movements across the globe and identify the areas with weak or strong tectonic phenomena, it is necessary to accurately determine the coordinates of the reference points. This problem can solve modern satellite location systems (Glonass, GSM). Radar satellite systems are an overview of the Earth's surface (continental plates) to form a radar image (LI). To form a radar image data are used with the device location station synthetic aperture (synthetic aperture radar).

SAR (Synthetic aperture radar)—a method that allows to obtain radar images of the earth surface and all embedded objects.

The advantage is the availability of data regardless of the weather conditions and the level of natural light areas with detail comparable to aerial photographs. The data obtained in the microwave radio, are a unique source of information on the underlying ground surface. They allow you to define the vertical displacement with high accuracy (up to several millimeters), which is an alternative to the costly and labor-intensive ground-based measurements.

Technology Satellite-SAR (Fig. 4) is a complex system, where the final image is formed by locating on the basis of data from all satellites.

Our task must be to conduct highly accurate monitoring of at least three reference points located on the same plate.

The subsequent analysis is carried out in conjunction with all available geological and geophysical information and to minimize the costs for the design and implementation of land and marine geophysical and drilling operations, ensuring at all stages of the operational forecast are refined.

The result of the satellite system is a high-precision control of changing the position of the reference points and the direction of the continental plate (Figs. 5 and 6).

For the full application of SAR-data for solving the problem of modeling, the movements of continental plates have been developed data processing software in the form of software modules.

The developed model is monitoring each of the continental plate.

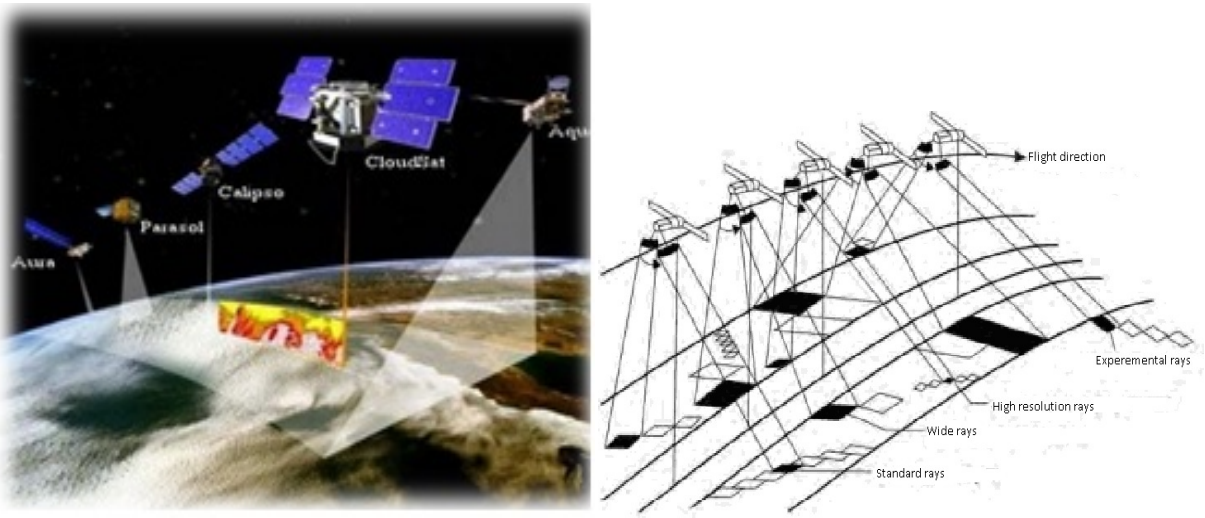

Fig. 4 System of synthetic aperture radar satellites.

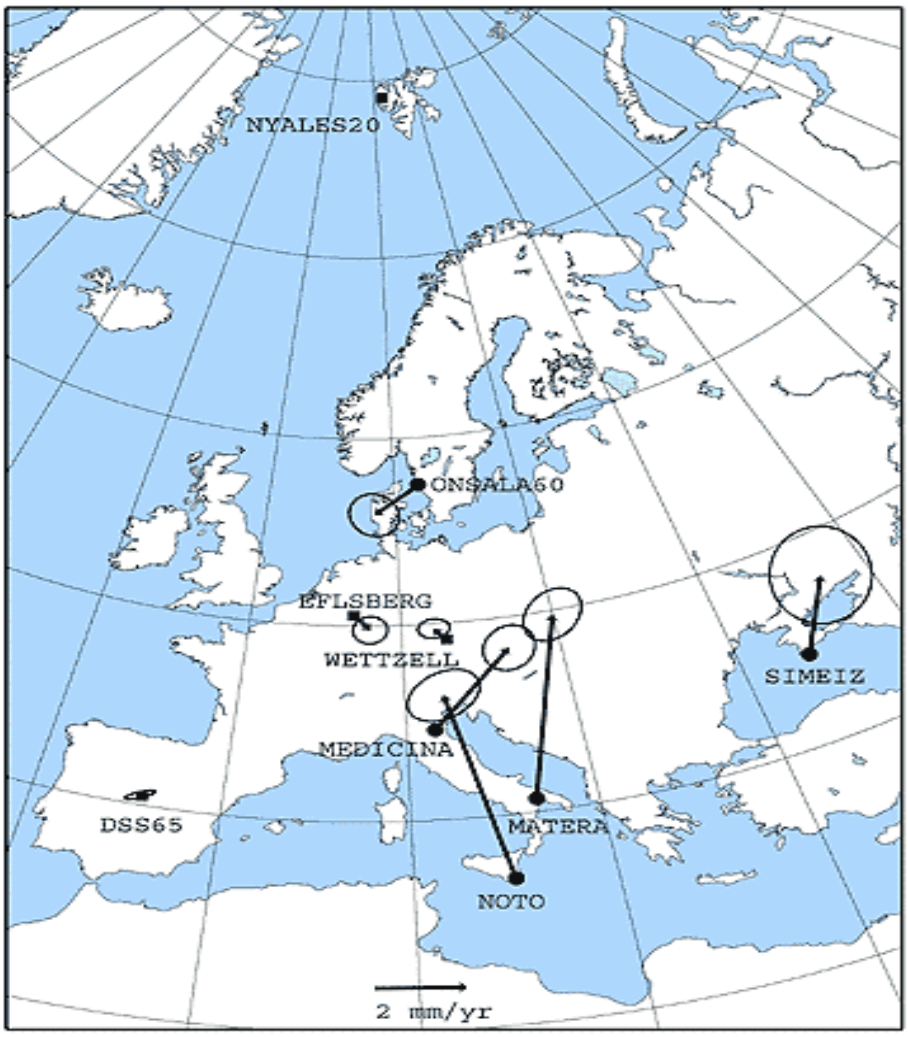

Fig. 5 Continental plate with control points and direction.

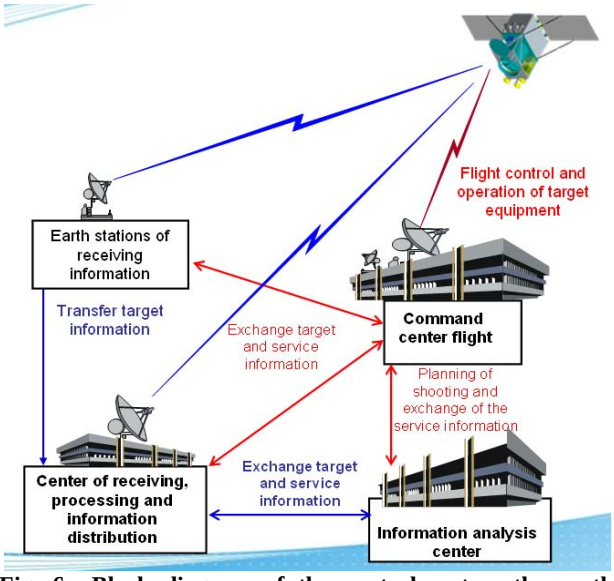

Fig. 6 Block diagram of the control system the earth surface.

4. Conclusions

First the mathematical simulation of the movement of continental plates had proposed by means of linguo-combinatorial approach. The general scheme of earthquake prediction should include blocks of simulation of the plates movement and blocks of measurements of position and velocity of real plates with the help of satellite navigation. Model parameters have to be adjusted according to the results of measurements. There will be more points of measurement of these parameters, the prediction of earthquakes will be more exact. To create a real system of earthquake prediction, more scientific research and international cooperation are required.

References

[1] A. Wegener, The Origin of Continents and Oceans, Akademizdatcenter “Nauka” RAS, Moscow 1984.

[2] A. Koch, R. Hart, Plate Tectonics, Mir-publishers, Moscow, 1989.

[3] M.B. Ignatyev, Holonomical automatic systems, Leningrad, AN USSR, Moscow, 1963.

[4] M.B. Ignatyev, Theory of complex systems and cybernetic picture of the world, St. Petersburg, 2011.

[5] M.B. Ignatyev, T.S. Katermina, The method of redundant variables for monitoring and diagnosis of computing processes in real time, Journal Proceedings of the SPIIRAS 3 (26) (2013).

[6] V.I. Krylov, Space Geodesy, Moscow, 2002.

[7] B.H. Wellenhof, GPS—Theory and Practice, Wien, 2009.

[8] B.C. Verba, L.B. Neronsky, I.G. Osipov, Radar systems zemleobzora space-based, Communications Technology Publishing, Moscow, 2010.

[9] Y.D. Shirman. Computer Simulation of Aerial Target Radar Scattering Recognition, Detection and Tracking, Artech House, Boston, London, 2002, p. 294.

[10] D. Barton, G. Ward., Handbook of Radar Measurements, in: M.M. Veysbeyn (Ed.). Sov. radio, Moscow, 1976, p. 392.

[11] J.D. Shearman, Electronic systems: Fundamentals of the Theory Handbook, Communications Technology Publishing, Moscow, 2007, p. 512.

[12] G.S. Kondratenkov, Radars view of the earth, in: G.S. Kondratenkov, V.S. Potekhin (Eds.), Radio and Communication Publishing, Moscow, 1983, p. 272.

[13] P.I. Dudnik, Multifunction radar systems: Studies, in: P.I. Dudnik, A.R. Ilchuk(Eds.), Mgeoid, Annual for High Schools, Drofa, 2007, p. 283.

[14] M.B. Ignatyev, Cybernetic Picture of the World, Complex Cyber-Physical Systems, SUAI Publishing, St-Petersburg, 2011, p. 472.

Journal of Geological Resource and Engineering 1 (2013) 46-54

Seismic Behavior of Offshore Wind Turbine with Gravity Foundation

Hao Yu and Xiangwu Zeng

Department of Civil Engineering, Case Western Reserve University, Cleveland 44106, Ohio, USA

Abstract: The development of offshore wind energy becomes very fast in recent years due to its clean, safe, and high efficiency. However, the issue that quite a few offshore wind farms have been built in seismic active areas raises a great engineering challenge for the selection, design, and seismic evaluation of offshore wind turbine foundations. Earthquake is one of the most critical hazards for offshore wind turbines. The softening of soil due to pore water pressure buildup can sharply reduce the bearing capacity of the foundation, and consequently result in stability failure. The induced strong structural vibration has adverse impact on the normal operation of wind turbine as well as on the efficiency of power generation. In this study, a group of earthquake centrifuge tests was performed on a physical model of a wind turbine with gravity foundation. The seismic behavior of both the structure and the foundation soil was analyzed based on the recorded accelerations, pore water pressures, lateral displacements and settlements. The emphasis was on the interaction between foundation and soil. The results showed that gravity foundation can effectively resist the overturning moment induced by the superstructure. However, it was quite sensitive to the subsoil conditions. The large settlement and tilt in the offshore foundation might affect the performance of a wind turbine.

Key words: Offshore wind turbine, gravity foundation, seismic responses, centrifuge tests.

1. Introduction

For offshore wind farms located in seismic active regions, a great challenge has been the seismic analysis and design of the foundation for wind turbines. However, without any proven experience and failure cases, the studies on seismic resistance of offshore wind foundations are quite immature.

The gravity base is one of the most preferred foundations for offshore wind turbines as a result of its low installation cost. This type of foundation is widely used in shallow water with the depth of up to 20 m, by directly sitting on the seabed or embedding some portion into the soil. The dimension of the reinforced concrete base typically ranges from 12 m to 18 m and the weight is up to thousands of tons [1]). Accordingly, the gravity foundation depends mainly on the massive self-weight to provide stability against the loads transferred either from the superstructure or from the surrounding soils and water.

The seismic analysis of gravity foundation for offshore wind turbines is particularly complicated due to the distinct structural features and harsh offshore environment. The stability of a foundation under earthquake loading is one of the most important issues. In particular, if the soil in the foundation is sand, the seismic-induced liquefaction might cause significant failures. Currently, the studies of wind turbine stability under earthquake conditions are based on the local building codes, i.e. Eurocode 8 [2], International Building Code [3], and American Society of Civil Engineers 7-05 [4]. However, these criteria cannot directly address the wind turbine problems because of the different structural properties. Quite a lot of model tests, both physically and numerically, were conducted on the similar structures under seismic loading (Yoshimi and Tokimatsu [5], Liu and Dobry [6], Bazeos et al. [7], and Chakrabortty et al. [8]). The results of those researches may help to understand the behavior of offshore foundations for wind turbines.

Corresponding author: Hao Yu, Ph.D., research field: geotechnical engineering. E-mail: hxy88@case.edu.

The centrifuge test, as an accessible and economically viable modeling technique, has been widely used in the field of offshore engineering (Finn et al. [9], Madabhushi and Schofield [10], Martin [11]). In this study, a group of earthquake centrifuge tests was conducted on a wind turbine model with gravity foundation. The seismic behaviors of the model were measured in both dry and saturated condition in order to compare the seismic resistance of gravity foundation for onshore and offshore turbines. In addition, the soil behaviors in the free field and adjacent to the foundation were studied in the two different conditions.

2. Test Program

2.1 Test Facilities and Soil Deposit

The wind turbine model was tested on the geotechnical centrifuge at Case Western Reserve University. The centrifuge has a 1.37 m radius and 20 g-ton capacity. A hydraulic shaker designed by TEAM Corporation is mounted on the centrifuge platform. It can generate 1-D earthquake shaking during the flight. The details of the Case Western Reserve University centrifuge were reported by Figueroa et al. [12]. The container is a rigid rectangular box with internal dimensions of 53.3 cm (length) × 24.1 cm (width) × 17.7 cm (height).

The soil layer was constructed at 1 g (g = acceleration of gravity) by using the well graded Toyoura sand with D_{50} = 0.17 mm. The sand was uniformly poured from the height of 80 cm to keep the relative density at about 68%. The thickness of soil deposit was 4.5 m (in prototype scale under 50 g). In saturated tests, the soil was saturated by de-aired water under vacuum. The water table was maintained 1.5 m above the ground surface to simulate the offshore condition.

2.2 Model Configuration and Test Procedures

The model was prepared according to the structural features of offshore wind turbines in the real situation, which can be divided into three parts: tower head, wind tower, and foundation. As shown in Fig. 1, the tower head was simplified as a lumped mass, including the mass of the nacelle, generator, gearbox, etc. at the top of the tower rod with large slenderness ratio. Such tower-like structure was expected to induce strong vibration and large overturning moment during the earthquakes. The gravity foundation was modeled by using an aluminum block which is much heavier than the superstructure. The gravity base was embedded 1.5 m in the soil to prevent lateral sliding and the average contact pressure of the structure on the subsoil was about 70 kPa. The details of each part were described in Table 1. It should be pointed out that due to the size limitation of the centrifuge model, the prototype structure simulated by the tests was about one fourth of the size of a typical offshore wind turbine. However, the essential characteristics of such a structure were captured by the model and the results of the study can still provide insights about the seismic behavior.

The testing model was instrumented by ACC (accelerometers), PPT (pore pressure transducers), and LVDTs (Linear Variable Differential Transducers). The detail model profile as well as the instrument layout was depicted in Fig. 1. A 1-D synthetic earthquake (Fig. 2) was applied along the base when the model spun to a 50 g gravitational field. In the meantime, acceleration, pore pressure and displacement time histories were recorded by the installed sensors. The settlements of both the structure and the soil were measured by the corresponding LVDTs. Centrifuge scaling laws [13] were employed to evaluate the corresponding prototype behavior of the model.

Table 1 Wind turbine models in the centrifuge tests.

Component	Dimension (m)	Weight (t)
Tower head	1.75 × 1.75 × 1.25	10.6
Wind tower	L = 13; D = 0.5	6.25
Gravity base	3.75 × 3.75 × 2	75.9

In prototype units; L = length; D = diameter.

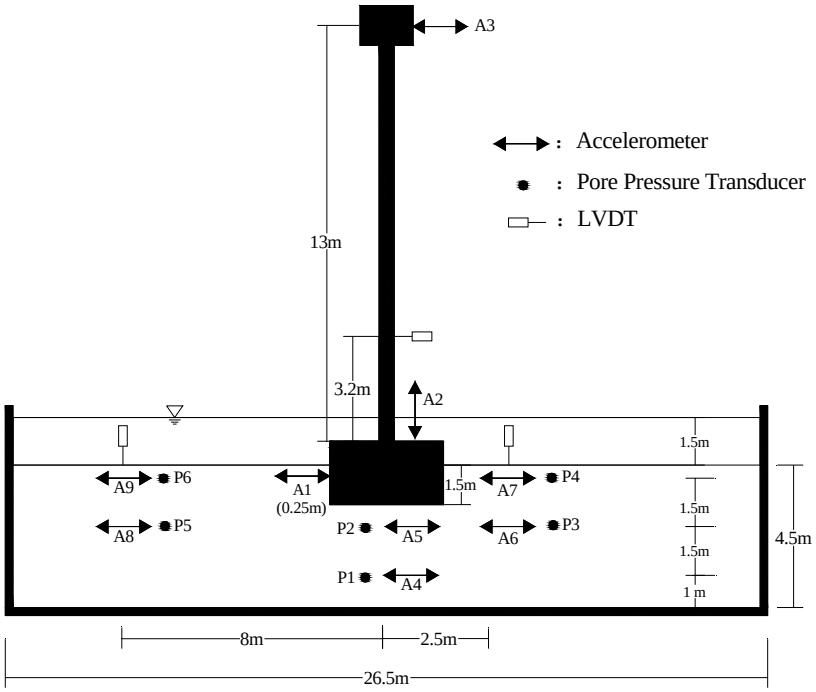

Fig. 1 Model configuration in the saturated tests (in prototype unit).

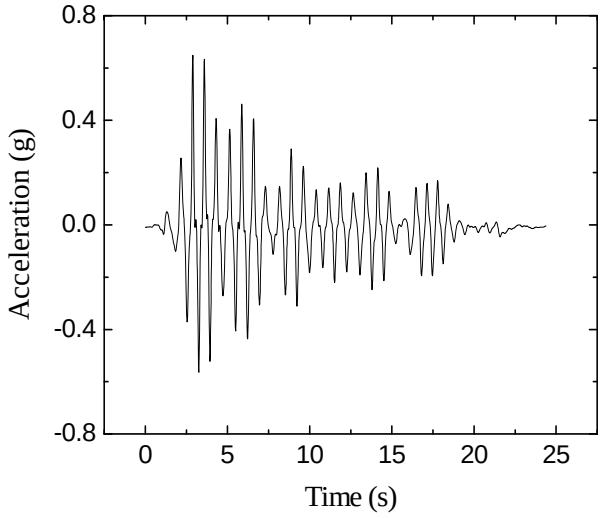

Fig. 2 Typical input acceleration.

3. Test Results

3.1 Seismic Behavior of Model in the Dry Test

The model test in dry condition was aiming to examine the behaviors of onshore wind turbine under earthquake loading. As shown in Fig. 1, the soil accelerations under seismic loading were measured in three different locations: underlying the structure (ACC4 & 5); adjacent to the foundation (ACC6 & 7); and in the free field (ACC8 & 9) where the soil would not be affected by the structure or the boundary of container. In the dry tests, the recorded time histories of accelerations in the prescribed locations (Fig. 3) exhibited identical waveform and magnitude to the input motion as shown in Fig. 2. Therefore, the dense dry sand could be considered as an efficient media for seismic wave propagation.

A majority of earthquake energy imparted from the stiff soil to the embedded structure. Consequently, there was relatively strong response measured in the gravity base by ACC1 and in the tower head by ACC3 (Fig. 4a). ACC2 was installed vertically on the foundation but some distance away from the center (Fig. 1). Thus the recorded time histories by ACC2 could, to some extent, represent the rocking condition of the gravity foundation, which seemed negligible in the onshore condition. The lateral displacement of the turbine was illustrated in Fig. 5a. The residual displacement of the structure was quite small during the seismic loading. Even during the strong shaking period, the huge mass of gravity base foundation could provide enough stability to the superstructure

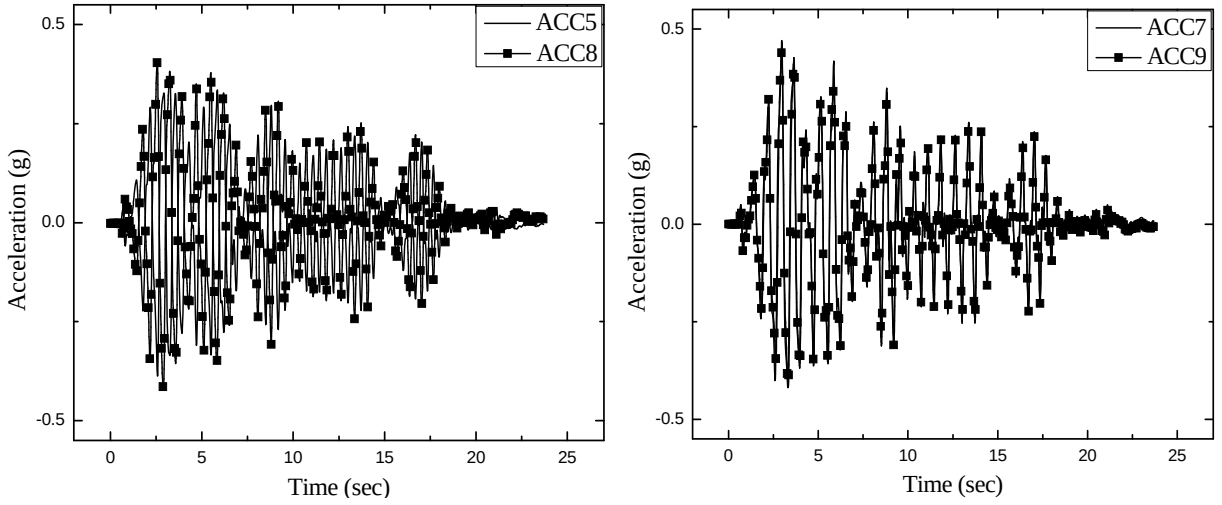

Fig. 3 Recorded time histories of accelerations in the dry soil.

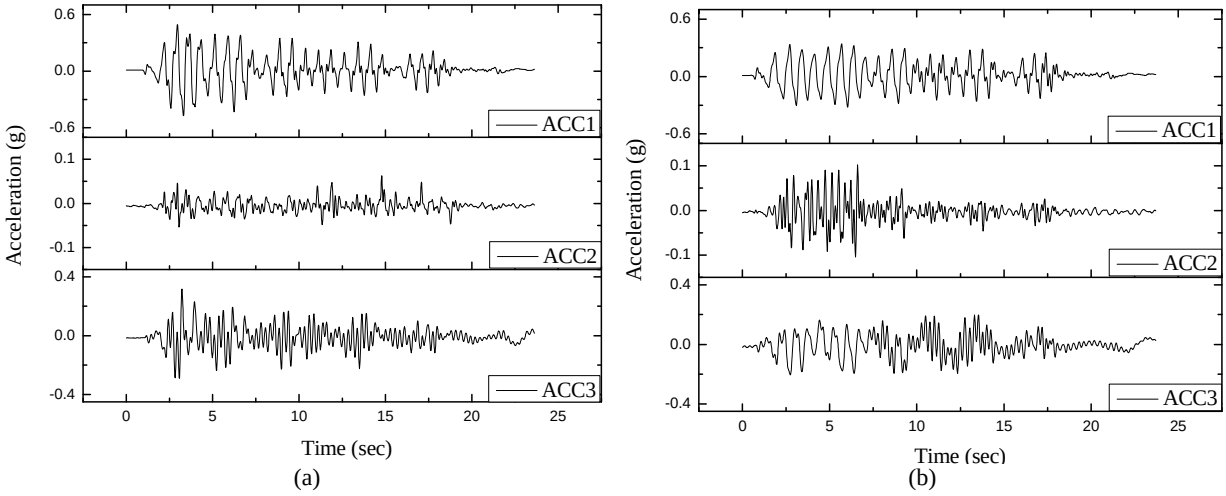

Fig. 4 Accelerations of gravity model in (a) dry test and (b) saturated test.

against the dynamic vibration.

Fig. 6 compared the recorded settlements of the wind turbine structure and the ground surface. It was found that the settlements in the dry condition were quite insignificant. The soil layer was compacted by only 6 cm after shaking. And the structure settled even less than the ground surface. However, there were many obvious oscillations in the time history curve, which might reveal the rocking of the foundation. In addition, little difference was observed between the settlements in the adjacent field and in the free field. Therefore, in the dry condition, the existence of structure might not influence the seismic behavior of adjacent soils.

3.2 Seismic Behavior of Model in the Saturated Test

The model test was performed in the saturated condition in order to simulate the offshore wind turbine under earthquakes. In this case, the soil showed quite different behaviors in the different locations due to the development of pore water pressure. The pore pressure transducers were installed in pair with the accelerometers at the corresponding locations (Fig. 1).

The existence of water has also largely changed the structural behavior during the earthquake. The extensively excess pore water pressure softened the soil layer and consequently increased the soil damping

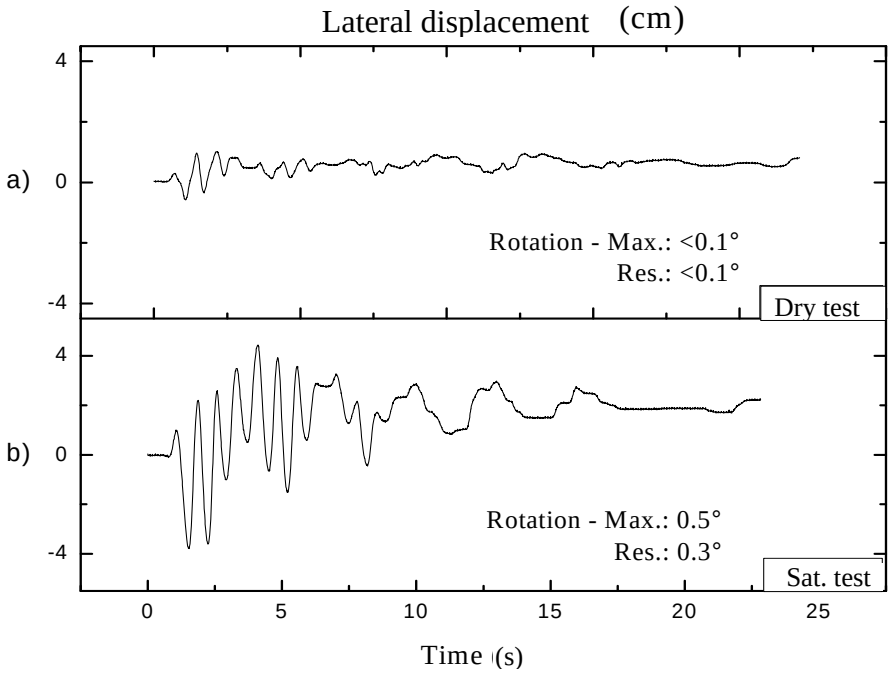

Fig. 5 Recorded time histories of superstructure lateral displacements in (a) dry test, (b) saturated test (Max. = maximum rotational angle; Res. = residual rotational angle).

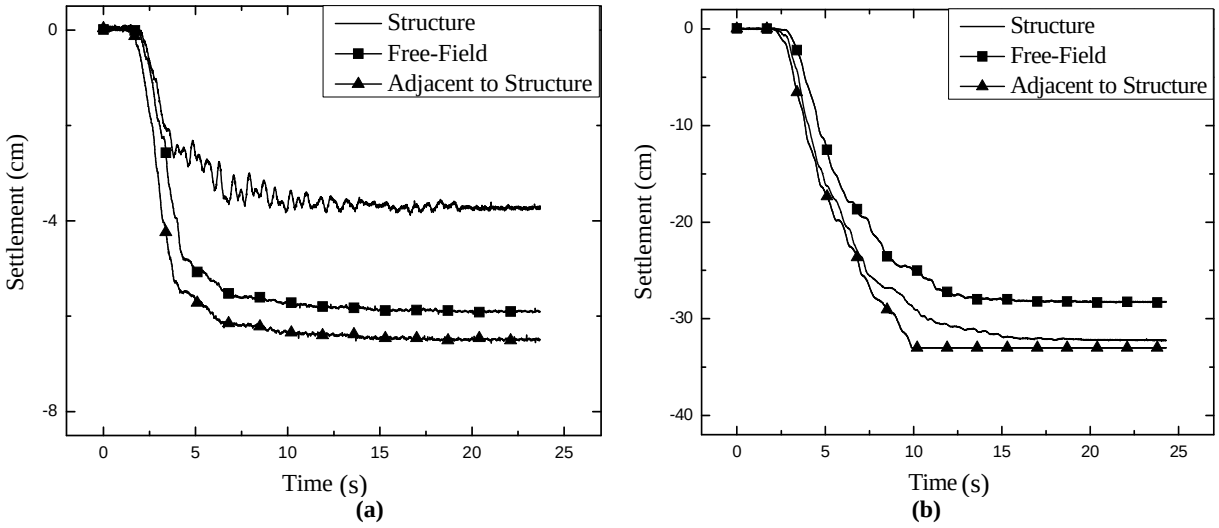

Fig. 6 Settlements of structure and ground surface in (a) dry test and (b) saturated test.

to the propagating earthquake energy. As seen in Fig. 4b, the recorded accelerations in the foundation (ACC1) and tower head (ACC3) were reduced compared with those in the dry condition. However, the rocking of gravity base (ACC2) was significantly amplified during the strong shaking. Accordingly, the vibration of superstructure was evidently increased. As shown in Fig. 5, the maximum lateral displacement during the shaking was about 4 cm in the saturated condition, which was much larger than that in the dry condition. However, the residual tilt was still within the acceptable level. The conclusion could thus be drawn that the gravity base foundation has a great resistance to the overturning moment during the seismic loading.

The settlements of structure and ground surface also exhibited huge difference in the saturated condition. As shown in Fig. 6b, the structure and ground sunk more than 25 cm which was much larger than those in

the dry test. In particular, the structure settled a bit faster than the ground in the free field. It was observed that most part of the structural settlement occurred during the strong shaking (2-7 s) while the dissipation of pore water pressure after strong shaking contributed quite a small portion. In addition, the structural settlement surpassed the ground settlement in the free field, which might cause adverse impacts on the stability and normal operation of the wind turbine. Moreover, it was noticed that the settlements of soil in the adjacent field was larger than that in the free field, which might be affected by the interaction with the foundation.

According to Fig. 7a, the pore pressure ratios (ratio of increment of pore water pressure to the effective stress of soil) were compared in the depth 2 m under the ground surface. Clearly, the pore pressure ratio generated under the structure (PPT2) was much smaller than in the free field (PPT5). Correspondingly, the response measured by ACC5 under the structure (Fig. 8) did not change too much compared to that measured in the dry test. However, with the significant increase of pore water pressure in the free field, the soil was largely softened associated with the stiffness reduction in the soil near ACC8 (Fig. 8b) during the corresponding period 2-7 s. After that, pore water pressure began to dissipate and the soil gradually regained its stiffness.

In the top layer, the pore pressure ratio of soil in the free field reached to 1 at the 4th second (PPT6, Fig. 7b) when the soil was completely liquefied. The acceleration in ACC9 (Fig. 8c) was greatly attenuated and the liquefaction process lasted through the 12th second. The recorded pore pressure ratios in the soil adjacent to the foundation (PPT3 & 4) were a bit smaller than those at the same depth in the free field (Fig. 7), which might be influenced by the confining pressure and the dynamic soil-structure interaction. Accordingly, the attenuations of soil responses in the adjacent field (ACC6 & 7, Fig. 8), by contrast, seemed to be smaller during the strong shaking.

4. Analysis of Testing Results

The effectiveness of gravity foundation depends primarily on the soil condition, although it exhibited great seismic resistance to the overturning moment induced by the wind tower. In comparison of the onshore turbine and offshore turbine under the identical earthquake loading, it was found that the soil and structure exhibited quite different responses in these two conditions. The stiff dry soil could provide sufficient bearing to the wind turbine. In this condition, the structural settlement and tilt were minimized. However, the pronounced seismic response in the

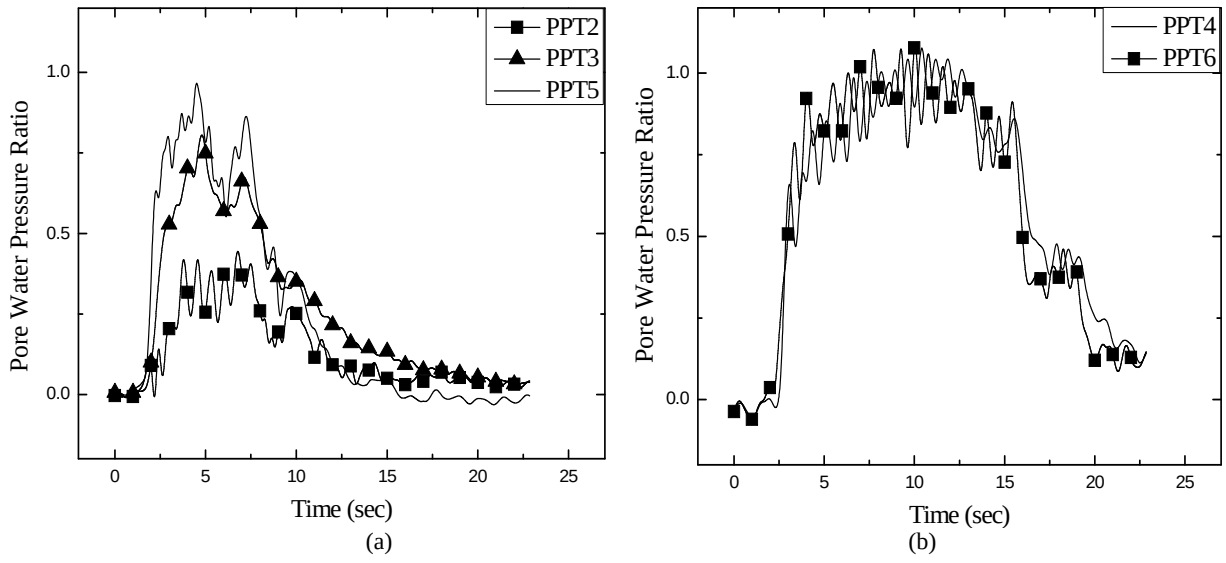

Fig. 7 Recorded time histories of pore pressure ratio in the saturated soil.

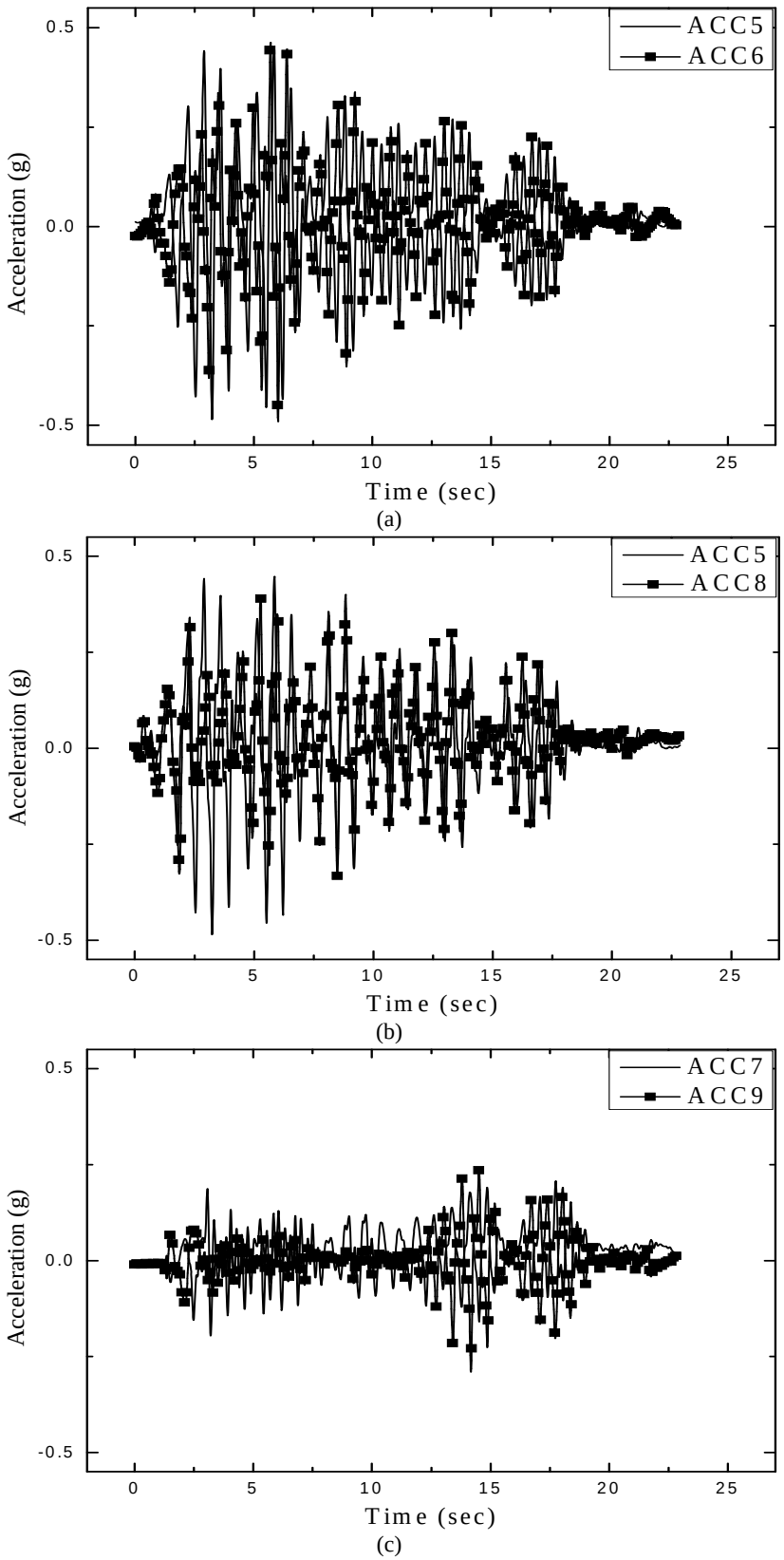

Fig. 8 Recorded time histories of accelerations in the saturated soil.

foundation and superstructure would amplify the dynamic vibration imposed on the onshore wind turbine. On the other hand, the softened soil in the saturated condition could strongly attenuate the propagating seismic energy to the gravity base. But the excessive structural settlement was expected which may cause damage the offshore wind turbine [14].

In spite of the complexity and uncertainty, the SSI (soil-structure interaction) under earthquakes has been widely studied in recent decades, Stehmeyer, Bhattacharya and Adhikari [15-17]). The effect of SSI was expected to be more pronounced in the softer soil than in the stiff soil [18] (Rizos and Stehmeyer). By contrast, the frequency and response of structural motion in the saturated test decreased while the rocking of structure was amplified attributing to the buildup of pore water pressure under the structure. In addition, the soil around the foundation (PPT4) liquefied, at which time the lateral support of soil to the embedded portion of gravity base was totally lost. As seen in Fig. 5, the dynamic peak rotational angle increased from less than 0.1° in the dry condition to 0.5° in the saturated condition. It was also found in Fig. 7a that, due to the increased overburden pressure, the soil underlying the structure exhibited higher resistance to pore pressure generation. The excessive structural settlement was due not only to the compression of the soil layer, but also to the local subsidence induced by the amplified structural rocking. Similar researches have been conducted by Bartlett [19], Martin and Lam [20], Pecker and Pender [21], and Gajan et al. [14]. It was found that the amplified rotation periodically decreased the contact area of foundation base on each side. The yielding of soil underlying the base occurred, contributing to accumulated settlement of the structure by extruding the weakest soil away from underneath the structure [22]. In addition, the inertial force induced by superstructure vibration tended to amplify this mechanism. However, such deduction needs further validation by numerical analysis [23].

In the development of multi-megawatt offshore wind turbine, the gravity foundation with large mass and base area is needed to provide sufficient stability to the large-scale superstructure. However, the structural settlement and tilt are still the most challenging risks, which were found to be directly related to the contact pressure of the structure and its height/width ratio [24]. The mitigation schemes of shallow foundations under earthquakes have been widely researched. Most of efforts were spent on improving the structural design and employing alternative foundations (e.g., use pile foundations or new type gravity base foundation) [25]. However, the application of such schemes on offshore wind turbines needs to be validated in further studies.

5. Summaries and Conclusions

In this paper, a group of centrifuge model tests for seismic response of offshore wind turbine with gravity foundation have been performed in order to exam the structural stability. The model test in the dry condition simulated the condition of onshore wind turbine, which was also used to compare the seismic behavior with the offshore condition. Based on the measured responses in both soil and structure, the results can be concluded as:

(1) Gravity base foundation can provide sufficient stability in the onshore condition. However, the pronounced structural acceleration will amplify the dynamic vibration imposed on the onshore turbine.

(2) The offshore wind turbine with gravity base foundation exhibited great resistance to the overturning moment and toppling under earthquakes. However, the softened soil, due to the buildup of pore water pressure, tends to cause larger structural settlement and tilt in addition to the effect of soil-structure interaction.

(3) Without proven experience of offshore wind turbine under earthquake loadings, the analysis of structural behaviors and mitigation schemes for gravity foundation need to be further verified through

physical modeling and numerical simulation.

References

[1] G. Gerdes, A. Tiedemann, S. Zeelenberg, Case Study: European Offshore Wind Farms—A Survey for the analysis of the experiences and lessons learnt by developers of offshore wind farms, Technical report for Pushing Offshore Wind Energy Regions, Deutsche Windguard Department, University of Groningen, 2006.

[2] Eurocode 8: Design provisions for earthquake resistance of structures, DD ENV 1998-1-1, BSI, 1996.

[3] International Building Code 2006, International Code Council, Country Club Hills, US, 2006.

[4] Minimum Design Loads for Buildings and Other Structures, ASCE 7-05, American Society of Civil Engineers, 2006.

[5] Y. Yoshimi, K. Tokimatsu, Settlement of building on saturated sand during earthquakes, Soil and Foundations 17 (1) (1977) 23-38.

[6] L. Liu, R. Dobry, Seismic response of shallow foundation on liquefiable sand, Journal of Geotechnical and Geoenvironmental Engineering 123 (6) (1997) 557-567.

[7] N. Bazeos, G.D. Hatzigeorgiou, I.D. Hondros, H. Karamaneas, D.L. Karabalis, D.E Beskos, Static, seismic and stability analyses of a prototype wind turbine steel tower, Engineering Structures 24 (2002) 1015-1025.

[8] P. Chakrabortty, R. Popescu, J.H. Prevost, Tower structures on liquefiable soil excited by random seismic input [CD-ROM], in: 9th ASCE Specialty Conference on Probabilistic Mechanics and Structural Reliability, ASCE, Albuquerque, NM, 2004.

[9] W.D.L. Finn, R.S. Steedman, M. Yogendrakumar, R.R. Ledbetter, Seismic response of gravity structures in a centrifuge, in: 17th Offshore Technology Conference, Houston, Texas, 1985.

[10] S.P.G. Madabhushi, A.N. Schofield, Centrifuge modeling of tower structure on saturated sands subjected to earthquake perturbations, Geotechnique 43 (4) (1993) 555-565.

[11] C.M. Martin, Impact of centrifuge modeling on offshore foundation design, in: Proceedings of International Symposium “Constitutive and Centrifuge Geotechnical Modelling: Two Extremes”, Ticino, Switzerland, 2002, pp. 135-153.

[12] J.L. Figueroa, A.S. Saada, H. Dief, Development of the geotechnical centrifuge at Case Western Reserve University, Centrifuge 98 (1) (1998) 3-8.

[13] A.N. Schofield, Cambridge geotechnical centrifuge operations, Geotechnique 30 (3) (1980) 227-268.

[14] S. Gajan, B. Kutter, J. Phalen, T. Hutchinson, G. Martin, Centrifuge modeling of load-deformation behavior of rocking shallow foundations, Soil Dynamic and Earthquake Engineering 25 (2005) 773-783.

[15] J. Stewart, R. Seed, G. Fenves, Empirical Evaluation of Inertial Soil-Structure Interaction Effects, Technical report for Pacific Earthquake Engineering Research Center, University of California, Berkeley, California, 1998.

[16] E.H. Stehmeyer, Computational simulations of linear soil-foundation-structure systems under dynamic and seismic loading, M.S. Thesis, Department of Civil Engineering, University of South Carolina, 2003.

[17] S. Bhattacharya, S. Adhikari, Experimental validation of soil-structure interaction of offshore wind turbines, Soil Dynamics and Earthquake Engineering 31 (2011) 805-816.

[18] D. Rizos, E. Stehmeyer, Simplified seismic analysis of soil-foundation-structure systems including soil-structure interaction effects, in: 13th World Conference on Earthquake Engineering, Vancouver, B.C., Canada, 2004.

[19] P.E. Bartlett, Foundation rocking on a clay soil, M.S. Thesis, University of Auckland, School of Engineering, New Zealand, 1976.

[20] G. Martin, I.P. Lam, Earthquake resistance design of foundation: Retrofit of existing foundations, in: Proceedings of GeoEngineering 2000 Conference, Melbourne, Australia, 2000, pp. 19-24.

[21] A. Pecker, M. Pender, Earthquake resistance design of foundation: New construction, in: Proceedings of GeoEngineering 2000 Conference, Melbourne, Australia, 2000, pp. 19-24.

[22] S. Dashti, J.D. Bray, J.M. Pestana, M.R. Riemer, D. Wilson, Mechanisms of seismically-induced settlement of buildings with shallow foundations on liquefiable soil, Journal of Geotechnical and Geoenvironmental Engineering 136 (1) (2010) 151-164.

[23] D. Pitilakis, M. Dietz, D.M. Wood, D. Clouteau, A. Modaressi, Numerical simulation of dynamic soil-structure interaction in shaking table testing, Soil Dynamics and Earthquake Engineering 28 (2008) 453-467.

[24] R. Sancio, J.D. Bray, T. Durgunoglu, A. Onalp, Performance of buildings over liquefiable ground in Adapazari, Turkey, in: Proceedings of 13th World Conference on Earthquake Engineering, 2004, pp. 935.

[25] U. Hartwig, T. Bierer, J. Sommer, Full-scale model tests on a gravity base foundation for offshore wind turbines, in: 21st International Offshore and Polar Engineering Conference, Maui, Hawaii, USA, 2011.

Journal of Geological Resource and Engineering 1 (2013) 55-60

Cooling Systems for Borehole Tools

Benedict Holbein, Jörg Isele and Luigi Spatafora

Institute of Applied Computer Science, Karlsruhe Institute of Technology, Herrmann-von-Helmholtz-Platz-1, Eggenstein-Leopoldshafen, Baden-Württemberg 76344, Germany.

Abstract: Since 2012 the work on a cooling system for borehole probes is going on at the IAI. It is supposed to allow the usage of standard electronics, as a first approach in borehole environments at 5 km depth, with 200 °C and 600 bar. Within ZWERG, the cooling system serves as base to realize different measurement operations without time limitations. Therefore it contains an insulation to reduce outer heat input, an active cooling system to cool down components which are sensitive to heat inside, like electronics, as well as a cooled room where the electronic can be installed. The first approach based on the example borehole in Soultz-sous-fôret, France (5 km, 200 °C) shall initiate further project in this field, with the perspective to conduct measurement operations in even hotter boreholes. Alternative methods of heat management in borehole probes investigated and developed at IAI, are high temperature electronics and PCM-systems.

Key words: Cooling, deep geothermal energy, borehole tools, down-hole monitoring.

1. Introduction

The deep geothermal energy has the potential to play an important role for the energy supply of the future although it stays behind his possibilities so far. This is caused by several problems the technology has to fight with. There is a high investment risk which is linked to the difficulties of aiming exactly at the aquifer. Additionally it is impossible to optimize running plant processes without real-time data of the open[1] hole. Risks caused by seismic activities cannot be predicted either and the public acceptance is suffering. All this problems are mainly influenced by a lack of information of geothermal wells during the whole life cycle, starting with the drilling until the energy production [1].

Because of the extreme conditions in geothermal boreholes, namely the high temperatures and pressures pared with highly corrosive thermal waters, like in Iceland, the use of measurement devices is difficult [2]. Many standard electronics do not stand temperatures above 70 °C, high-temperature components are rare and very expensive [3]. These circumstances make a cooling system necessary. For short operations of a few hours, a PCM (phase change material) concept, where the PCM i.e. ice takes away the harmful heat while changing its phase that can do the job. The cooling effect in this case is limited by the mass of PCM material carried inside the probe. An increased mass of carried PCM for longer cooling also increases the length of the probes. This brings difficulties for their handling with it and provokes higher heat-input from outside [4]. Another method, the cooling by Peltier-elements only enables low cooling capacities, which will not be sufficient for most applications [5]. Therefore, it would be helpful for widespread borehole investigations to have a functional unlimited-cooling-system as basic module of a system platform for various measurement operations called ZWERG, with which is help it be possible to quickly construct different tools for different application, serving “blueprints” for repeating components [6]. To realize operation-times of several weeks, we are developing an active cooling system at the Institute of Applied Computer Science. This system is based on the principle of a cooling-machine and make it

Corresponding author: Benedict Holbein, B.Sc. main research field: cooling of in borehole tools. E-mail: benedict.holbein@kit.edu.

possible to perform measurement and monitoring operations over the complete life-cycle of geothermal wells, starting with the drilling phase and ending with the running plant. Doing so, it makes an important contribute to overcome the lack of borehole-data and the problems of geothermal energy in general.

2. Applications

The cooling system will be usable within the complete lifecycle of boreholes (Fig. 1). Thereby it allows generating widespread information in all phases of geothermal energy production.

The cooling system could for example cool a SPWD (seismic prediction while drilling) unit to realize the investigation already during the drilling phase. This would help targeting exactly the aquifer [7]. Afterwards it could be used for widespread pre-investigations of water chemic to specifically adjust plant parameter and components. While energy production, by a cooled probe generated real-time data would allow risk predictions and enable intervention and process optimization in time.

3. Conditions and Concept

The expected operation conditions for the cooling system corresponding to the operation depth of 5 km are: surrounding temperatures up to 200 °C and surrounding pressure up to 600 bar.

To realize the cooling function during time periods of several weeks, the system conducts a thermodynamic cycle process with a refrigerant. The refrigerant evaporates at a temperature below 70 °C inside the cooled room and gets compressed by a compressor at a pressure higher than the vapor pressure (of refrigerant) at 200 °C. Like this the refrigerant can condense at a temperature above the surrounding temperature (200 °C) while it transfers heat to the borehole.

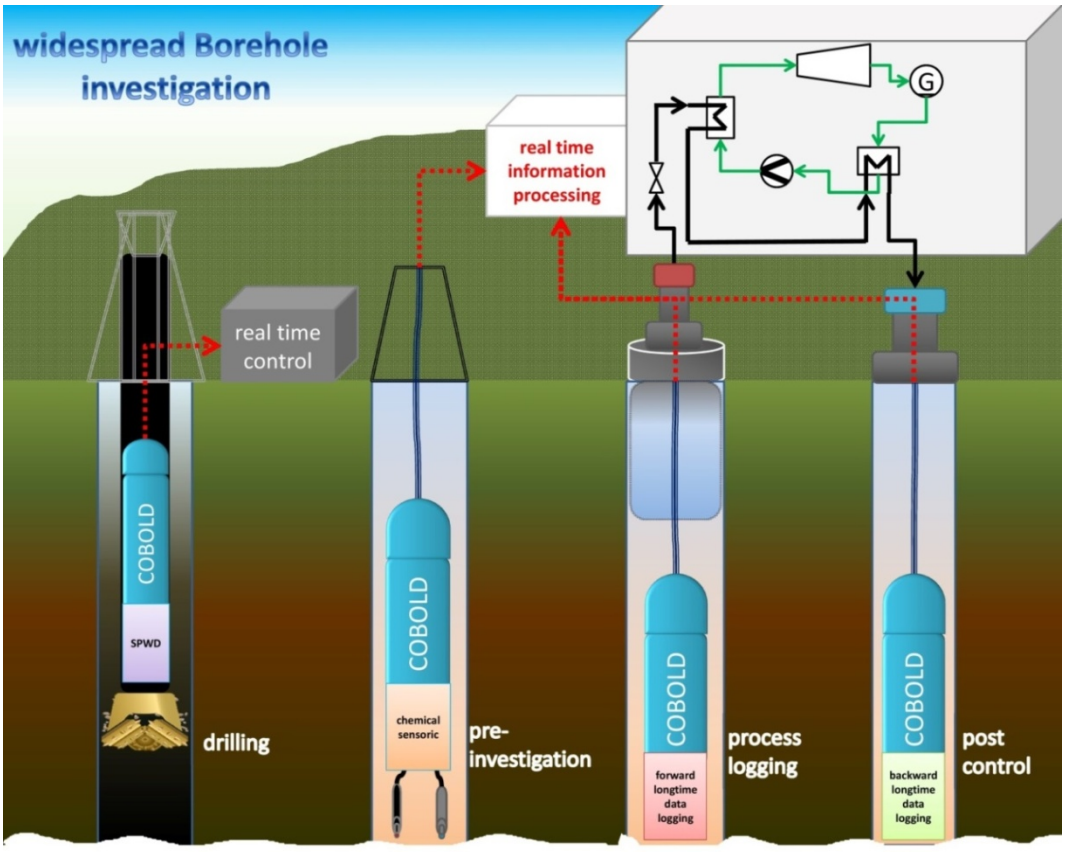

Fig. 1 Overview over different application options for the cooling system.

To close the process, the condensed substance passes an expansion to start-pressure and start-temperature.

4. The Cooling Machine

4.1 Cycle Process

As refrigerant, acetone is regarded at the moment. The evaporation temperature at atmospheric pressure is about 56.5 °C, which is far enough below 70 °C. This means that electronics temperatures can be kept below 70 °C as well. The condensing temperature when compressed at 40 bar is 220 °C, thus the temperature gradient to the borehole temperature is sufficient to transfer the heat to the surrounding. Fig. 2 shows the complete cycle in a log p-h (pressure enthalpy) plot.

The compression process is assumed as polytropic compression. With Eq. (1) the required compression effort can be calculated. The achievable cooling capacity can be estimated with the enthalpy balances of the plot (Fig. 2) or calculated using Eq. (2).

$$P_{com.} = \mathrm{d}m/\mathrm{d}t \times R \times T \times \frac{n}{n-1} \times [(\frac{p_2}{p_1})^{\frac{n-1}{n}} - 1] \quad (1)$$

where, dm/dt is mass flow, R is gas constant, T is temperature and p is pressure.

$$\dot{Q}_{cool.} = \mathrm{d}m/\mathrm{d}t \times [\frac{\mathrm{d}p}{\mathrm{d}T} \times T_1 \times x \times (v'' - v') \quad (2)$$

where, in the equation after Clausius Clapeyron, dp/dT is the temperature dependent pressure gradient; T_1 is the evaporation temperature, x the liquid ratio, v'' the specific superheated and v' the specific saturated steam volume [9].

Table 1 shows the most important process parameters, calculated with different approaches. The polytropic compression approach seems to generate the most realistic results compared with first experimental results. According to that, a cooling capacity of 100 W could be achieved with nearly similar effort for the compression.

Experiments for the validation of the insulation of the cooling housing showed that outer heat inputs of around 20 W have to be expected. Thus approximately 80 W heat could be transferred from the probe in the described constellation. For many of the electronic systems this would be sufficient. In case of higher heat input, this system is flexible, thus cooling capacity can be increased according to an increased mass-flow by increasing the compressor frequency.

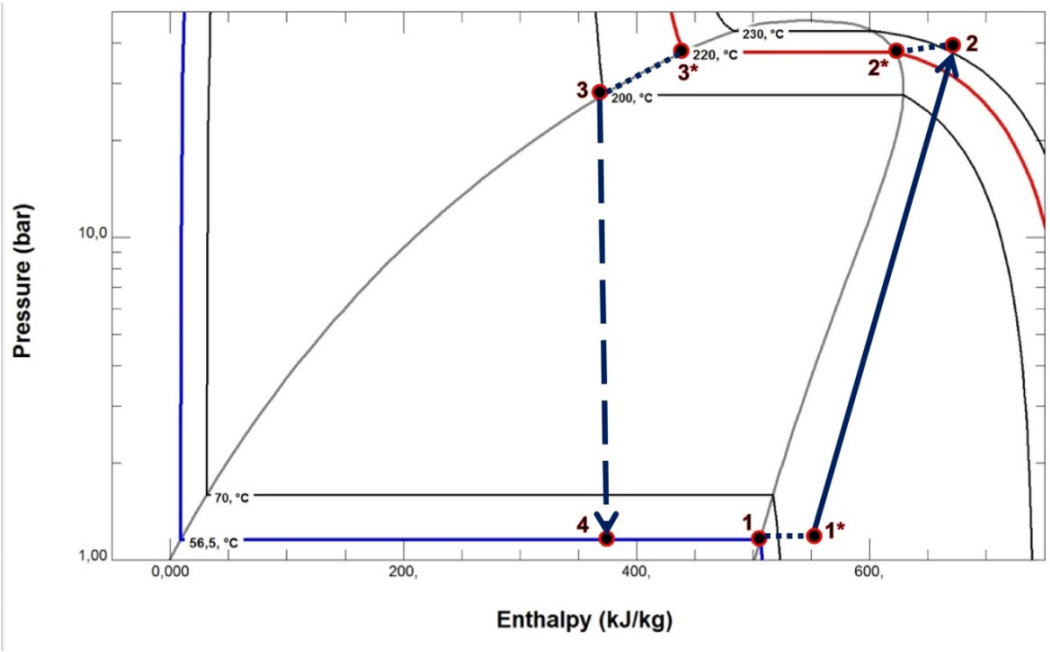

Fig. 2 Log p-h plot of the cooling cycle [8].

Table 1 Calculated process parameter.

Used input parameters						
Adjusted mass-flow d*m*/d*t* (kg/h)	Evaporation temperature T_1 (K)	Starting pressure p_1 (bar)	Final pressure p_2 (bar)	Gas constant *R* [J /(kg-K)]	Pressure gradient d*p*/d*T* (bar/ K)	Measurement mass-flow d*m*/d*t* (kg/h)
2	324.15	1.19	40.93	143.15	0.05	~ 1.97
Calculated process parameters						
Calculation approach	Cooling capacity (W)	Compression effort (W)	Heat output (W)	Liquid ratio *x*	Polytropic exponent *n*	
Idealistic approach	353.7	77.28	431	-	-	
Polytropic compression approach	114.49	112.35	118.14	0.4	1.13	
Measurement projection approach	94.3	96	190.37	0.38	-	

4.2 Materials

The material question is an important one as four every down-hole tool. It is a great field and will not be discussed in detail in this paper. So far, nickel-based alloys i.e. Inconel 718 are preferred for outer elements such as the housings and the condenser. Because of their high mechanical strength combined with high corrosion and temperature resistance, they are a good choice.

Their disadvantages are the high costs and low machinability, thus a lot of effort is put in the development of manufacture techniques and geometrical simple design. For the seal problematic perfluorinated rubber seals, which stand high temperatures and aggressive refrigerant substances are tested.

4.3 Probe Engineering

To realize the described process, the central components evaporator, compressor, condenser and expansion valve are required. Furthermore, a cool-room-housing with sufficient insulation and installation surface for the components, which has to be cooled down. The insulation consists of a vacuum, located in the double wall of the housing and MLI (Multi Layer Insulation) at the inner wall. Experiments showed that this structure can reduce the outer heat input significantly [10].

Fig. 3 shows a possible assembly of the components. From the right you can see a sensor unit as exemplary application which is connected to the cool-room-housing. Inside the evaporator with installed electronic is located. The compressor housing which also contains the expansion valve is connected to the evaporator. An electrical driven version (fitted) for the use with wire line, as well as a hydraulic driven variant for drill string operations is showed. At the upper end the condenser as outer heat exchanger is mounted. The whole system is closed as cycle.

5. Results and Current Works

So far, the experiment results show good properties for the heat transfer and support the impression of the suitability of acetone as refrigerant. Other refrigerants are tested parallel.

Fig. 4 shows the possible cooling process with R113. At the moment, we are realizing an experimental assembly to display the complete cooling process with realistic surrounding conditions. Therefore, an experimental compressor with pneumatic engine which reaches the required final pressure has been engineered and manufactured (Fig. 5). An evaporator prototype as well as a condenser

Fig. 3 Computer aided design illustration of the cooling system.

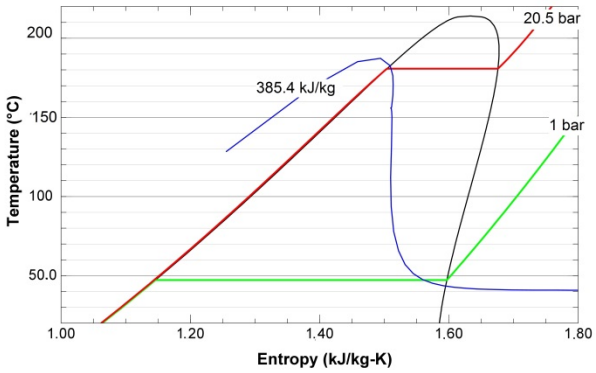

Fig. 4 Cooling process with R113 in *T*-s (temperature-entropy)—plot at 170°C.

Fig. 5 Laboratory compressor.

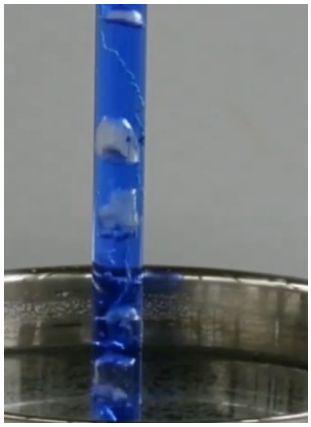

Fig. 6 Evaporation of colored acetone at 57 °C.

prototype get currently manufactured and will be ready soon. Further experiments are planned.

Based on previous experiments concerning the evaporation behavior of acetone (Fig. 6), fluid flow models are developed. The models are used for the simulation of heat transfers. These simulations will help adjusting optimal process parameters and designing optimized components.

6. Conclusions

The previous results allow an optimistic view in the future. The active cooling concept seems to be promising, thus its realization will be continued with great effort.

Additionally, the work on the process validation, component design optimization and ways of integrating the demands of geothermal technology in the processes will be intensified in the following years.

A project-application in cooperation with different scientific and industrial partners has been submitted to the BMU (Federal Ministry of Environment, Germany). The approval is very likely to be granted in summer 2014 and will support the further development a lot.

References

[1] Energy Target 2050: 100% Electricity from Renewable Energy Sources (Ger.: Energieziel 2050: 100% Strom aus Erneuerbaren Quellen), Federal Ministry of Environment Nature Conservation and Nuclear Safety BMU, Dessau-Roßlau, Germany, 2010.

[2] J. Jonsson, Simulation of output curves and wellhead pressure from high enthalpy wells in the Svartsengi geothermal field, M.S. Thesis, SW-Iceland, Faculty of Earth Sciences, University of Iceland, 2012.

[3] C. Bauer, Construction of a board with the heat-resistant micro-controller TI SM470R1B7M-HT and tests under alternating temperatures (Ger.: Aufbau einer Platine mit dem temperatur-beständigen Mikrocontroller TI SM470R1B1M-HT und tests unter wechselnden Temperaturen), Project Work, BA Karlsruhe, Karlsruhe, 2010.

[4] C. Strubel, Development of a Cooling System for a Geothermal Borehole Probe (Ger. Entwicklung eines Kühlsystems für eine Geothermie Bohrlochsonde), M.S. Thesis, HS Karlsruhe and ENSMM Besançon, 2010.

[5] A. Eberle, Pre-Investigation for the design of a Cooling Module for Borehole Probes based on Peltier-Elements (Ger. Voruntersuchung zum Entwurf eines Kühlmoduls für Bohrlochsonden auf Basis von Peltierelementen), Report, BA, Karlsruhe, 2009.

[6] J. Isele, B. Holbein, Development of a research probe for geothermal boreholes, in: 38th Workshop on Geothermal Reservoir Engineering, Stanford, Calif., Feb. 11-13, 2013.

[7] R. Giese, A. Jurcyk, P. Otto, U. Polom, G. Borm, Seismic Source and Procedure for the Generation of Seismic Shear Waves (Ger. Seismische Quelle und Verfahren zur Erzeugung seismischer Scherwellen), German Patent, DE 102005024367 B4 (2005).

[8] REFPROP — Reference Fluid Thermodynamic and Transport Properties, NIST Standard Reference Database 23, Version 9.1, Applied Chemicals and Materials Division, National Institute of Standards and Technology NIST, Colorado, Boulder.

[9] V.D.I. Wärmeatlas, VDI - Heat Atlas 2006, Society of German Engineers VDI – Association for Process Technology and Chemical Engineering GVC, Springer Publisher, Heidelberg, Germany, 2006..

[10] B. Holbein, Development of a cooling system for geothermal borehole probes, in: 38th Workshop on Geothermal Reservoir Engineering, Stanford University, Stanford, California, USA, 2013.

Geological Resource and Engineering
Volume 1, Number 1, December 2013
David Publishing Company
240 Nagle Avenue #15C, New York, NY 10034, USA
Tel: 1-323-984-7526, 323-410-1082; Fax: 1-323-984-7374, 323-908-0457
http://www.davidpublishing.com
geology@davidpublishing. com

ISSN 2328-2193
12
9 772328 219136